Effect of transmembrane potential on the diffusion of Na^+/H^+ exchanger of human red blood cell

Dissertation

zur Erlangung des Grades
des Doktors der Naturwissenschaften
der Naturwissenschaftlich-Technischen Fakultät III
Chemie, Pharmazie, Bio- und Werkstoffwissenschaften
der Universität des Saarlandes

Von

Aravind Pasula

Saarbrücken
2010

Tag des Kolloquiums:

Dekan:

Berichterstatter:

Vorsitz:

Akad. Mitarbeiter:

Dedicated to my family

Table of contents

Abbreviations

ABC	ATP binding cassette
a.u.	Arbitrary unit
AM	Acetoxymethyl
BCECF	2', 7'-bis-(2-carboxyethyl)-5-(and-6)-carboxyfluorescein
Caco-2	Human colon carcinoma cells clone-2
Ca^{2+}_i	Intracellular calcium concentration
Cs A	Cyclosporin A
CCD	Charged couple devices
DMSO	Dimethylsulfoxide
ED	Ethylene diamine
EGTA	Ethylene glycol tetra acetate
ETC	Easy To Clean
FCS	Fluorescence correlation spectroscopy
GPTS	Glycidoxypropyltrimethoxysilane
HIS	High ionic strength
LIS	Low ionic strength
MEM	Minimal Eagle medium
NSVDC	Non selective voltage dependent cation channel
PGA	Polyglucolic acid
P-gp	P-glycoprotein
pH_i	Intracellular pH
PLA	Polylactic acid
PLGA	Polylactic-co-glycolic acid
PLL	Poly-L-lysine
PMMA	Polymethylmethacrylate
PMT	Photomultiplier tube
RBC	Red blood cell
R18	Octadecyl rhodamine B chloride
TAU	Taurine coated surface
WGA	Wheat germ agglutinin

Chapter 1: Introduction

The present work is aimed at understanding and addressing the following problems which are investigated in detail.

A. Effect of transmembrane potential on the lateral diffusion of Na^+/H^+ exchanger of human RBCs.

B. Mechanism behind the Ca^{2+} loss of single Caco-2 cells.

C. Influence of nano-structured surfaces and nano-particles on the physiological processes of human RBCs and Caco-2 cells.

The Na^+/H^+ exchanger is an ubiquitous plasma membrane protein which transports Na^+ (some also K^+) across cell membranes in exchange for H^+ (Muerer *et al*., 1976; Richter *et al*., 1997). Existing in few copies per cell, their presence has been identified in almost all cell types (Grinstein *et al*., 1984; Tse *et al*., 1993; Rindler *et al*., 1981). The exchanger has a critical role in maintaining the intracellular pH (Deitmer and Ellis, 1980; Aickin *et al*., 1977) and cell volume (Siebens *et al*., 1985; Lew *et al*., 1986).

Very little is known about the effect of the transmembrane potential and volume change on the lateral diffusion of integral membrane proteins and lipids. Lateral motion of membrane constituents has many physiological significances in a biological system (Axelrod *et al*., 1983; McCloskey *et al*., 1984). We have investigated the influence of transmembrane potential on the lateral diffusion of Na^+/H^+ exchanger labeled with Bodipy-FL amiloride and the cell permeant lipid probe β-Bodipy-FL-C12-HPC in RBCs. Therefore, we altered the ionic strength of the extracellular solution by changing the transmembrane potential, took into account the volume change, and analysed the diffusion constants of Na^+/H^+ exchanger using the fluorescence correlation spectroscopy (FCS).

In the second part of the thesis, we have investigated the mechanism behind the Ca^{2+} loss of single Caco-2 cells in physiological conditions. Ca^{2+} is the most abundant ion in the human body which is responsible for many cellular processes. Ca^{2+} acts as a universal intracellular messenger which regulates neurotransmission, muscle contraction, etc. Cells regulate the intra- and extra-cellular Ca^{2+} levels very precisely, which is important for the cell growth, differentiation and apoptosis (Santella *et al*., 1998; Nicotera *et al.,* 1998).

Dramatic Ca^{2+} loss has been observed when the Caco-2 cells are in physiological conditions and without any external Ca^{2+} source in the environment with the aid of fluorescence microscope. Specifically, the objective of this study is to find the pathway behind the Ca^{2+} loss and the conditions responsible for it. Different inhibitors which specifically inhibit Ca^{2+} channels and Ca^{2+} pumps have been applied in these investigations.

In the present thesis, we have also made an attempt to study the effect of important physiological processes like Ca^{2+} transport and pH changes of RBCs and Caco-2 cells during their interactions with various nano-structured surfaces and nano-particles. The changes in intracellular pH and Ca^{2+} content give important information about the cell homeostasis and proper function of cell metabolism.

Nano-structured surfaces and nano-particles have a revolutionary impact in the present decade. The architecture and features of nano-structures at the contact of cell surface may induce some changes in the migration, growth and differentiation of certain cell types. The nano structured surfaces can be defined as structures ranging few nanometers (1-100 nm) and offer high surface to volume ratio which is characteristic feature of these materials (Alivisatos *et al*., 2004; West *et al*., 2000). Fundamental understanding of these interactions at the substrate level would certainly help in the manufacture of better materials. The investigated surfaces differ in the composition and texture of the material, physically and chemically. The membrane crossing ability of nano-particles and their influence on cell morphology has been studied using single cell fluorescence imaging system. Thus, we made an attempt to study the effect of various surfaces obtained from different sources on the Ca^{2+} transport and pH changes of both RBCs and Caco-2 cells.

The present work has been carried out under the supervision of Prof. Dr. Ingolf Bernhardt in the Laboratory of Biophysics, University of Saarland.

Chapter 2: Basic knowledge

2.1 Biological membrane and dynamics of membrane constituents

The cell membrane functions like a barrier between cell entity and the surrounding environment. According to the fluid mosaic model proposed by Singer and Nicolson (1972) the proteins "float in the lipid sea" and the lateral diffusion of proteins and lipids is allowed in the plane of membrane. This model considers the bilayer as a two-dimensional fluid in which lipids and proteins are free to diffuse. In recent years, considerable evidence has accumulated demonstrating that biological membranes are highly dynamic structures in which all components can undergo Brownian motion. However, the fluid mosaic model couldn't predict the influence of cytoskeleton and the diversity in the free diffusion of membrane components at that time. The arrangement and lateral distribution of proteins and lipids is essential for many cellular processes like transport, signal transduction and cell-cell recognition to occur (Kathleen, 2007). The asymmetry of a biological membrane is preserved and is necessary for the cell survival (Zwaal *et al.*, 1997). The three-dimensional view of a cell membrane structure is shown in Fig. 1.
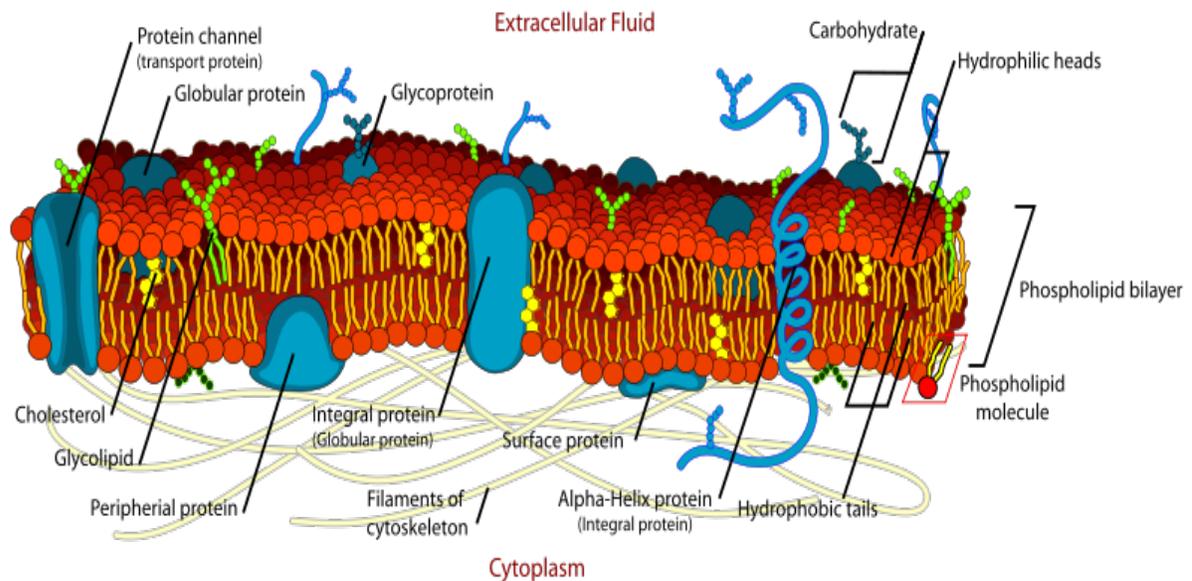
Fig. 1: Three-dimensional view of cell membrane structure (Image taken from the website: http://cellbiology.med.unsw.edu.au/units/images/Cell_membrane.png).

The mobility of a membrane constituent depends on the size of the molecule, lipid composition, its interactions with other molecules and temperature. Measuring the lateral diffusion of the diffusing component in membranes yields the information about the mobility rates which are related to cell physiological functions and the dynamic view of the surrounding environment. The fluidity of membrane depends on cholesterol content, temperature, configuration and composition of fatty acid chains. The distance covered by membrane lipids and proteins can be calculated using the Eq. (1):

$$X^2 = 2Dt \ \ \text{or} \ \ X = \sqrt{(2Dt)} \tag{1}$$

where X is the distance, D is the diffusion coefficient and t is the time. Thus, the characteristic diffusion constant (D) obtained for a lipid in the fluid-crystalline state or protein surrounded by lipid in fluid-crystalline state is 10^{-8} cm^2/s and diffuses a distance of 1 μm in 1 s. In case of lipids, the lateral (in-plane) diffusion is relatively rapid at rates 10^{-10} cm^2/s in crystalline state and 10^{-8} cm^2/s in fluid-crystalline state. The rotational mobility of lipids is rapid at rates of 10^{-9}–10^{-10} s in fluid-crystalline state. The transverse or flip–flop movement of phospholipids is very rare and unspecific with half-times in the order of hours or even days (Zachowski *et al*., 1993). On the contrary, the energy (ATP) dependent transport of aminophospholipids (PS and PE) from exoplasmic to cytoplasmic side is quick and highly specific (Seigneuret and Devaux, 1984). Specific proteins called translocases or flippases mediate such transport and are also involved in the origin of transmembrane asymmetry. The lateral and flip–flop movement of lipids in membrane is shown in Fig. 2.
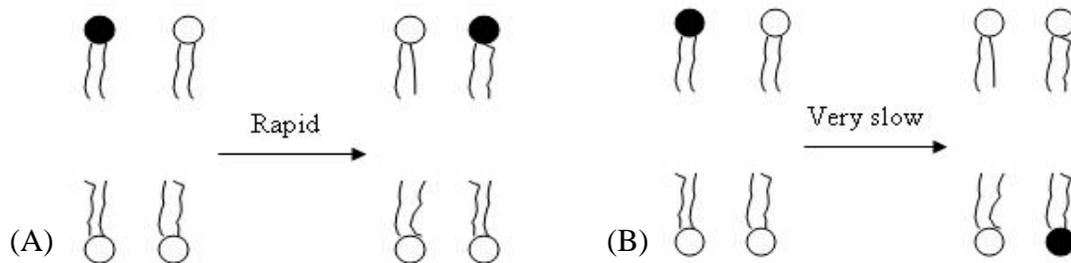
Fig. 2: Lipid movement in membrane. A) Lateral diffusion, and B) Flip-flop diffusion.

The lateral mobility of lipids in the outer membrane layer is greater compared to the inner membrane lipids. The restricted mobility of inner membrane lipids is attributed to the interactions of phospholipids with the cytoskeleton. Protein mobility varies to a greater extent. It has been observed that some proteins are free to move and others are attached to structures in the cytoplasm or extracellular spaces, thus restricting their movement. Various reports have established and confirmed the role of cytoskeletal matrix controlling the lateral mobility of proteins (Dennis *et al*., 1981; Sundqvist *et al*., 1976). The lateral diffusion of proteins found to be in the order of 10^{-8}–10^{-10} cm^2/s and depends on the state of lipid environment. The rotational mobility of proteins is very rapid in the order of 20–500 μs. Proteins, in contrast to lipids, do not exhibit flip-flop movement in membranes. Some models used to analyze possible rotational and translational motion of membrane constituents within membranes are shown in Fig. 3.

(I)   (II)   (III)

(IV)   (V)   (VI)
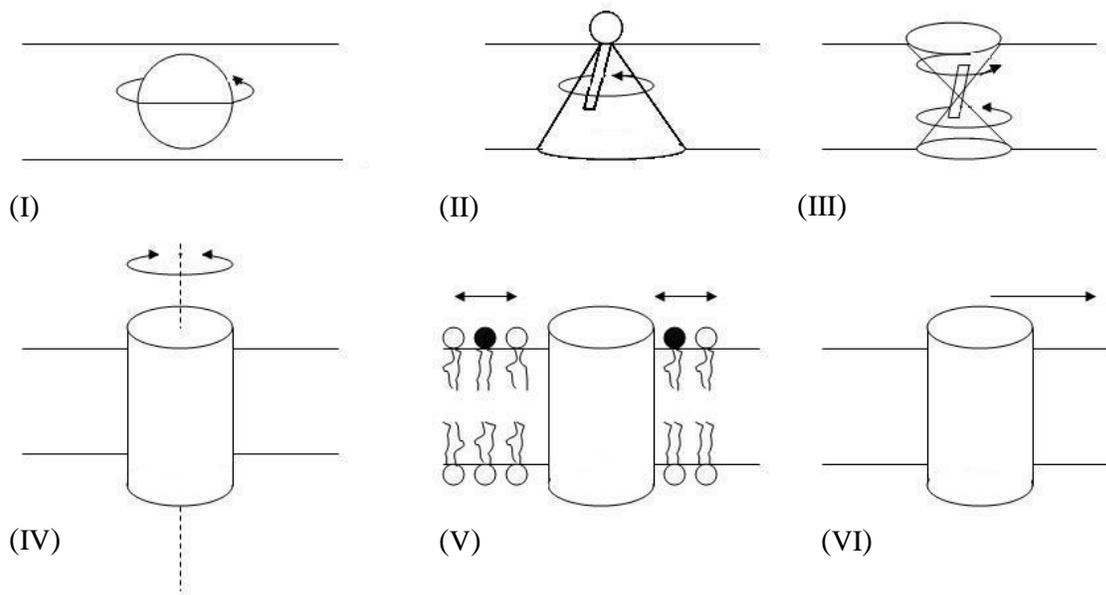
Fig. 3: Some models used to analyze rotational and translational motion within membranes. I) Isotropic rotation of a spherical molecule within the hydrophobic core of the membrane. II) Wobbling-in-cone model for a "rod-like" molecule tethered at the surface and able to move rapidly within a cone-shaped region defined by an angle with respect to the bilayer normal. III) Wobbling-in-cone model for rod-like molecule within the hydrophobic core. IV) Rotation of a cylindrical transmembrane protein. V) Lateral motion of lipids within the bulk (left side) and exchanging between bulk lipid and lipid adjacent to protein (right side). VI) Lateral motion of a cylindrical transmembrane protein.

The human RBC membrane has been served as a favourite model for studying the structural and mechanical properties of membrane for quite a long time. Advantages like availability, lack of nucleus, lack of intracellular organelles and the relatively homogeneous structure makes it suitable to investigate many properties related to membrane structure and dynamics. The lateral motion of lipids and proteins depends on the conditions like low ionic strength or high temperature that effects directly or indirectly the submembraneous spectrin-actin protein matrix of the membrane (Koppel *et al*., 1981). Human RBCs with lacking spectrin association also increase the diffusion rate of the integral proteins, whereas the lateral diffusion rates of membrane lipids are largely unaffected.

2.2 The transmembrane potential, surface potential and the electric field in the membrane

The transmembrane potential plays an important role in many physiological processes of cells (Cone, 1971; Sundelacruz *et al*., 2008). The disparity and the permeability coefficients of the different ions between the outer and inner sides of a biological membrane give rise to transmembrane potential. The transmembrane potential can be calculated only for the conditions where the sum of all partial ion fluxes is zero (for steady-state conditions only!). Thus, $\Sigma Z_i F J_i = 0$, where J_i are the electrodiffusive fluxes of the ion species and F is the Faraday constant. Considering only K^+, Na^+, and Cl^- the transmembrane potential can be calculated using the Goldman-Hodgkin-Katz equation:

$$\Delta \psi = \frac{RT}{F} \ln \frac{P_K c^o{}_K + P_{Na} c^o{}_{Na} + P_{Cl} c^i{}_{Cl}}{P_K c^i{}_K + P_{Na} c^i{}_{Na} + P_{Cl} c^o{}_{Cl}} \qquad (2)$$

The expression for the transmembrane potential of RBCs is derived from the following considerations (Eq. 3 and Eq. 4). The electric transmembrane potential ($\Delta\psi$) can be expressed as a diffusion potential of K^+ and Na^+. Because, under physiological conditions, the net ion movement of K^+ and Na^+ compared to Cl^- across the RBC membrane is very low. So, the electric transmembrane potential can be described as a diffusion potential of K^+ and Na^+ only:

$$\Delta \psi = \frac{RT}{F} \ln \frac{P_K c^o{}_K + P_{Na} c^o{}_{Na}}{P_K c^i{}_K + P_{Na} c^i{}_{Na}} \quad (3)$$

Which is identical to Nernst potential for chloride ions and protons:

$$\Delta \psi = \frac{RT}{F} \ln \frac{P_{Cl} c^i{}_{Cl}}{P_{Cl} c^o{}_{Cl}} = \frac{RT}{F} \ln \frac{P_H c^o{}_H}{P_H c^i{}_H} \quad (4)$$

In Eqs. (3) and (4), P_K, c_K, P_{Na}, c_{Na}, P_{Cl}, c_{Cl}, P_H, c_H are the permeability coefficients and concentrations for K^+, Na^+, Cl^-, and H^+, respectively. Symbols o and i represent the outside and inside of the membrane. R is the gas constant, F is the Faraday constant, and T is the absolute temperature.

In the present thesis, we made an attempt to study the effect of transmembrane potential and the volume changes of the cell on the diffusion constant of Na^+/H^+ exchanger of human RBCs under isotonic conditions. In physiological conditions RBCs maintain a negative membrane potential of -8 to -10 mV (Jay and Burton, 1969; Freedman and Hoffman, 1979; Deutsch *et al.*, 1979). Altering the ionic strength of the solution surrounding the RBCs causes several changes in the electric potential profile of the cell and leads to structural changes in the glycoproteins and glycolipids. In low ionic strength (LIS) conditions, considerable alterations in the physical characteristics like density profile and thickness of the membrane glycocalyx can be observed. Electrophoretic measurements of human RBCs suspended in LIS solution of 10 mM NaCl have shown that the glycocalyx of the cells increased in thickness from 5.5 (in HIS solution) to 12 nm (Bernhardt, 1994). Increase in the electric potential under LIS conditions is attributed to the mutual intra- and inter-molecular attraction and repulsion of the charged ionic groups. Membrane electric field inside a biological membrane can influence membrane constituents significantly. The electric field inside a cell membrane is determined by the gradient of the electric potential in all three dimensions. The electric field in the direction perpendicular to the cell membrane is given by the difference between the actual electric potentials on both sides of the cell membrane divided by the membrane thickness (assuming zero charge density inside). Thus it is clear that the

transmembrane potential as well as the inner and outer surface potential is of importance for determining the electric field inside a cell membrane. The electric field strength in a RBC membrane under physiological conditions is assumed to be in the order of 10^6 V/m. So, it is quite obvious that a reduction in the ionic strength of the extracellular solution results in a change of the electric field inside the membrane due to alterations of the transmembrane potential and also the outer surface potential. The situation is clearly explained in Fig. 4. The electric potential profile across the cell membrane is not linear because of electrically charged and polarizable groups are present around and are located in different positions relative to both sides of the membrane surface. This concerns not only the head groups of the membrane phospholipids which contribute with a dipole potential of about 100 mV to the overall potential profile in the membrane but also regions of charged membrane proteins. Additionally, a change of the electric potential gradient leads to significant alterations of the mechanical tension inside the cell membrane, as given by the Maxwell stress, P_e:

$$P_e = \frac{\varepsilon \varepsilon_o (d\psi / dx)^2}{2} \qquad (5)$$

where ε is the permittivity, ε_o is the dielectric constant and $d\psi/dx$ is the electric potential gradient in the membrane.
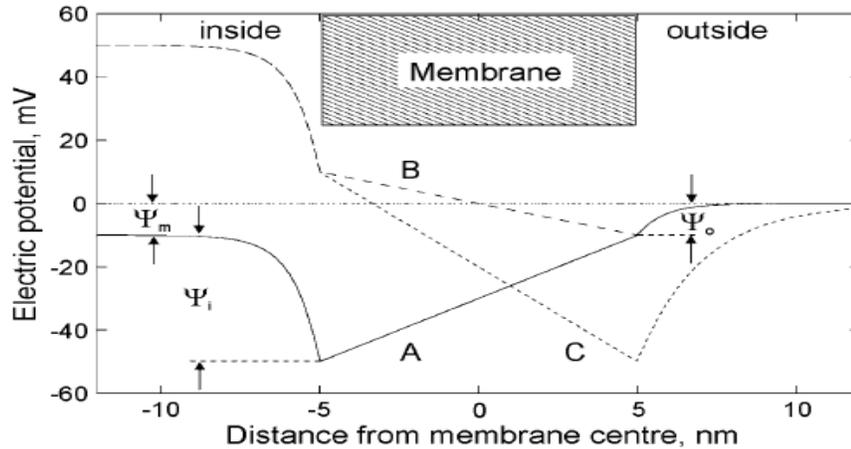
Fig. 4: Electric membrane potential profile across the RBC membrane: Ψ_m transmembrane (diffusion) potential, Ψ_o outer surface potential, Ψ_i inner surface potential, A physiological ionic strength solution, e.g. NaCl solution, B solution with reduced Cl$^-$ concentration but constant ionic strength (compared to A), e.g. sodium tartrate solution, C solution of low ionic strength (LIS), e.g. sucrose solution (Taken from Bernhardt and Weiss, 2003).

The electric field in the cell membrane in the direction of the plane of the cell membrane depends on the present localization of the membrane constituents (proteins and lipids). Specifically, the distribution of charged and polarized membrane constituents as well as their lateral movement is important (McLaughlin and Poo, 1981). Additionally, electrogenic pumps and electrodiffusive pathways contribute to the actual electric field in the membrane also (Fromherz, 1988). It has been reported that the electric field inside a biological membrane influences the mobility and the position of the hydrocarbon chains of the phospholipids as well as the phase transition temperature of the membrane phospholipids (Träuble and Eibl, 1974; Jähnig, 1976; Forsyth *et al*., 1977). The electric field strength is also known to affect the head groups of the phospholipids. Membrane electric field can influence membrane proteins either directly or indirectly via changes in the phospholipids environment of the proteins, thereby affecting the lipid-protein interaction.

2.3 Red blood cell morphology

Human RBC is a biconcave disc in shape with 8-10 µm in diameter, 2 µm of thickness and with a volume of 90 μm^3. This characteristic shape is maintained by cell's active metabolism. The primary function of a RBC is to distribute oxygen to the body cells and dispose CO_2 and protons generated during tissue metabolism. The average life span of a RBC is about 120 days. During this period, it travels around 500 km making about 170,000 circuits (Lux, 1979) through heart and small penetrations in capillaries for numerous times. This discocyte shape is advantageous as it offers a high surface to volume ratio to facilitate gas exchange. The normal human RBC can have discocytic (discoid), stomatocytic (cup) or echinocytic (crenated) shapes (Fig. 5).

(A)   (B)   (C)
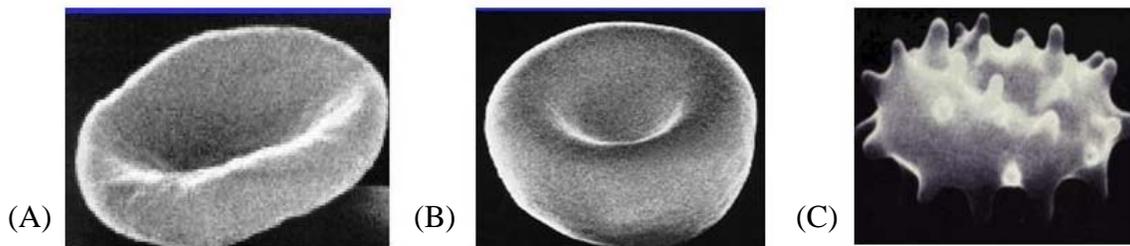
Fig. 5: Shapes of human RBCs: A) Discocyte B) Stomatocyte and C) Echinocyte.

2.4 Red blood cell membrane proteins

Human RBC membrane is constituted by three major components:

a) Integral membrane proteins (e.g., anion exchanger (AE 1), glycophorin, membrane transport proteins)

b) Skeletal proteins (e.g., spectrin, protein 4.1 and actin)

c) Anchoring proteins (e.g., ankyrin, protein 4.2)

A schematic diagram representing the organization of the major RBC proteins and their interactions with various proteins of the cytoskeleton is shown in Fig. 6.
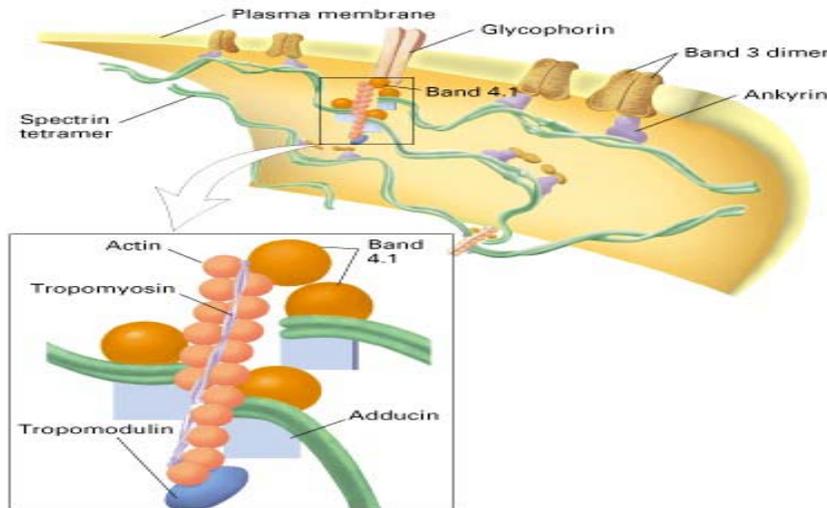
Fig. 6: Schematic diagram representing the organization of the major RBC proteins and their interactions with different proteins of the cytoskeleton (Taken from the website: http://bioweb.wku.edu/courses/Biol22000/27Actin/Fig.html).

2.4.1 Integral membrane proteins
Band 3 protein or anion exchanger

It is a major and most abundant (with approx. one million copies per cell) integral transmembrane protein of the human RBC plasma membrane (Fairbanks *et al*., 1971; Steck, 1978). It occupies about 25% of the total membrane protein weight with a molecular weight of 100 KDa. It exists mainly as a dimer and participates in the efficient transport of bicarbonate across the RBC membrane in exchange for Cl⁻ ion. The N-terminal of band 3 protein anchors to the membrane skeleton by associating with ankyrin

and protein 4.1. Additionally, it also binds to glycolytic enzymes, haemoglobin and other proteins including protein 4.2. The cytoplasmic domain can be cleaved from the membrane without altering the band 3-catalyzed anion transport. The C-terminal membrane spanning domain is heterogeneously glycosylated with a molecular mass of 52 KDa. The membrane hydrophobic C-terminal participates in the Cl^-/HCO_3^- anion transport of the RBC (Fujinag *et al*., 1999).

Glycophorins

Most of the negetive surface charge (60%) of the RBC is imparted by the glycophorins. Each RBC membrane contains approximately 200,000 copies of glycophorins accounting for 1.5% of the membrane weight. The transmembrane protein glycophorin is composed of three distinct domains:

a) Hydrophilic amino terminal located external to the membrane with oligosaccharide side chains

b) Hydrophobic region inside the lipid bilayer

c) Hydrophilic region rich with charged amino acids inside the cytosol

The oligosaccharides are O-glycosylated to serine or threonine (except one N-glycosilated). Glycophorins along with the protein 4.1 take part in the RBC integrity and shape. Additionally, the glycophorins also contain antigens for M and N blood groups.

Membrane transport proteins

Membrane transport proteins are involved in the movement of ions, small molecules, or macromolecules across the RBC membrane. These are integral membrane proteins, with alpha helices, which exist within and span across the membrane and transport substances by three principle transport mechanisms like passive or gradient diffusion, facilitated diffusion, and active transport. A detailed description to different membrane proteins participating in RBC membrane transport and their function are explained in the section 2.6.

2.4.2 Skeletal proteins

The major peripheral proteins include spectrin, ankyrin, proteins 4.1, 4.2 and actin. These proteins play an important role in the structure of human RBC cytoskeleton and integration.

Spectrin (bands 1-2)

Spectrin constitutes most of the RBC membrane skeleton mass with 200,000 molecules per cell (Steck, 1974) located on the cytoplasmic surface. It is composed of two subunits namely α (280 KDa) and β (246 KDa) which are structurally distinct and encoded by different genes. Both subunits form heterodimers (αβ) by winding around each other and self assemble head to head to form heterotetramers ($\alpha_2\beta_2$). These tetramers at the tail end linked with actin and are attached to band 4.1. The head end with ß-chains attach to ankyrin which is further connected to band 3. This interaction is enhanced by band 4.1. Spectrin plays a vital role in maintaining the structure and visco-elastic properties of human RBCs. It also provides support to the lipid bilayer and thereby is involved in the lateral mobility of integral membrane proteins.

Actin (band 5)

In human RBCs, actin (β-actin) is believed to exist in non-filamentous form with $400-500\times10^3$ copies per cell (Tilney *et al*., 1975). It exists as a short, double helical F-actin with 12 to 13 monomers of 35 nm in length. It gives stability to the RBC membrane by interacting with spectrin, protein 4.1 and tropomyosin. It is assumed that in human RBCs actin along with spectrin restrict the lateral movement of membrane-penetrating particles and thereby controlling RBCs shape and deformability.

2.4.3 Anchoring proteins
Ankyrin (band 2.1-2.3)

Ankyrin serves as a cross linker between the membrane skeleton via spectrin binding and the lipid bilayer via band 3 binding. This association is important in maintaining the membrane stability. Abnormalities in ankyrin result in typical heriditary spherocytosis (HS).

Protein 4.1 and protein 4.2

In human RBCs, these proteins regulate the physical properties of mechanical stability of the membrane. They stabilise the spectrin-actin network and maintain the membrane skeleton integrity. They also enhance the interaction between spectrin to the lipid bilayer through their association with transmembrane proteins band 3 and glycophorin. Protein 4.1 contains two polypeptides referred to as 4.1a and 4.1b which differ in molecular weight by 2 KDa. The primary role of protein 4.2 is to stabilize the association of spectrin, actin and ankyrin complex with band 3. It is also involved in protecting the membrane skeleton from premature ageing. Protein 4.1 is an important structural protein with a molecular mass of 78-80 KDa.

2.5 Red blood cell membrane lipids

Lipids occupy approximately half of the membrane area in human RBCs. The major lipids include phospholipids, glycolipids and cholesterol. The phospholipids phosphatidylserine (13%), phosphatidylethanolamine (27%) and phosphatidylinositol (2-5%) are distributed mainly in the inner or cytoplasmic leaflet of the membrane, whereas sphingomyelin (26%) and phosphatidylcholine (28%) are in the outer leaflet. Lipids can form all-trans (saturated) or kinks (unsaturated) configuration of fatty acids. For each type of phosholipid, a characteristic phase transition temperature exists. Below the phase transition temperature fatty acyl chains are in crystalline state and above this temperature they are in fluid-crystalline state. Glycolipids are membrane components composed of lipids that are covalently bonded to mono- or polysaccharides. Human RBCs also contain certain amount of cholesterol in unesterified form with a primary role to maintain membrane fluidity. Thus the membrane asymmetry is maintained, which is crucial for the cell survival. Flippases are the enzymes which participate in the translocation of phosphatidylserine and phosphatidylethanolamine to the inner leaflets using ATP.

2.6 Red blood cell membrane transport

The procees of ion transport through biological membranes can be classified into four principal mechanisms: pumps, carriers, channels and residual transport. Various techniques are available to determine transport rates include radioactive tracers and fluorescence-labeled dyes (flux measurements). Alternatively, electrophysiological

methodology including the patch-clamp is applicable to electrogenic transport. An overview of various transport systems for Na^+ and K^+ of human RBCs is illustrated in Fig. 7.
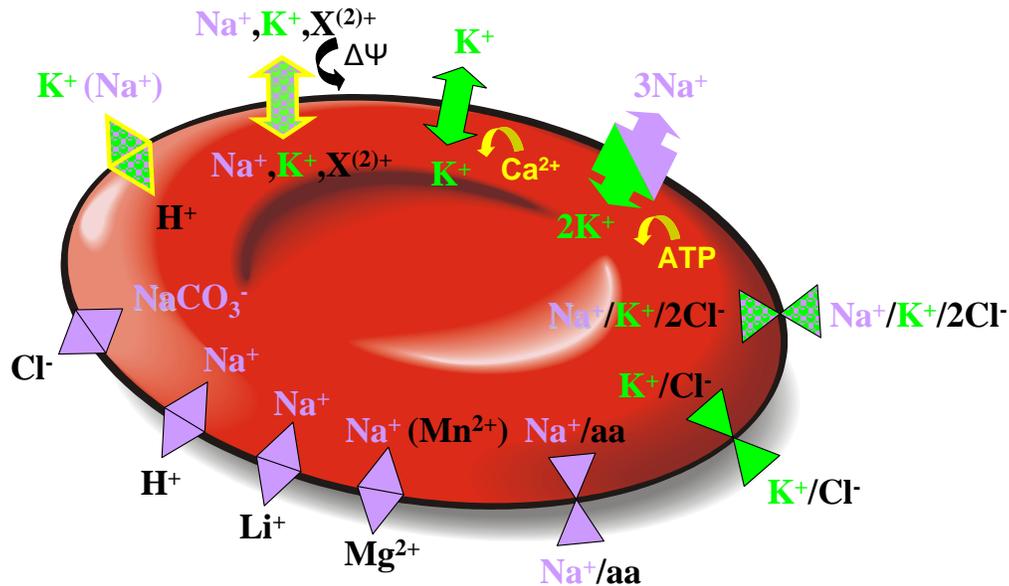
Fig. 7: Overview of various transport systems for Na^+ and K^+ of human red blood cells. The transport mechanisms shown: Na^+/K^+ pump; $Na^+/K^+/2Cl^-$ symporter; K^+-Cl^- symporter; Na^+-dependent amino acid transport; $NaCO_3^-/Cl^-$ exchange; $Na^+(Mn^+)/Mg^{2+}$ antiporter; Na^+/Li^+ antiporter Na^+/H^+ antiporter; nonseclective voltage-dependent cation channel (NSVDC); $K^+(Na)^+/H^+$ antiporter and Ca^{2+}-activated K^+ channel (Gardos channel) (Taken from Bernhardt and Weiss, 2003).

2.6.1 Pumps

Pump action is mediated by active transport (or primary active transport) characterized by one or more ions moving against the electrochemical potential(s) through direct coupling to metabolic energy (ATP). The enzymes which hydrolyze ATP to harness energy for solute movement are termed ATPases. They often need cosubstrates, for example, Na^+ and K^+ for the Na^+ K^+-ATPase, Ca^{2+} and H^+ for the Ca^{2+}-ATPase. In functional terminology, they are called pumps, for example, Na^+/K^+ pump or Ca^{2+} pump. During the transport, there is a conformational change of the pump protein, driven by energy released during ATP hydrolysis. Human RBCs containing important pumps are described below.

Na⁺/K⁺ pump

Human RBCs played an important role in identification and characterization of the Na^+/K^+ pump. This pump is responsible for maintaining the high internal K^+ concentration and low internal Na^+ concentration (Sarkadi and Tosteson, 1979). The pump extrudes Na^+ in exchange for K^+ in 3:2 stoichiometry using 1 ATP molecule as energy source. The Na^+/K^+ pump is known to be present in nearly all animal cell types (except in RBCs of carnivora). It utilizes up to 70% of the total cellular ATP of a cell. The gradient established by the Na^+/K^+ pump is used by different transpoters like K^+/Cl^-, $Na^+/K^+/2Cl^-$ and the Na^+/H^+ exchanger. The ion gradients generated by this pump serves as an energy source for the coupled transport of other ions. The Na^+/K^+ pump consists of two subunits α (catalytic site) and β (glycosylated site) with molecular weights of ~100 KDa and 55 KDa, respectively. Another subunit termed γ (10 KDa) has also been identified in purified preparations of the enzyme. This pump can be specifically inhibited by ouabain. The subunit α contains the binding sites for ATP and ouabain and takes part in most of the functions of the Na^+/K^+ pump. This subunit also has a pivotal role during the conformational changes, which accompany occlusion, and translocation of ions in the Na^+/K^+ transport cycle (Jorgensen *et al*., 1982). The smaller β subunit is involved in the activity of the complex. It also facilitates the plasma membrane localization and activation of the α subunit.

Ca²⁺ pump

Human RBCs maitain low intracellular Ca^{2+} levels in the range of 0.01-0.1 µM. It is strictly regulated by a Ca^{2+}-activated, Mg^{2+}-dependent Ca^{2+} pump. Ca^{2+} pump was first described by Schatzmann (1975). It consists of a single polypeptide chain of 138 KDa. There are about 1000 copies per cell. It belongs to the P-type of ATPases and is the largest of all known P-type ion pumps. The pump is structurally organised with ten transmembrane helices. The cytoplasmic domain contains three protrusion units consisting of antiparallel β-sheets, α-helices and parallel β-sheets. The first protrusion unit is located between the 2nd and 3rd transmembrane domains and permits the coupling of ATP hydrolysis to the transport of Ca^{2+} ions. The second protrusion unit is between transmembrane domains 4 and 5.

The C-terminal of this part contains the active sites of the pump for aspartyl-phosphate formation and the binding site for ATP. It is attached to the membrane by a flexible 'hinge' which allows the catalytic aspartic acid to approach the bound ATP during the catalytic cycle. The third and last protrusion is present at transmembrane domain 10 with the N-terminal. Calmodulin-binding domain is located next to the C-terminal region. The Ca^{2+} pump is activated by calmodulin binding (Jarrett and Penniston, 1977). Vanadate, a known inhibitor, acts by inhibiting the phosphorylated intermediate (an aspartyl-phosphate) during the catalytic cycle.

2.6.2 Channels

Channels often consist of several transmembrane α-helices spanning the cell membrane. In the inner part of the protein, several helices together can form a channel structure. Such structural organization allows a more-or-less specific transport of ions. Channels exhibit two general features include a mechanism for opening and closing and a selectivity filter. The high-frequency switch between the open and closed state of the channel is termed gating, and the duration of opening is called open time. The selectivity filter is responsible for the more-or-less specific transport of one or several ion species. Human RBCs containing important channels are described below.

Aquaporins

Aquaporins or water channels are the membrane proteins which mediate water transport across the membrane. Human RBCs adjust according to the osmolarity of the surrounding environment. Human aquaporin-1 channel is capable of transporting roughly 3 billion water molecules per second. Aquaporins are first detected and localized as a polypeptide of 35‒60 KDa by Benga in 80's (Benga *et al*., 1986b; Benga *et al*., 1986c). Peter Agre and his coworkers have shown that the chip 28 protein (now named as aquaporins) is associated with with six membrane spanning alpha helices of human RBCs (Preston *et al.,* 1991).

Gardos channel

The Ca^{2+}-activated K^+ channel is also called Gardos channel after its discoverer in ATP depleted RBCs (Gardos, 1958). This specific channel is activated with a rise of the

cytoplasmic Ca^{2+} content of the cell. The Gardos channel in human RBCs is irreversibly inactivated in the absence of extracellular K^+ and has a low conductance in the order of about 20 pS (Alvarez and Garcia-Sancho, 1989). It is reported that normal RBCs contains approximately 150 channels per cell. Its potential role as a mediator during the sickle cell dehydration has been established. Specific inhibitors like chinin, chinidin, clotrimazol and charybdotoxin are known to inhibit the channel (Brugnara *et al*., 1993; De Franceschi *et al*., 1994).

Nonselective voltage-dependent cation channel

The existence of non selective voltage-dependent channel (NSVDC) was demonstrated by inside-out and whole-cell patch clamp recordings (Christophersen and Bennekou, 1991). Depolarizing the human RBC membrane from negative to positive values, the NSVDC channel starts to respond. This channel transports Na^+, K^+, Rb^+, NH^+_4 and Ca^{2+}, Mg^{2+} and Ba^{2+}. Based on an estimate of the patch area and the number of channel observations, the number of channels assumed to be 300 per RBC (Kaestner *et al.*, 2000). The NSVDC channel of RBC is blocked by the inorganic substances ruthenium red and La^{3+} and inactivated by the sulfhydryl protein reagents, NEM and IAA (Bennekou *et al*., 2004). Several reports have identified an important role of this channel in eryptosis induced by osmotic shock, oxidative stress, and energy depletion. Eryptosis is the suicidal death of RBC which is characterized by cell shrinkage, membrane blebbing, activation of proteases and phosphatidylserine exposure at the outer membrane leaflet.

2.6.3 Carriers

Proteins acting as carriers mediate the transport of ions or other substrates by making use of a periodic repeated conformational change of the protein. Thus, it becomes possible for the transported substrate to gain access to its binding site at both the inner and outer membrane surface. Sometimes, an intermediate folded conformational state is seen. In this transitional stage, the bound substrate is denied access to the aqueous solutions on either side of the membrane. In general, carrier-mediated transport can be divided into two different mechanisms: uniport and cotransport. A uniport mediates transport of a single ion or other substrate. The transport via uniporters can only occur

''downhill'', that is, along the concentration gradient of the transported substance (or along its electrochemical gradient in case of charged species). It is also termed as facilitated diffusion. Cotransporters can be classified into symporters and antiporters. The term cotransport is used as synonym for symport, while an antiport function is synonymous to exchange or countertransport. A symporter binds ions or substances (two or more substrates) and transports them together in one step in the same direction through the membrane. Movement of one substrate down its chemical or electrochemical gradient is used to power the ''uphill'' transport of the cotransported substrate(s), that is, against their chemical or electrochemical gradients. An antiporter or countertransporter mediates exchange of an ion (or substance) for another ion (or substance) transporting them in opposite directions. The antiporter can carry out its transport process in one step similar to the symporter. Human RBCs containing important carriers are described below.

K^+/Cl^- cotransporter

This transporter is involved in the cotransport of K^+ and Cl^- in an interdependent manner with a 1:1 stoichiometry (Brungara et al., 1989). It is more functional in reticulocytes and its activity diminishes with the cell age. The major activators of K^+/Cl^- cotransporter include cell swelling, low pH, Mg^{2+} depletion, and thiol modification. In mature RBCs the transporter can be activated by various oxidant agents that stimulate dephosphorylation of the transporter (Brugnara, 1997). The K^+/Cl^- cotransporter is responsible for the RBC dehydration in sickle cell anaemia (Brugnara, 1995). This cotransporter is sensitive to loop diuretics like bumetanide and furosamide (Bernhardt et al., 1988).

Na^+/Mg^{2+} exchanger

Na^+-dependent Mg^{2+} transport was first described by Günther and Vormann in chicken and turkey RBCs (1985). This transporter is strictly dependent on the extracellular Na^+ concentration. Abnormalities in the Na^+/Mg^{2+} exchanger result in the pathogenic diseases like primary hypertension and cystic fibrosis. Though the exchange stoichiometry varies between cell types and functional status of cell, but in general it is 2 Na^+ for 1 Mg^{2+}. This transporter can be inhibited by amiloride, quinidine and imipramine.

Na$^+$/Li$^+$ antiporter

The Na$^+$-dependent Li$^+$ transporter in human RBCs was first described by Duhm and Becker (1977). The exchanger primarily transports Na$^+$ for Li$^+$ and it can also accept Na$^+$. The Li$^+$ efflux occurs in the presence of external Na$^+$ but not K$^+$, Rb$^+$, Cs$^+$, choline, Mg^{2+}, or Ca^{2+} and is insensitive to ouabain. This extrusion is inhibited by phloretin, and does not require any cellular ATP. However, the total Li$^+$ influx of human RBCs is partly ouabain-sensitive and partly ouabain-insensitive but phloretin-sensitive. An increase in the activity of Na$^+$-Li$^+$ countertransporter (SLC) is observed in patients who have essential hypertension and can be regarded as the possible marker of type 2 diabetes (Canessa *et al*., 1980).

Glucose transporter

RBCs require glucose for metabolic needs and therefore it is supplied constantly by the glucose transporter. It is the most extensively characterised transport systems of the facilitated diffusion in human RBCs. Human RBCs contain little glucose compared to the blood plasma (~5 mM). Glucose enters the cell down the concentration gradient through glucose transporter. Glucose transporters are transmembrane proteins with 12 membrane spanning helices and exist as a monomer. It accounts for 2% of the total membrane protein in the RBC.

Na$^+$/K$^+$/2Cl$^-$ cotransporter

The Na$^+$/K$^+$/2Cl$^-$ cotransporter was first described by Wiley and Cooper in human RBCs in 1970s (Wiley and Cooper, 1970). The net salt movements mediated by this cotransport exhibit a stoichiometry of 1Na:1K:2Cl. In human RBCs, Na$^+$/K$^+$/2Cl$^-$ cotransporter may play a role in the maintenance and regulation of cell volume (Duhm and Gobel, 1984). It has been reported that the depolymerization of cytoskeletal actin activates the Na$^+$/K$^+$/2Cl$^-$ cotransporter during the changes of cell volume. The transport can be inhibited by loop diuretics like bumetanide, benzmetanide, and furosemide.

2.6.4 Residual transport

The residual transport can be explained as the membrane transport after all the known specific pathways (pumps, channels, and carriers) are inhibited. The residual K^+ transport is insensitive to ouabain, bumetanide and EGTA. Thus the possible involvement of the Na^+/K^+ pump, the $Na^+/K^+/2Cl^-$ cotransport, and the Ca^{2+}-activated K^+ channel can be excluded. K^+/Cl^- cotransporter is silent in adult human RBCs and activated only under specific conditions (Hall and Ellory, 1986). The K^+ and Na^+ transport (unidirectional influxes and effluxes as well as net effluxes) in LIS conditions, but at isotonic osmolarity, are significantly increased in human RBCs (Bernhardt *et al*., 1991; Denner *et al*., 1993). Additionally, in solutions containing Na-gluconate or Na-glucuronate (replacing NaCl) does not result in a significant change of the K^+ influx, although such conditions lead to the similar change of the transmembrane potential as compared with solutions where NaCl is replaced by sucrose. Thus it has been concluded that the residual transport is not based on a simple electrodiffusion (Bernhardt *et al*., 1988, 1991).

Richter and his co-workers have shown that the transport operates under situations far from the physiological conditions (Richter *et al*., 1997). Further evidence came from the study of intracellular pH changes under various conditions using the fluorescent dye BCECF. The obtained data of H^+ efflux can be correlated with the (ouabain + bumetanide + EGTA)-insensitive K^+ efflux (Kummerow *et al*., 2000). The possible role of a proposed $K^+(Na^+)/H^+$ exchanger seems to be more convincing for explaining the residual transport (Bernhardt *et al*., 2001).

Chapter 3: Materials and Methods

3.1 Chemicals and sources

The chemicals and their sources used for the present work are listed in the Table 1:

Table 1: Chemicals and their sources

Chemicals	Sources
D(+)- sucrose, N-2-hydroxyethylpipe-razin-N'-2-ethanesulfonic acid (HEPES), NaOH, Dimethylsulfoxide (DMSO)	Roth, Karlsruhe, Germany
BCECF-AM, Bodipy-FL amiloride, Fluo-4 AM, Fura-2 AM, Pluronic F-127 (20% solutions in DMSO), β-Bodipy-FL-C12-HPC, Octadecyl rhodamine B chloride (R18)	Invitrogen, Inc., Karlsruhe, Germany
Sodium-ortho-vanadate	Alexis Biochemicals, Gruenberg, Germany
NaCl, KCl, $CaCl_2$, $MgCl_2$, D(+)-glucose, Diltiazem-Cl, Poly-L-lysine solution 0.1% w/v in distilled water, Nigericin, 4-Bromo-calcium A23187, Ethylenglycoltetraacetate (EGTA), Nifidepine, Cyclosporin A	Sigma-Aldrich, Munich, Germany
Ethanol	Chemical store, University of Saarland
Baysilone paste	Bayer, Leverkusen, Germany

3.2 Buffers and solutions

Different buffers and solutions with their composition used in the present study are listed below.

High ionic strength (HIS) solution:

        145 mM NaCl
        10 mM glucose
        7.5 mM KCl
        10 mM HEPES / NaOH, pH 7.4

Low ionic strength (LIS) solution:

        250 mM or 200 mM sucrose
        10 mM glucose
        7.5 mM KCl
        10 mM HEPES / Tris or NaOH, pH 7.4

Sodium tartrate solution:

        107 mM Na tartrate
        10 mM glucose
        7.5 mM KCl
        10 mM HEPES / NaOH, pH 7.4

pH-calibration solution:

        135 mM KCl
        10 mM NaCl
        10 mM glucose
        10 mM HEPES / Tris,
        with pH: 6.8, 7.1, 7.4 or 7.8

The structural formulae of the most important substances used and their absorption and emission spectra are shown from Fig. 8‒Fig. 18.

(A)

(B)
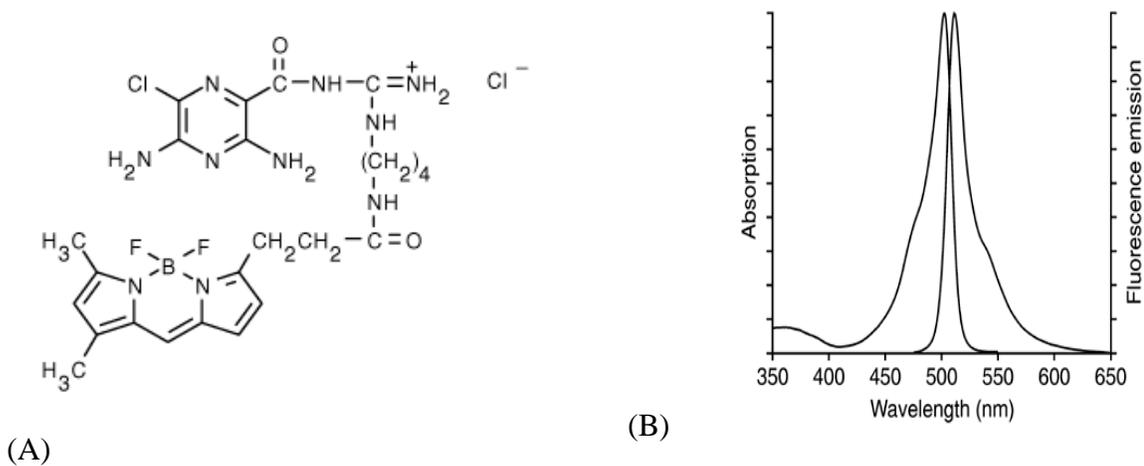
Fig. 8: A) Structural formula and B) absorption (λ_{max}= 488 nm) and emission (λ_{max} = 510 nm) spectra of Bodipy-FL amiloride (Taken from www.invitrogen.com).
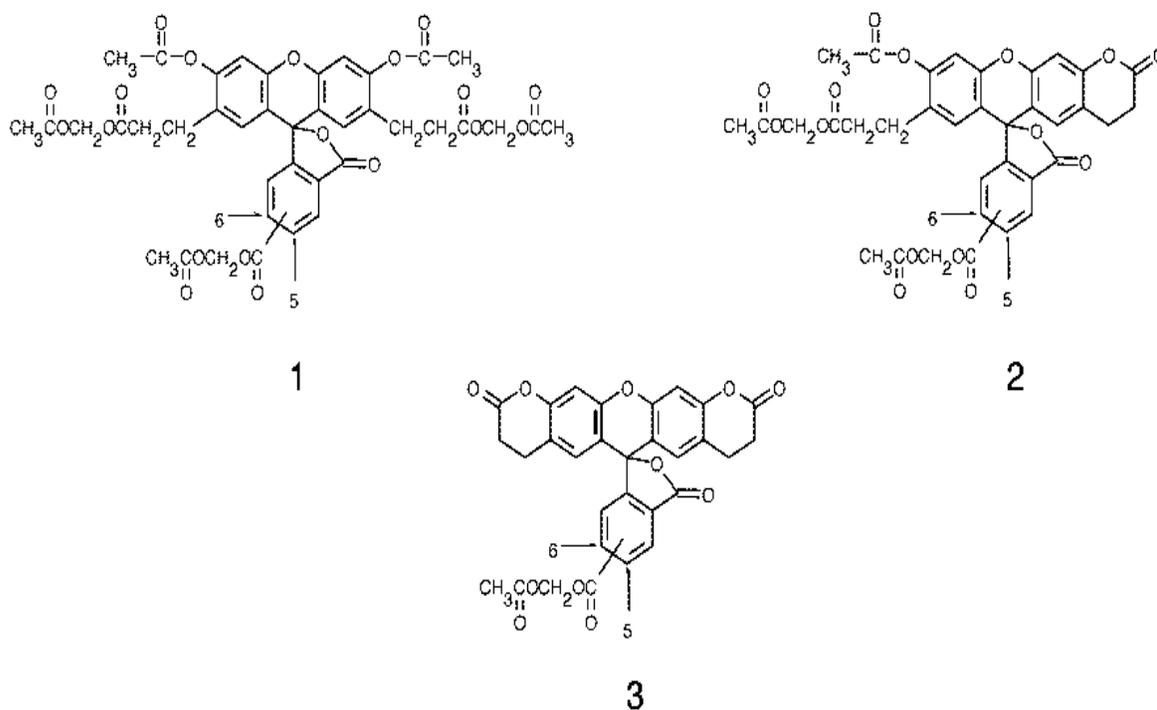
Fig. 9: Three different molecular structures of AM-Esters of BCECF (Taken from www.invitrogen.com).
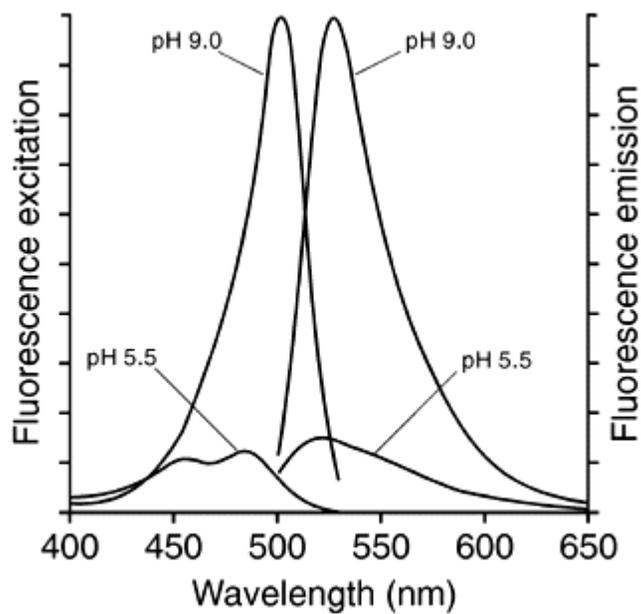
Fig. 10: Absorption ($\lambda_{max} = 490$ nm) and emission ($\lambda_{max} = 510$ nm) spectra of BCECF-AM at pH 9.0 and 5.5 (Taken from www.invitrogen.com).

(A)

(B)
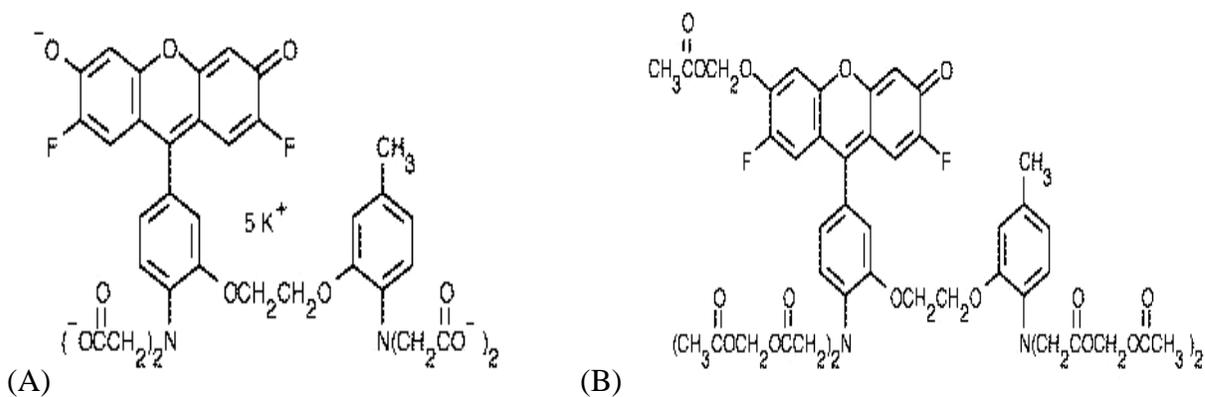
Fig. 11: Structural formula of Fluo-4 (A) and the AM-Ester of Fluo-4 (B) (Taken from www.invitrogen.com).
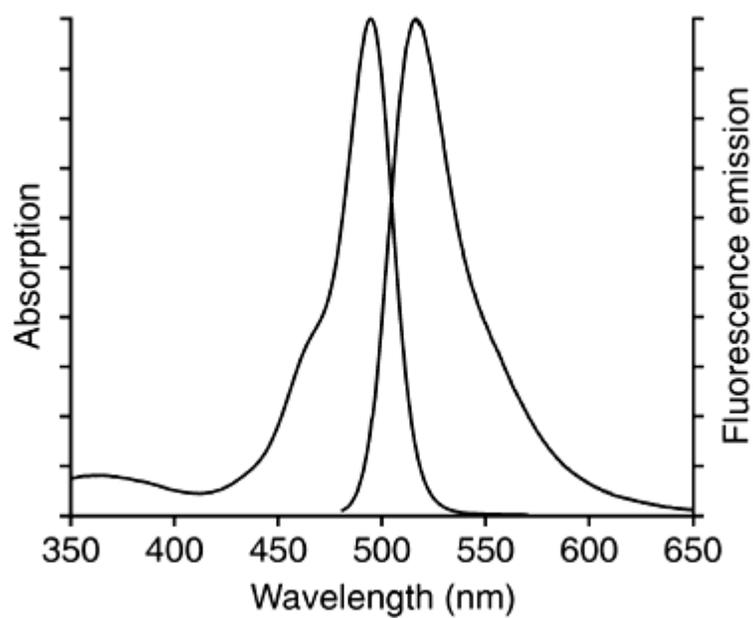
Fig. 12: Absorption (λ_{max} = 490 nm) and emission (λ_{max} = 530 nm) spectra of Fluo-4 AM (Taken from www.invitrogen.com).
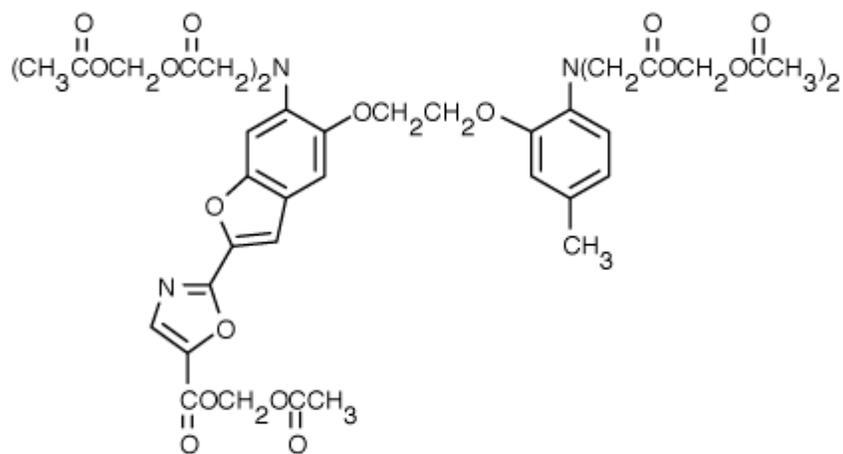
Fig. 13: Structural formula of Fura-2 AM (Taken from www.invitrogen.com).
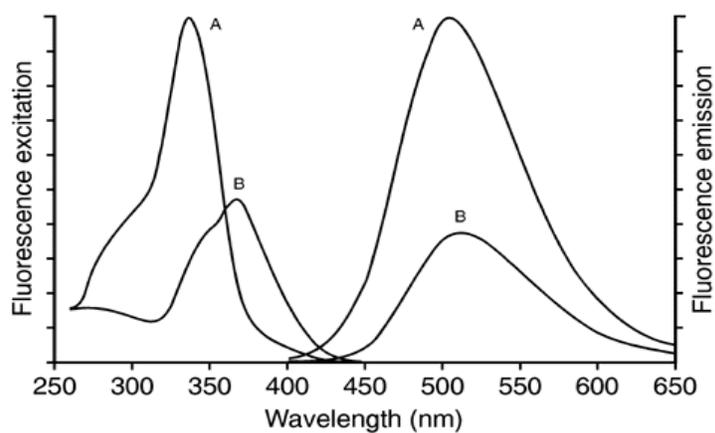
Fig. 14: Fluorescence absorption (λ_{max} = 340 nm) and emission (λ_{max} = 510 nm) of Ca^{2+}-saturated (A) and Ca^{2+}-free (B) Fura-2 in pH 7.2 buffer (Taken from www.invitrogen.com).
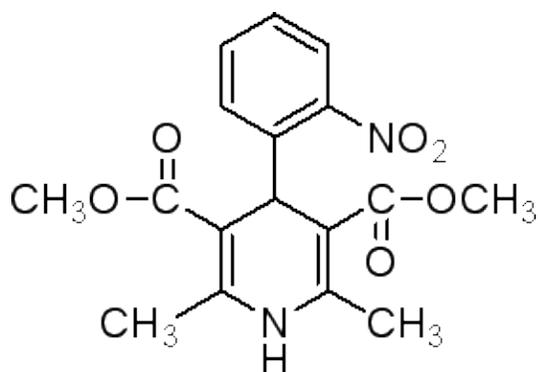
Fig. 15: Structural formula of nifedipine (Taken from www.sigmaaldrich.com).
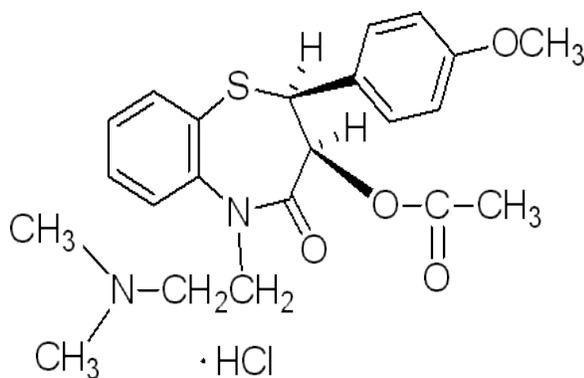
Fig. 16: Structural formula of diltiazem-Cl (Taken from www.sigmaaldrich.com).
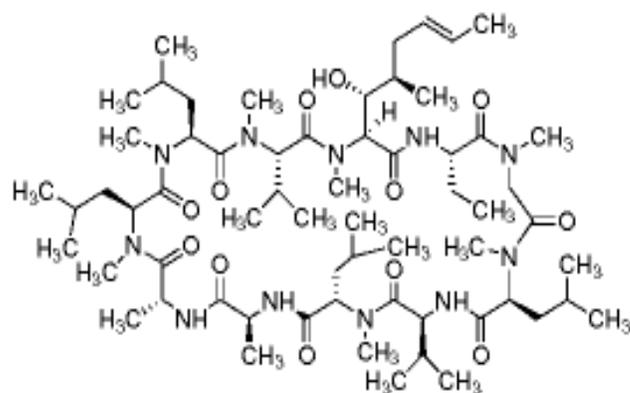
Fig. 17: Structural formula of cyclosporin A (Taken from www.sigmaaldrich.com).

(A)

(B)
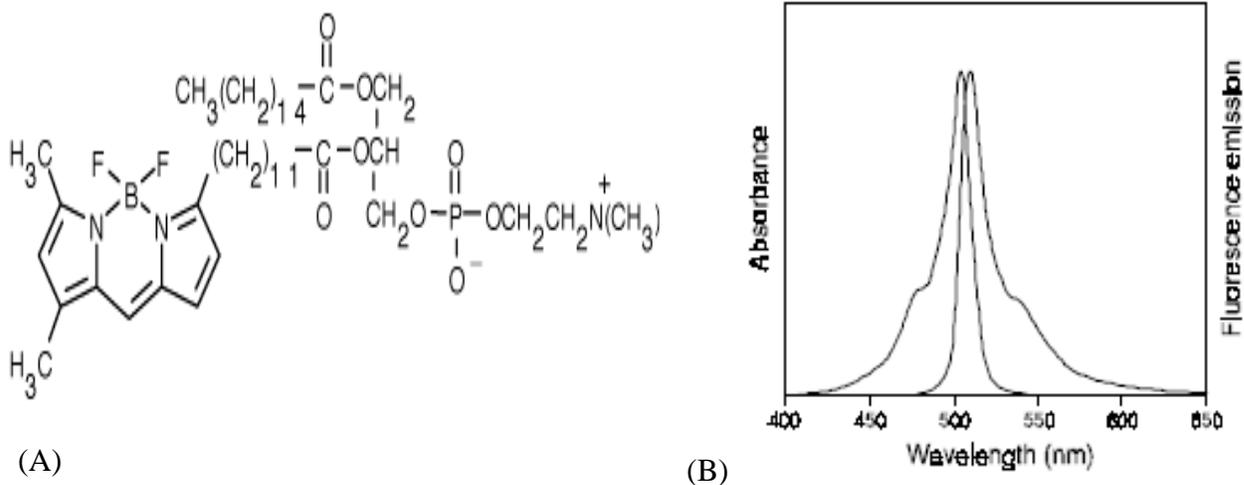
Fig. 18: A) Structural formula and B) Absorption (λ_{max} = 503 nm) emission (λ_{max} = 510 nm) spectra of β-Bodipy-FL-C12-HPC (Taken from www.invitrogen.com).
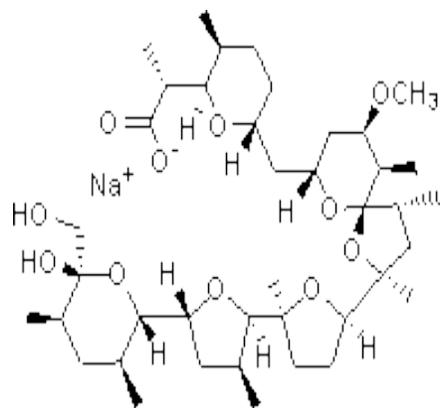
Fig. 19: Structural formula of nigericin (Taken from www.sigmaaldrich.com).
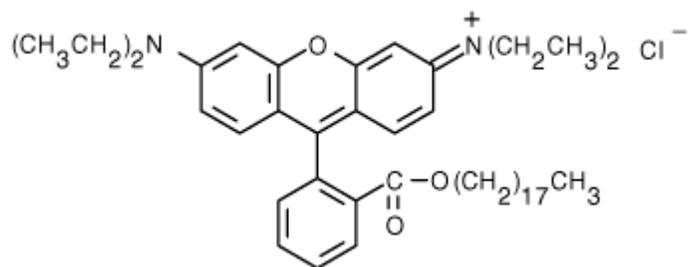
Fig. 20: Structural formula of octadecyl rhodamine B chloride (R18) (Taken from www.invitrogen.com).

3.3 Sample preparation for FCS measurements

Heparin stabilized blood samples of healthy volunteers were obtained from the University clinic, Homburg and the Sports Centre, Saarbruecken, Germany. The human RBCs were obtained after washing the blood sample by centrifuging three times at 2000 g for 5 min in physiological (high) ionic strength (HIS) solution. After every wash the supernatant containing plasma and buffy coat were aspirated carefully. For labeling the Na^+/H^+ exchanger, washed RBCs (1% haematocrit) were incubated with Bodipy-FL amiloride (400 nM) for 30-40 min at 37°C in the dark. After incubation, the RBCs were quick washed in HIS solution to remove the unlabeled fluorescent dye and were re-suspended (0.01 % haematocrit) in the same HIS solution. For experiments with low ionic strength (LIS) solutions (pH 7.4), contain 250 mM or 200 mM sucrose instead of NaCl to maintain a constant osmolarity and cell volume, respectively. We have also used a sodium tartrate (107 mM) solution to maintain a high ionic strength and positive transmembrane potential. Furthermore, two slightly changed physiological solutions (145 mM NaCl, HIS solution), one with reduced concentration of NaCl (120 mM) and the other with added 30 mM sucrose (HIS Sucrose solution) are used. In both the solutions, the surface potential of RBCs remains similar to HIS solution but the volume is affected.

The measurements with LIS solutions or sodium tartrate solutions the final washing procedure has been carried out in the corresponding solution. The incubation period in these solutions remained the same as stated above. RBCs (1% haematocrit) were incubated with octadecyl rhodamine B chloride (R18) (1 nM) for 30 min (Takahashi *et al.*, 2003). Nonpolar β-Bodipy-FL-C12-HPC (1 µM) was incubated with washed RBCs (1% heamatocrit) for 30 min at 37°C. After incubation, the unbound dye has been washed out carefully using HIS solution, and for the measurements in LIS solutions or sodium tartrate solutions the last washing procedure has been carried out in the corresponding solution.

3.4 Experimental setup and data analysis for FCS measurements

All the FCS experiments have been performed with a home built confocal setup based on an inverted microscope (Axiovert 2000, Zeiss). The laser light from the frequency-doubled diode laser (Picarro, Soliton), operating at $\lambda_{exc} = 488$ nm and a fiber

laser (Guided Color Technologies GmbH), operating at $\lambda_{exc} = 546$ nm were focused to the microscope body without using any further lenses. The incoming laser light was deflected by a dichroic mirror (495 DRLP, Chroma for Bodipy-FL amiloride labeled experiments and 555 DRLP, Omega for R18 labeled experiments) and was focussed on to a diffraction limited spot in the sample using a water immersion objective lens (63x NA 1.2 WI, Zeiss). The obtained fluorescence coming out of the sample was collected by the same objective, passed via the same dichroic mirror and was focussed by a tube lens to a pinhole (50 µm diameter). A band pass filter (HQ 525/50, AHF Analysentechnik, for Bodipy-FL amiloride and HQ 590/70, AHF Analysentechnik, for R18) was used to suppress the remaining scattered light. The fluorescence was split by a beam splitter and detected by two sensitive avalanche photodiode modules (SPCM-14-AQR, PerkinElmer Optoelectronics). The collected TTL-signals were collected and processed by a hardware correlator (FLEX 02 D, www.correlator.com) yielding the autocorrelation function $g^2(\tau)$ with nanosecond time resolution. The FCS set up is calibrated by a test fluorescein and rhodamine B solution. The obtained correlation curves were recorded with applied excitation intensity I in the range of 2.6-3.9 kWcm^{-2}. The measured fluorescence autocorrelation functions $g^2(\tau)$ were fitted with two-component model by using commercial software (Origin Pro 7.5, Origin Lab, MA, USA):

$$g^2(\tau) = 1 + \frac{f}{N}\left(\frac{1}{1+\dfrac{\tau}{\tau_{d1}}}\right) + \frac{(1-f)}{N}\left(\frac{1}{1+\dfrac{\tau}{\tau_{d2}}}\right) \qquad (6)$$

where, N represents the number of fluorescence molecules within the detection volume, τ_{d1} is the diffusion time of the fraction f, and τ_{d2} is the diffusion time of the remaining fraction of labelled molecules. The diffusion time τ_d is the average time taken by a molecule to diffuse through the radial part of the observation volume of the fluorescence microscope. However, the diffusion time depends on the size of the observation volume, wavelength of laser excitation and the optical properties of the instrument. The diffusion

coefficient D is a property of a diffusing molecule in a given solvent and better suited to characterize experimental data than the diffusion time. The diffusion coefficient D can be calculated from the corresponding diffusion time according to:

$$\tau_d = \frac{\omega_0^{\,2}}{4D} \qquad\qquad (7)$$

where, ω_0 denotes the beam waist of the detection volume, which is formed from the Gaussian beam profile convolved with the pinhole profile.

Images were obtained by TimeHarp 200 PC-board (PicoQuant GmbH, Germany) and the images were viewed by PicoQuant SCX View software (PicoQuant GmbH, Germany). The power of the laser beam entering the microscope was set to 10-15 µW for the FCS experiments. For better adhesion of RBC, the glass coverslips have been pre-treated with poly-L-lysine (0.001%). The laser beam was either focused on the cell membrane after scanning with the piezo scanner and moving the coverslip by using TimeHarp 200 software or by positioning it manually. A schematic diagram representing the laser path is shown in Fig. 21. Dual-autocorrelation curves were taken immediately after positioning the laser beam on the membrane using a hardware correlator (FLEX 02 D).
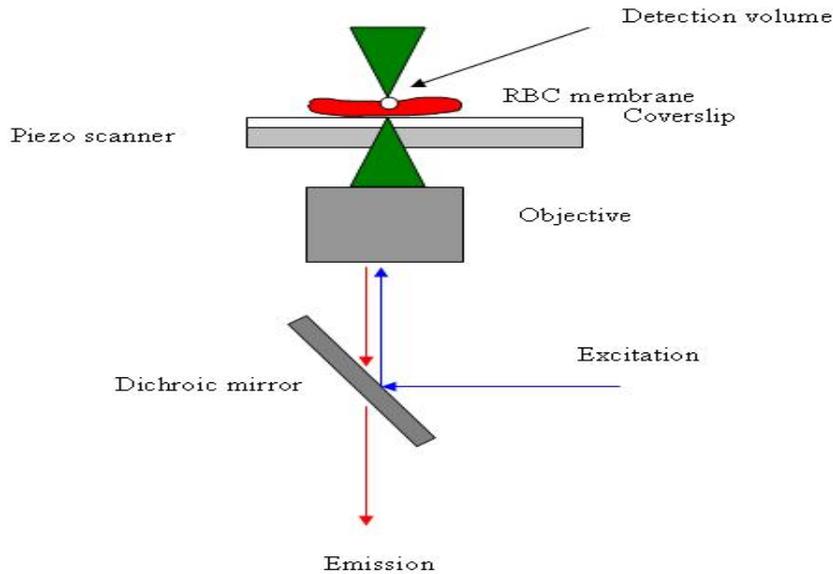
Fig. 21: Schematic illustration of focussing the laser path on the cell membrane.

3.5 Microscope setup

All the investigations at the single cellular level are performed using inverted single cell fluorescence microscope (Eclipse TI 2000 E, Nikon). The microscope is with all necessary components like a continuous light source (Xenon-Lamp, UX L-75XE, USHIO), filters or monochromator, photo detector and software programme to perform fluorescence recordings and films (Fig. 22). The monochromator provides a wide spectrum of wavelengths between 300-600 nm. It also allows switching between any desired wavelengths within few milliseconds. Additionally, the microscope allows performing ratiometric measurements.
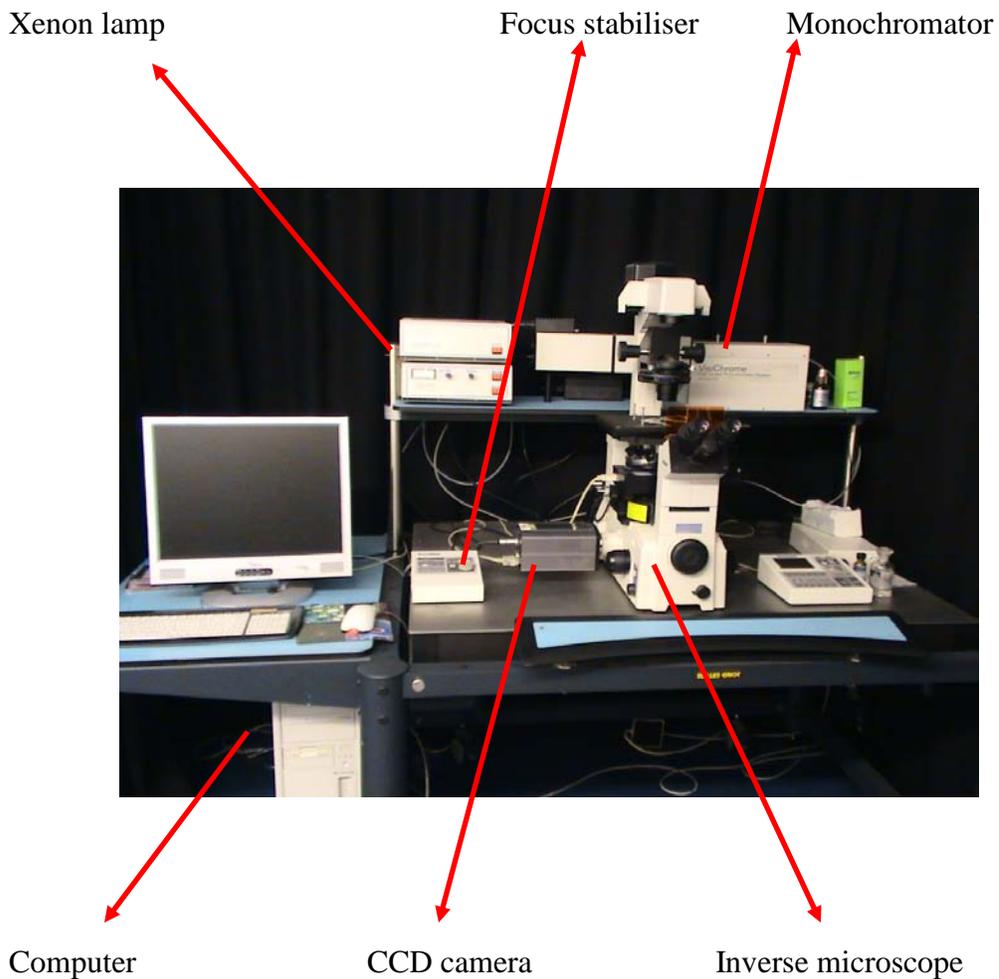
Fig. 22: Fluorescence microscope with components used for single cell imaging.

The microscope is equipped with an advanced and sensitive photo-detector (Visitron System, Puchheim, Germany). The photodetector detects the fluorescent light and converts it into a digital signal. The CCD (charged coupled devices) is a very sensitive chip integrated with cameras and allows in attaining both spatial and temporal resolution. At the bottom of microscope filters for different wavelengths are mounted which are available between the positions back and forth. The microscope is additionally equipped with a focus stabiliser which allows us to perform experiments for longer time periods. The computer is an integral part of the workstation which controls and allows processing of the acquired images with the Meta view software.

3.6 Dye loading of human RBCs

The investigations for determining the intracellular pH and qualitative determination of Ca^{2+} content are carried out using the pH-sensitive fluorescent dye BCECF-AM and Fluo-4 AM, respectively. The cells were obtained after washing the blood 3 times in HIS solution at 2000 g. The procedures for dye loading of RBCs are described below.

3.6.1 Intracellular pH measurements

The intracellular pH was determined by using BCECF-AM (Tsien, 1989). Washed RBCs at a haematocrit of 1% were suspended in a total volume of 0.5 ml of HIS solution. The RBCs were then incubated with the fluorescent indicator BCECF-AM (5 μM) for 45 min at 37°C in the dark. After the incubation with the dye, RBCs were washed with HIS solution three times to remove the unbound fluorescent dye, and were re-suspended (0.015% haematocrit) in the same solution. A calibration curve of the fluorescence intensity is plotted depending on obtained pH, using the K^+/H^+ ionophore nigericin (Kummerow *et al*., 2000). Cells were loaded with 5 μM nigericin and suspended in the calibration buffer solutions containing (mM): KCl 135, NaCl 10, glucose 10 and HEPES/NaOH 10. The obtained calibration curve was linear in the pH range 6.8-7.8.

After mounting the cells over the glass surface coated with 0.001% poly-L-lysine (PLL). Images were taken at every 20 s (exposure time 500 ms) over a period of 30 min for each experiment. All the experiments were performed at ambient temperature and in a

dark room. Investigations for RBCs were done using a 100×1.4 (NA) oil immersion lens. Approximately 10 to 15 cells were observed in the field of view for each experiment.

3.6.2 Intracellular Ca^{2+} content measurements

RBCs (1% haematocrit) after washing in HIS solution were incubated with the Ca^{2+}-sensitive fluorescent dye Fluo-4 AM at a concentration of 4 μM for 45 min at 37°C (Kaestner *et al.*, 2006). The non-ionic detergent was used to assist in dispersion of the non-polar AM ester in aqueous media. Cells were then quick-washed in HIS solution (with HEPES/NaOH buffer) to remove the unbound fluorescent dye and were re-suspended (0.015% haematocrit) in the same solution. The kinetics of trapped dye molecules were monitored by exciting with xenon lamp at a wavelength of 488 nm and the emission was collected at 520 nm. Aliquots of Fluo-4 AM were prepared with pluronic F-127 (20% DMSO in H_2O) to give a final concentration of 1 M (stock solution).

Single cell measurements were carried out similar to the intracellular pH measurements with similar experimental conditions explained before.

3.7 Caco-2 cells

Caco-2 cells were kindly provided by Prof. Dr. Lehr (Institute for Biopharmacy and Pharmaceutical Technology, University of Saarland). The cells were cultured at 37°C in a humidified atmosphere of 5% CO_2 and were propagated in minimal essential medium (MEM) with 2 mM L-glutamine and Earle's balanced salt solution adjusted to contain 1.5 g/L sodium bicarbonate, 0.1 mM non-essential amino acids, and 20% of fetal bovine serum (FBS), 80% of 1.0 mM sodium pyruvate. The medium was changed regularly 1-2 times per week.

3.8 Dye loading for Caco-2 cells

For Caco-2 cells, intracellular Ca^{2+} measurements have been done both qualitatively and quantitatively using Fluo-4 and Fura-2 dyes, respectively. For intracellular pH measurements, fluorescent BCECF dye was used. All the above mentioned dyes are with acetoxymethyl ester which assists in traversing the cell

membrane. The RPMI medium containing Caco-2 cells was removed by centrifugation and cells were washed three times with HIS solution before loading of the dye.

3.8.1 Intracellular pH measurements

Caco-2 cells are incubated with 5 µM of BCECF dye for 30 min at 37°C in HIS solution and the intracellular pH was determined. Images were collected at 439 and 505 nm excitation, and emission at 530 nm was collected using appropriate filter settings. A calibration curve was plotted using the ionophore nigericin by incubating BCECF-labeled cells in a high K^+/H^+ buffer at a specific pH (6.6, 7.0, 7.4, or 7.8). After mounting the cells over the glass surface, images were taken at every 20 s (exposure time 500 ms) over a time period of 30 min for each experiment. All the experiments were performed at room temperature and in a dark room. Investigations were done using a 63×1.4 (NA) oil immersion objective and approximately 10 to 15 cells were observed in the field of view for each experiment.

3.8.2 Intracellular Ca^{2+} measurements

The change of intracellular Ca^{2+} concentration was examined by using a suitable dye like Fluo-4 AM. Caco-2 cells were incubated with 4 µM of Fluo-4 dye at 37°C for 30 min. After the incubation cells were then quick-washed in HIS solution (with HEPES/NaOH buffer) to remove the unbound fluorescent dye and were re-suspended in the same buffer. The kinetics of trapped dye molecules excited at 488 nm and emission at 505-530 nm was collected. Single cell measurements were carried out at similar experimental settings explained for intracellular pH measurements.

The intracellular Ca^{2+} concentration of Caco-2 cells was evaluated quantitatively by using the cell permeant, ratiometric fluorescent dye Fura-2 AM (Grynkiewicz *et al.*, 1983). The washed cells were incubated at 37°C for 30 min with 10 mM of Fura-2 AM with pluronic (0.02%) in HIS solution. The dye incorporates intracellularly as its acetoxy-methyl ester (Fura-2/AM). The unbound dye is washed out 3 times carefully and the cells are re-suspended again in HIS solution. The kinetics of fluorescence changes were measured at UV-excitation wavelengths of 340 and 380 nm with emission at 510 nm. For chelating the external calcium 10 mM EGTA is added to the buffer. Single cell measurements were carried out at similar experimental settings explained for intracellular

pH measurements. The fluorescence kinetics of the ratio images obtained provide the information of Ca^{2+} content of single Caco-2 cells.

3.9 Nano-structured surfaces

Nano-structured surfaces with different patterns and modifications are described in more detail below. The surfaces were used to investigate their influence on intracellular pH and Ca^{2+} content of RBCs and Caco-2 cells. The following structures were investigated:

- Micro/Nano-structured surfaces (GPTS04 and ETC01, ECT03)
- Nano-structured PMMA surfaces
- Glass surfaces coated with organic polymers
- Chemically modified surfaces

Micro/Nano-structured surfaces

Glycidoxypropyltrimethoxysilane, the precursor, used for the preparation of sol-gel derived nanoscaled hybrid polymer GPTS04. A schematic structural view of the GPTS04 surface is shown in Fig. 23. The GPTS04 surfaces were obtained from the Institute for New Materials (INM), Saarbruecken.
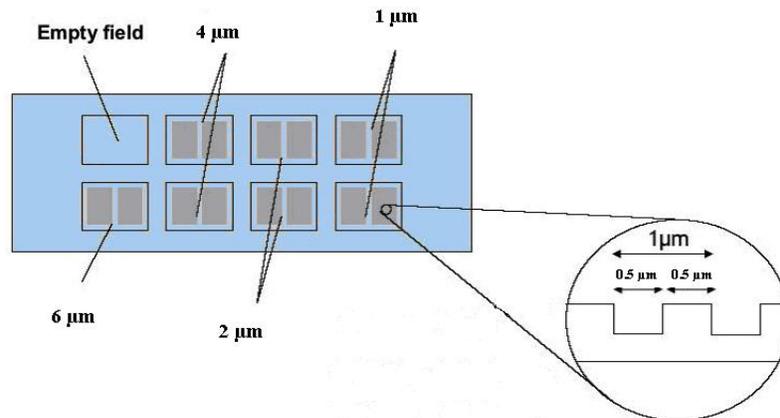
Fig. 23: The structural view of GPTS04 polymer surface.

The Easy To Clean (ETC) structures obtained from INM are very hydrophobic and lipophilic in nature. The ETC01 and 03 surfaces are coated with per-fluorinated organic

moieties which give them anti-adhesive property. ETC01 surface is treated thermally and ETC03 surface is treated by using UV radiation. Special characteristics of these ETC surfaces include:

- High microbiocidal effectiveness, even at low silver concentrations
- Long-lasting effect by slow and sustained release (controlled release)
- Easy to clean by anti-adhesive properties

Nano-stuctured surfaces

The nano-stuctured surfaces obtained from the University of Kaiserslautern are coated with glass pattern with a height of 100 nm and fields 0.9 nm x 0.9 nm. The image showing the nano-structured surface is shown in Fig. 24.
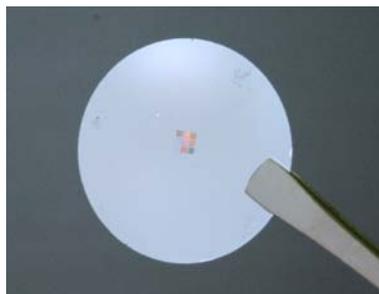
Fig. 24: Image of nano-structured surface.

Poly methyl methacrylate (PMMA) surfaces

The PMMA surfaces are 125 mm thick sheets of polymer (78 x 28 mm), which were rinsed with propan-2-ol and sterilized using γ radiation (25 kGy dose). The surface of the PMMA is slightly hydrophilic with a contact angle of 74.7° and transparent with surface roughness of 13 nm. There are two methyl groups which are held as methyl methacrylate in PMMA (Fig. 25). The methyl groups keep the material supple and non-brittle and allow the polymer chains to slide over one another on the surface. However, the acrylate pieces (vinegar-like structures) are still abundant and increase the surface reactivity, which significantly binds down proteins on the surface. The design of the polymer surface structure and their micro imprints and the patterns of the polymer surface are shown in Fig. 26. The PMMA surfaces were obtained from the Science Park, Barcelona.
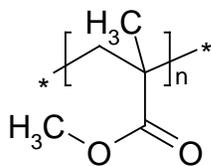
Fig. 25: The structural formula of PMMA precursor.

A:

B:

C:
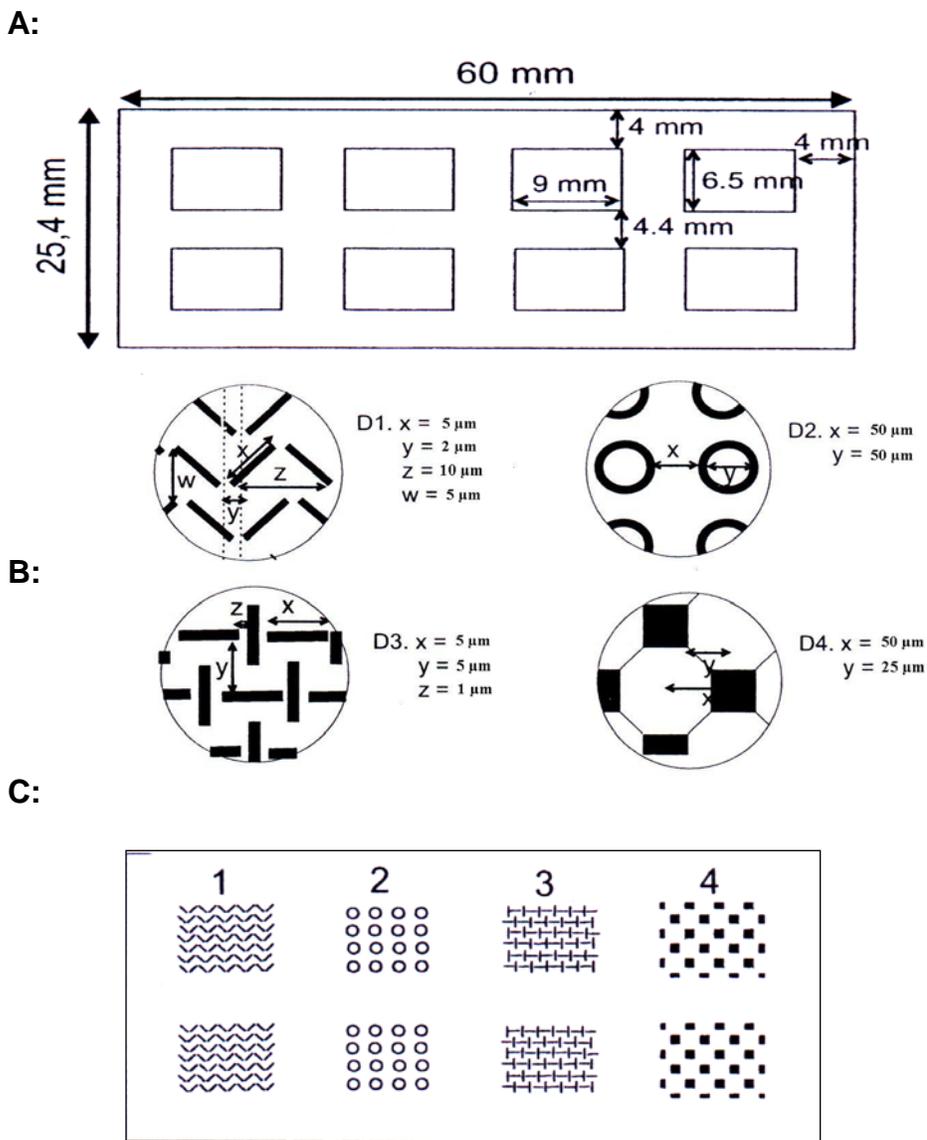
Fig. 26: Design of the polymer surface structure and their micro imprints. A: The dimensions of the polymer surface, B: Structure of the micro-imprint, C: Surface with eight different patterns.

Polymer coated glass surfaces

The polymer coated glass surfaces were obtained from the Department of Organic Chemistry, University of Sofia, Bulgaria. The structural formula of organic polymers is shown in Fig. 27, and a short description of the polymer composition is explained below:

- NVP/DMAEMPS= 6: Poly (N-vinil-2-pyrrolidone-co-N, N'-dimethhyl methacryloyloxy- ethylpropane sulfonate).

- AAm/DMAEMPS= 10/1: Poly (acrylamide-co-N, N'-dimethylmethacryloyl-oxyethylpropane sulfonate).

- AMPS/DMAEMPS= 7/3: Poly (2-acrylamido-2-methylpropanesulfonic acid-co-N, N'-dimethylmethacryloyl-oxyethylpropane sulfonate).
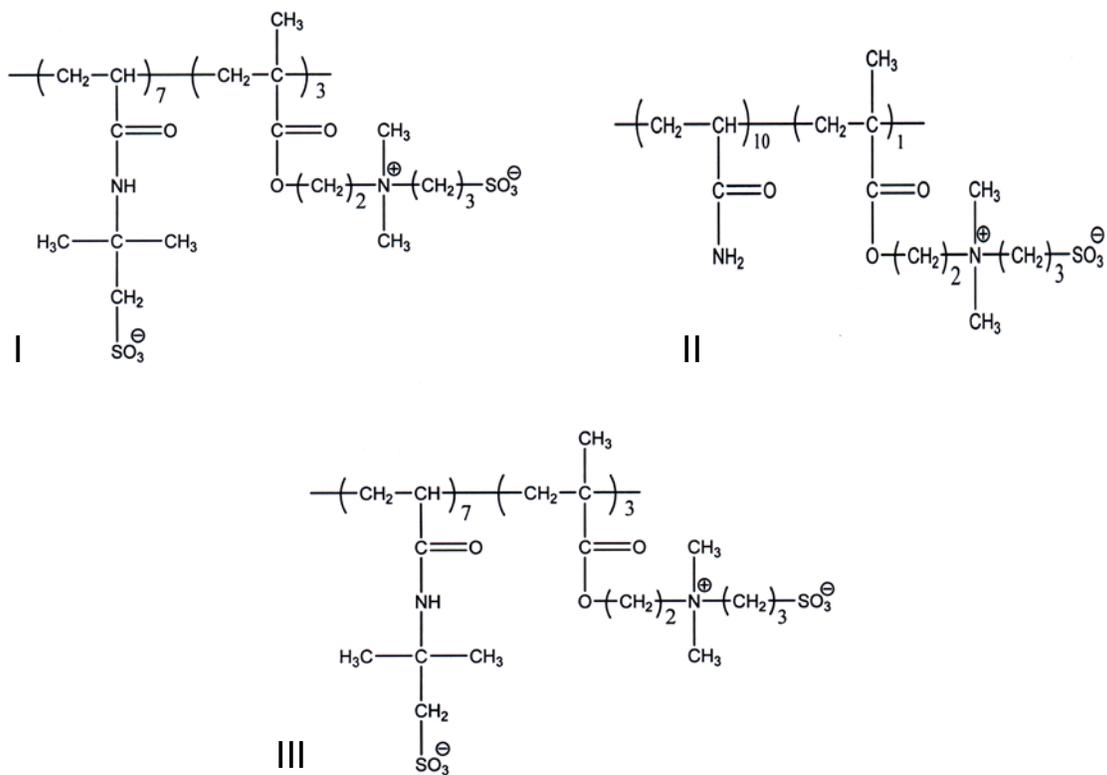
Fig. 27: Structural formula of the organic polymers I: NVP/DMAEMPS = 6, II: AAm/ DMAEMPS = 10/1, III: AMPS / DMAEMPS = 7/3.

Chemically modified surfaces

The glass surfaces coated with both positively charged (ethylene diamine) and negatively charged (taurine) coated surfaces have been investigated. These surfaces are prepared in the following steps:

1. The ordinary glass surfaces are placed for 10 min in dichloromethane, in an ultrasonic bath and later dried with N_2.

2. The surfaces were exposed at 80°C to hot ammonia (25%), hydrogen peroxide (35%)-water (1:1:4 v/v/v) for 20 min. After the exposure surfaces were rinsed with deionised water and dried again with N_2.

3. The surfaces were later transferred to ethanol-3-aminopropyl-triethoxysilan containing solution and kept for 10 min at 70°C. The surfaces were rinsed with ethanol and later dried again with N_2.

4. The surfaces were left overnight in a cellulose containing solution [o-(2-chloro-4-oxido-1, 3, 5-triazine-6-yl)-carboxymethylcellulose sodium salt] 21.0 mg/20 ml carbonate buffer with pH 8.48. Finally, the surfaces were rinsed with carbonate buffer and dried with N_2. The procedure remains the same for both the coatings up to here.

5. Preparation of taurine coated surface: Glass slides were suspended for 1 h in a 0.1 M-taurine solution (125.1 mg/10 ml carbonate buffer, pH 8.48).

6. Preparation of ethylene diamine surface: Glass slides were suspended for 1 h in a 0.1 M ethylene diamine solution (60.5 mg/10 ml carbonate buffer, pH 8.48).

7. The coated surfaces were later rinsed again with carbonate buffer and dried with N_2.

3.10 Nano-particles

Different nano-particles used for studying the membrane crossing ability of RBCs and Caco-2 cells include:

1. Fluorescent-labeled PLGA (f-PLGA+WGA) nano-particles
2. Nano-particles containing magnetic iron oxide

The other f-PLGA nano-particles coupled with WGA are 520 nm in diameter. For better adhesion of f-PLGA to the cell, lectin like WGA has been conjugated. The polymeric structural formula of PGA, PLA and PLGA particles is shown in Fig. 28. The cells are washed in HIS solution and incubated in the same solution for 30 min. These

nano-particles are observed at 488 nm. The f-PLGA nano-particles are kindly provided by Prof. Franz Gabor (Institute of Pharmaceutical Technology and Biopharmaceutics, University of Vienna, Austria).
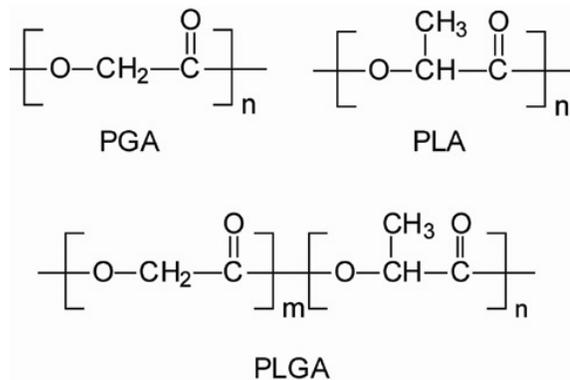
Fig. 28: Structural formula of PGA [poly (glucolic acid)], PLA [poly (lactic acid)] and PLGA [poly (lactic-co-glycolic acid)].

The magnetic iron oxide nano-particles obtained from the Institute of Physics and Chemistry of Materials, Strassbourg are of 12 nm in diameter. These nano-particles contain magnetic iron oxide core to which an organic layer (dye) is grafted with a phosphate entity. The cells were washed 3-4 times with HIS solution and incubated with nano-particles for 30 min at 4°C in the same solution. All the single cell experiments with the nano-particles containing magnetic iron oxide were carried out at 360 nm using fluorescence microscope suitable for single cell imaging.

Chapter 4: Effect of transmembrane potential on the diffusion of Na$^+$/H$^+$ exchanger of human red blood cell

4.1 Results

All the FCS curves were fitted by using the two component model (Eq. 5) and by applying the Eq. 6, and thus the diffusion constant D was calculated. The beam waist ω_o (at λ_{exc}= 488 nm) of the laser throughout the experiment was calculated to be ~450 nm which indicates a minute area of ~0.6 μm^2 within the RBC membrane in which the diffusion has been studied. The resolution in the *z*-direction for the measurements was about 7 μm. Long term exposure of laser on the cell membrane has been avoided as it causes photo damage to RBCs (Bloom *et al*., 1984; Wong *et al*., 2007). Confocal images of RBCs after labeling with Bodipy-FL amiloride, and the marked region where FCS has been performed are shown respectively, in Fig. 29 A and B. The amiloride is a reversible, selective, competitive inhibitor for the Na^+ site of the Na^+/H^+ exchanger.
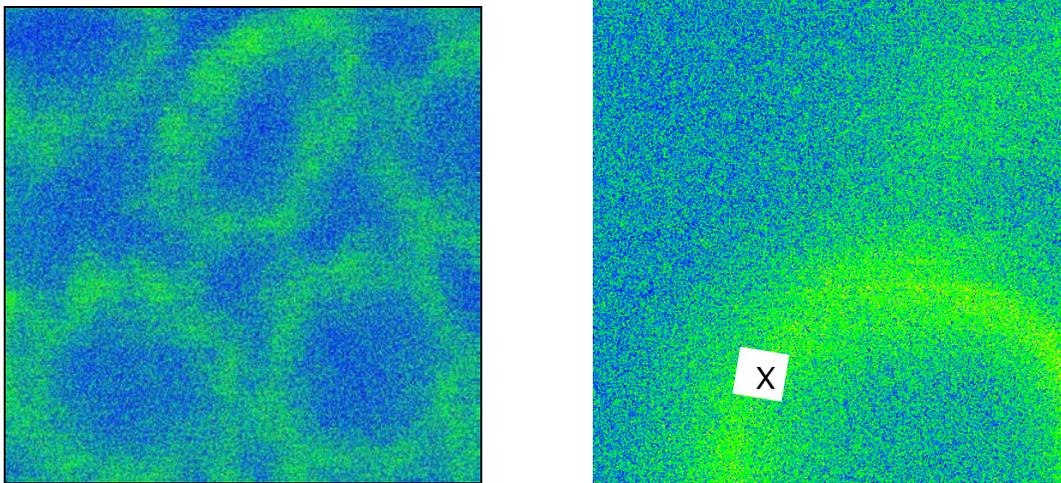
Fig. 29: A) Confocal images of RBCs labeled with Bodipy-FL amiloride, B) The marked region where FCS is performed in HIS solution.

4.1.1 Autocorrelation curve for the experiment

The obtained autocorrelation functions of the cell membrane measurements are well in agreement with previous reports for living cells (Politz *et al*., 1998; Schwille *et al*., 1999; Takahashi *et al*., 2003). Autocorrelation curves obtained in various solutions are shown in Fig. 30. More than one diffusion times were observed after the curves were normalized.
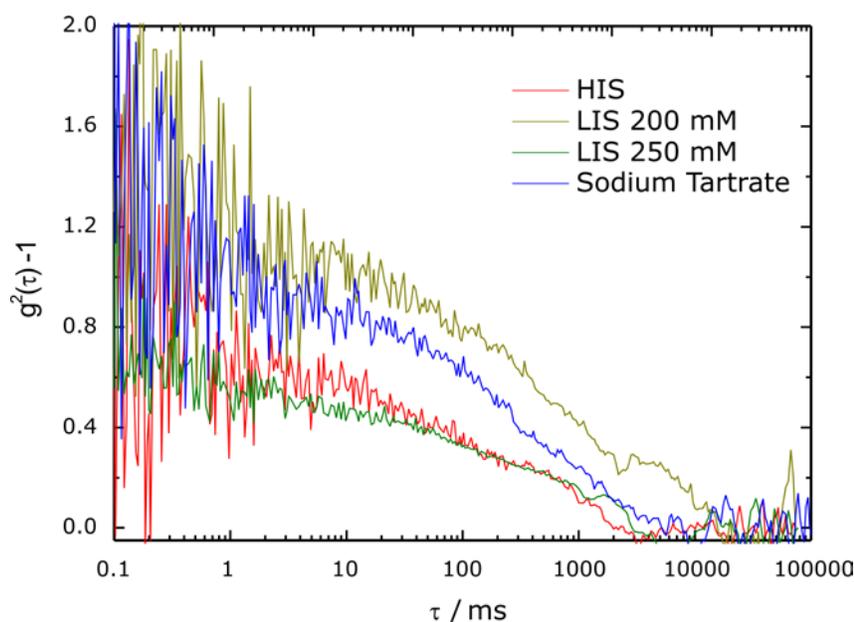
Fig. 30: Normalized fluorescence correlation curves of RBC membrane under different ionic strength solutions labeled with Bodipy-FL amiloride. Different solutions are shown with different colours.

4.1.2 Diffusion of the Na^+/H^+ exchanger labeled with Bodipy-FL amiloride

The obtained results were fitted using the two component model and apparently two diffusion constants for corresponding experimental solutions were obtained. The evaluation of correlation curves resulted in fast moving fluorescent species and in slow moving fluorescent species. In the beginning, we believed that the fast moving species (with higher diffusion constant) corresponds to the free dye and the slow moving species (with slower diffusion constant) corresponds to the labeled exchanger. This assumption is valid when approximately a similar diffusion time for the free dye throughout all the solutions is observed. However, it was not the case in our experiments. Moreover, the above assumption will not be applicable when there is ~100% labelling of the dye molecules. After the incubation of the dye, the cells were washed carefully to get rid of any unlabeled excess dye. So there is a little or no possibility of dye in the measuring system. Otherwise, it may hinder single molecule experiments with FCS. So, it is appropriate to assume that the fast moving species (particles with higher diffusion constant) reflect the non-hindered (free) diffusion of the Na^+/H^+ exchanger in the membrane and the slow moving species (particles with low diffusion constant) reflect the

hindered diffusion. The hindered diffusion can be attributed to the aggregation of two or more exchangers (i.e., bigger particles). Other possibilities might be due to the interaction between the protein-protein or protein with the underlying cytoskeleton. The different diffusion constants observed for the Na^+/H^+ exchanger are the result of interactions with the cytoskeleton network which is responding to the external changes (membrane potential or volume change). The fast and slow diffusion constants of Na^+/H^+ exchanger labeled with Bodipy-FL amiloride in different solutions are shown in Fig. 31 A and B respectively.

A

B
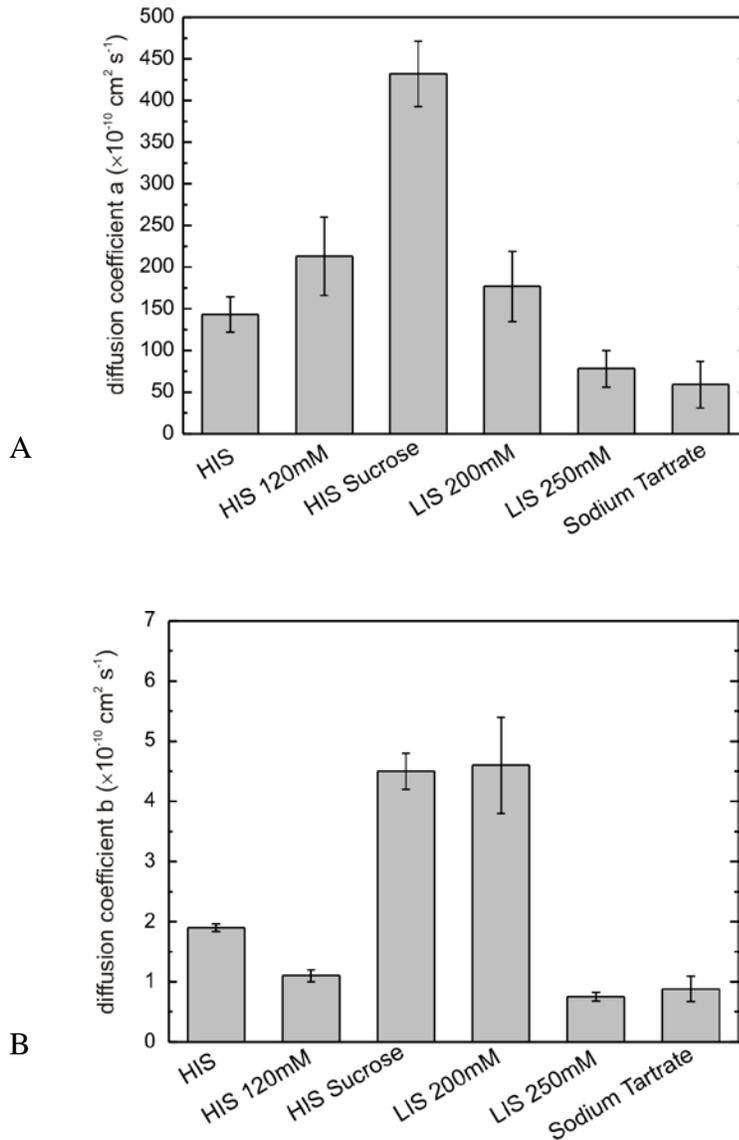
Fig. 31: The Diffusion constants (A: fast, B: slow) of Na^+/H^+ exchanger labeled with Bodipy-FL amiloride labeled in different solutions. Error bars represent the S.D. of 3-5 experiments, $p < 0.05$.

4.1.3 Influence of the transmembrane potential on the diffusion constant of Na^+/H^+ exchanger

FCS has been performed at the point of marked region shown in Fig. 27B of the cell membrane. The diffusion constant of the slower component with a fraction rate of 69%, obtained for the Na^+/H^+ exchanger in physiological solution is 1.9×10^{-10} cm^2/s .The value for faster component with a fraction rate of 31% is 143×10^{-10} cm^2/s. In low ionic strength solutions, LIS 250 mM, in which the transmembrane potential rises to a positive value of the slower component with a fraction rate of 71% and faster component with a fraction rate of 29% is 0.75×10^{-10} cm^2/s and 78×10^{-10} cm^2/s, respectively. The obtained values for slower component with a fraction rate of 65% and faster components with a fraction rate of 35% in LIS 200 mM are 4.6×10^{-10} cm^2/s and 177×10^{-10} cm^2/s, respectively. Furthermore, for sodium tartrate solution the values obtained for slower and faster components are 0.88×10^{-10} cm^2/s and 59×10^{-10} cm^2/s, respectively, and the slower component fraction rate is 52% while the fast moving fraction rate is 48%.

Thus, it can be concluded that the transmembrane potential has no significant effect on the lateral movement of the exchanger. The diffusion constant for Na^+/H^+ exchanger in sodium tartrate solution calculated to be 59×10^{-10} cm^2/s which is the slowest but the value is close to the LIS solutions. These results can be attributed to the similar transmembrane potential and alkalinization of the cells which occurs in both LIS and tartrate solutions. It is appropriate to consider the effect of volume change in LIS 200 solution along with the different HIS solutions.

The small difference between the diffusion constants of HIS and LIS 250 infer that the volume change has some effect on the lateral diffusion of the exchanger. The obtained values of slow or hindered component is found to be almost the same value in HIS (1.95×10^{-10} cm^2/s), HIS solution containing 120 mM NaCl (1.06×10^{-10} cm^2/s), LIS 250 mM (0.74×10^{-10} cm^2/s) and sodium tartrate (0.87×10^{-10} cm^2/s) (Fig. 29 B). However, the diffusion constant in LIS 200 mM solution (4.65×10^{-10} cm^2/s) is relatively higher than the diffusion constant in HIS and similar to HIS with 30 mM sucrose. In case of hindered diffusion of Na^+/H^+ exchanger the diffusion constant remains more or less similar. The precise mechanism behind such disparity of results for faster and slower components is

difficult to conclude. The influence of volume changes on the diffusion constant of Na$^+$/H$^+$ exchanger are discussed in the following section.

4.1.4 Influence of the volume change on the diffusion constant of Na$^+$/H$^+$ exchanger

In order to confirm the possible role of volume change on the diffusion constant of the exchanger, further investigations have been done. The HIS solution with 30 mM sucrose has been used to decrease the cell volume. Additionally, the 120 mM HIS solution has been prepared by reducing the NaCl concentration from 145 to 120 mM. These solutions maintain similar surface potential to the physiological solution. For HIS 120 solution, the obtained value for slower component with a fraction rate of 62% and faster components with a fraction rate of 38% are 1.1×10^{-10} cm^2/s and 213×10^{-10} cm^2/s respectively. A higher value of diffusion constant with a fraction rate of 62% has 5.1×10^{-10} cm^2/s and the slower component with a diffusion constant of 388×10^{-10} cm^2/s was observed for HIS with 30 mM sucrose solution.

Increase in the rate of protein diffusion comparable to that of a membrane lipid can be interpreted as an evidence for the destruction or uncoupling of the protein from the cytoskeleton. This assumption is more realistic in the case of Na$^+$/H$^+$ exchanger in HIS 120 mM+30 mM solution as a decrease in volume is observed. The decrease in volume in physiological conditions (HIS 120 mM) causes a constriction in the bilayer along with cytoskeleton thereby detaching the protein contact from the cytoskeleton. It is not clear at the moment that a small change in the ionic strength along with volume change result in the uncoupling of Na$^+$/H$^+$ exchanger from the cytoskeleton. The resulting diffusion constants D, diffusion time τ and fraction rate F of Bodipy-FL amiloride labeled Na$^+$/H$^+$ exchanger in different solutions are shown in Table 2.

Table 2: The Diffusion constant D, diffusion time τ and fraction rate F of Bodipy-FL amiloride Na^+/H^+ exchanger in different solutions.

Solutions	τ_{d1} (ms)	Da (10^{-10})	F1 (%)	τ_{d2} (ms)	Db (10^{-10})	F2 (%)
HIS	34	143	32	2446	1.9	69
HIS 120 mM	23	213	38	4540	1.1	62
HIS + 30 mM sucrose	11	432	23	1049	4.5	77
LIS 250 mM	65	78	42	6458	0.75	58
LIS 200 mM	28	177	73	1044	4.6	30
Na Tartrate	97	59	46	5692	0.88	54

4.1.5 Influence of the transmembrane potential on the diffusion of β-Bodipy-FL-C12-HPC

Our study was also extended to understand the effect of membrane potential on the lateral movement of membrane labeled lipids. The suitable dye for such experiments was the Bodipy conjugated lipid permeant β-Bodipy-FL-C12-HPC (β-BPC). The dye was successfully applied for studying the protein lipid interactions and measuring the kinetics of DNA release from lipoplexes (Keller *et al.*, 1995; Koynova *et al.*, 2007). Generally, lipids show the same order of diffusion constants compared to proteins at fluid crystalline state.

In HIS solution, the obtained value of diffusion constant for slower component with a fraction rate of 54%, obtained for the β-BPC is 15.2×10^{-10} cm^2/s. The value for faster component with a fraction rate of 46% is 280×10^{-10} cm^2/s. In low ionic strength (LIS) solutions, LIS 250 mM, the values of slower diffusion constant with a fraction rate of 71% and the faster component with a fraction rate of 29% are 12.5×10^{-10} cm^2/s and 257×10^{-10} cm^2/s, respectively. The obtained value for slower component with a fraction rate of 68.6% and faster components with a fraction rate of 31.3% in LIS 200 mM are 60×10^{-10} cm^2/s and 220×10^{-10} cm^2/s respectively. Further more, for sodium tartrate solution, the values obtained for slower and faster components are 36×10^{-10} cm^2/s and 287×10^{-10} cm^2/s, respectively. The slower component fraction rate is 42% and the fast moving fraction rate is 58%. The obtained diffusion constant of fast component (Fig. 30)

in all the experimental solutions with varying membrane potential were found to be almost similar ($\sim$250$\times$10^{-10} cm^2/s) and this is much higher than the expected value. The obtained values for slow diffusion constant are in good agreement with the previously published data where the characterisation of giant unilamellar vesicles was studied using fluorescence correlation spectroscopy (Korlach *et al.*, 1999). The faster and slower diffusion constants of β-BPC in RBC membrane in different solutions are shown in Fig. 32.
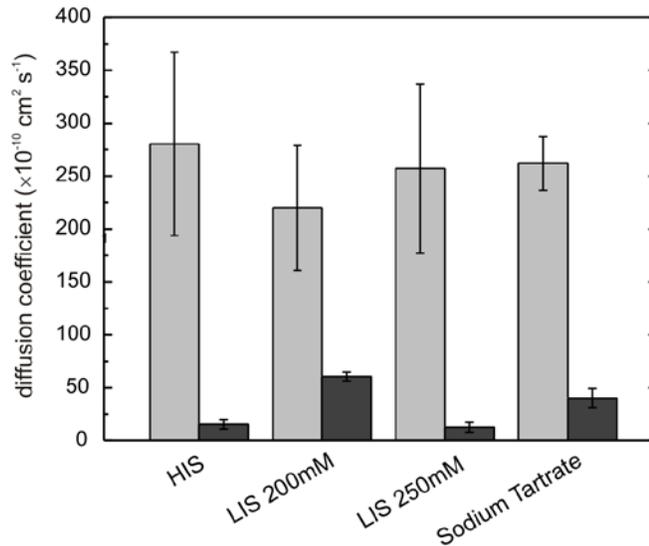
Fig. 32: Diffusion constants of β-Bodipy-FL-C12-HPC in the RBC membrane. Grey bars indicate the fast diffusion constants and black bars indicate the slow diffusion constants, respectively. Error bars represent the S.D. of 3-5 experiments, $p < 0.05$.

The diffusion constant values obtained for the slow moving component in HIS and LIS 250 mM are very similar: 15$\times$10^{-10} cm^2/s and 12$\times$10^{-10} cm^2/s. On the contrary, the obtained values of diffusion constants for LIS 200 and sodium tartrate solutions are 68$\times$10^{-10} cm^2/s and 40$\times$10^{-10} cm^2/s, respectively. Thus, with the obtained data it is unclear at the moment, which parameter is effecting the lipid diffusion and to what extent (transmembrane potential, surface potential, and/or cell volume). The resulting diffusion constants D, diffusion time τ and fraction rate F of labeled (ß-BPC) lipid in different solutions is shown in Table 3.

Table 3: The Diffusion constant D, diffusion time τ and fraction rate F of β-Bodipy-FL-C12-HPC labeled lipid in different solutions.

Solutions	τ_{d1} (ms)	Da (10^{-10})	F1 (%)	τ_{d2} (ms)	Db (10^{-10})	F2 (%)
HIS	18	280	46	334	15	54
LIS 250 mM	20	257	29	442	12	71
LIS 200 mM	23	220	31	442	60	68
Na Tartrate	18	262	54	124	40	45

4.2 Discussion

In the present work, we have studied the effect of transmembrane potential and volume changes on the diffusion of Na^+/H^+ exchanger of human RBCs using FCS. The fluorescence correlation curves are fitted using the two component model resulted in fast diffusing fluorescent species and slow diffusing fluorescent species. The fast moving species and slow moving species are assumed to be the non-hindered and hindered diffusions of Na^+/H^+ exchanger, respectively.

The diffusion constants for slow moving component of Na^+/H^+ exchanger in HIS (1.9×10^{-10} cm^2/s), LIS 250 mM (0.75×10^{-10} cm^2/s) and Na tartrate (0.88×10^{-10} cm^2/s) solutions are relatively similar. Thus, it can be concluded that the transmembrane potential has no effect on the lateral diffusion of Na^+/H^+ exchanger. However, the diffusion constant value in LIS (200 mM) solution is higher than in HIS solution and similar to HIS containing 30 mM sucrose solution. The obtained data for the fast moving component is more difficult to interpret and contrasting with the slow diffusing component. The diffusion constant values for HIS (143×10^{-10} cm^2/s) and LIS 200 mM (177×10^{-10} cm^2/s) solutions are more or less similar. In LIS 250 mM and Na tartrate solutions the diffusion constants are relatively similar. The value of slow diffusing constant in HIS 120 mM solution (1.1×10^{-10} cm^2/s) is similar to HIS solution though there is an increase in the RBC volume.

We attribute the differences in the diffusion of Na^+/H^+ exchanger in different solutions effecting the transmembrane potential and volume changes to the association

and interactions of Na^+/H^+ exchanger with the cytoskeleton of RBCs. It is still unclear at the moment, what factors influence the disparity between the slow and fast diffusing components.

Additionally, we have studied the effect of transmembrane potential on the diffusion of membrane permeant β-Bodipy-FL-C12-HPC labeled lipid. It has been observed that the transmembrane potential has no influence on the diffusion of fast moving component. The fast diffusing component has a constant value of ~250×10^{-10} cm^2/s in HIS, LIS (200, 250 mM) and Na tartrate solutions. Incase of slow moving component, the obtained data is insufficient to conclude the parameter which is effecting the lipid diffusion and to what extent (transmembrane potential, surface potential, and/or cell volume).

Chapter 5: Ca^{2+} loss of single Caco-2 cells under physiological conditions

5.1 Results and Discussion

The kinetics of Ca^{2+} transport of single Caco-2 cells is observed when no external Ca^{2+} source is available in the surrounding medium. We have observed a loss in the Ca^{2+} content of single Caco-2 cells and determined it qualitatively using the Ca^{2+} sensitive, fluorescent indicator Fluo-4 dye. Single Caco-2 cells showing this behaviour have been examined just after the cells are mounted on to the cover slips, and the mechanism behind this Ca^{2+} loss has been investigated using different inhibitors and drugs for Ca^{2+} channels and pumps. The observed kinetics of a single Caco-2 cell losing Ca^{2+} during a time period of 30 min is shown in Fig. 33.
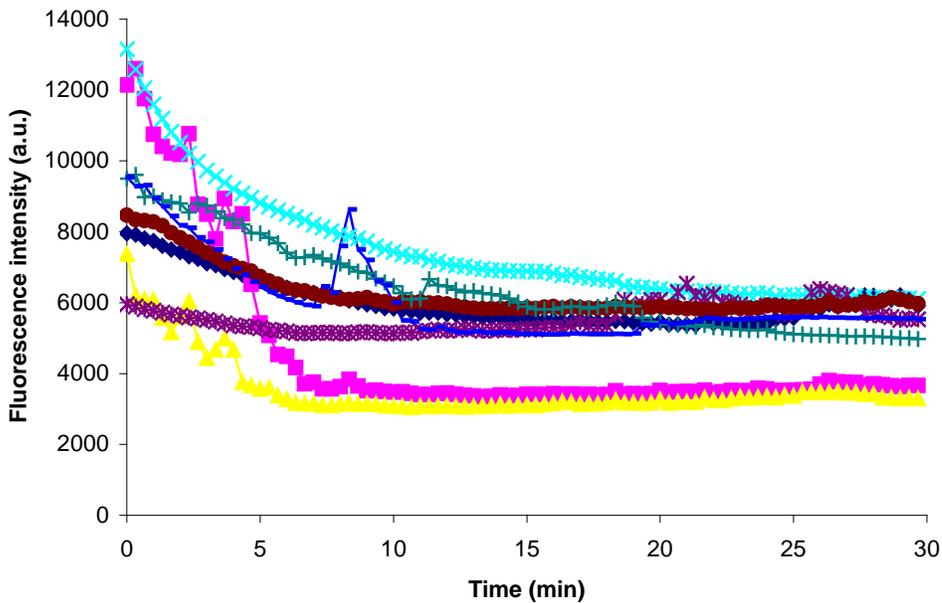
Fig. 33: Ca^{2+} transport of Caco-2 cells loaded with Fluo-4 and without any Ca^{2+} in the surrounding medium for a time period of 30 min. Each curve represents a single Caco-2 cell.

The Ca^{2+} loss of single Caco-2 cells has been studied in detail by adding different Ca^{2+} concentrations in the extracellular medium. It has been observed that the Caco-2 cells expel the Ca^{2+} in a dependent manner, i.e., the higher the external Ca^{2+} concentration the quicker the response by Caco-2 cells. Experiments are done with different external Ca^{2+} content (0, 2 and 10 mM) in the surrounding medium of Caco-2 cells (Fig. 34).
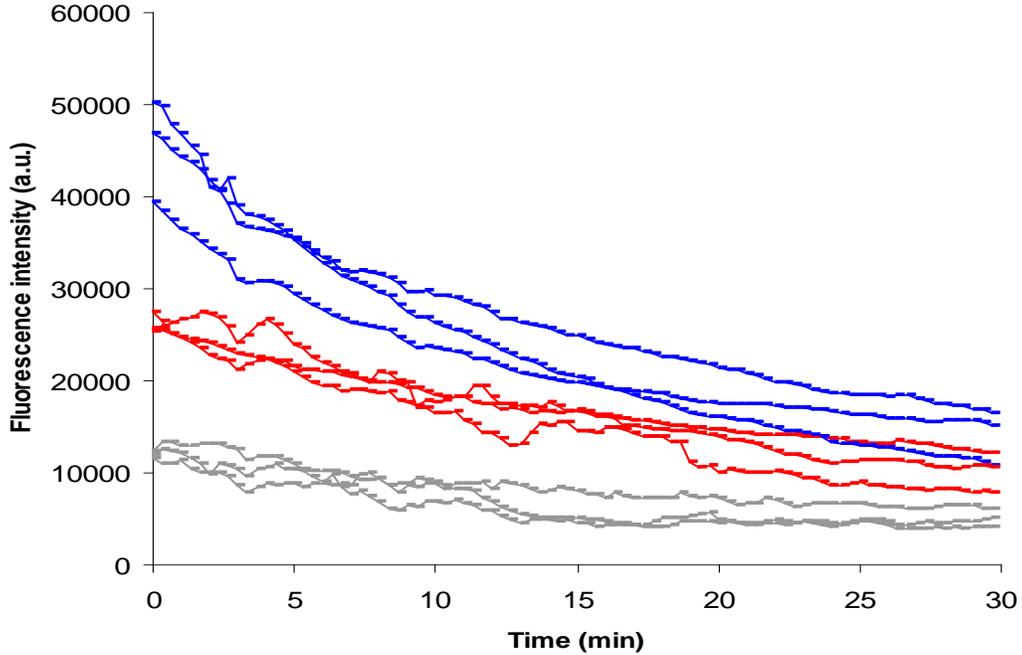
Fig. 34: Ca^{2+} transport in Caco-2 cells in physiological solution with different external Ca^{2+} concentrations. Three experiments are presented with different external Ca^{2+} concentrations for a time period of 30 min (▬ 10 mM Ca^{2+} , ▬ 2 mM Ca^{2+} and ▬ 0 mM Ca^{2+}). Each curve represents a single cell.

It is observed that the Ca^{2+} is entering the cell membrane and is pumped out by Caco-2 cells. The role of Ca^{2+} pumps is assumed, and suitable inhibitor like O-vanadate which inhibits most of the pump action has been used.

Caco-2 cells are preincubated with the fluorescent Fluo-4 dye and O-vanadate is added prior to the experiment. The above experiment is repeated in the presence of O-vanadate (80 µM) with external Ca^{2+} concentrations of 0, 2 and 10 mM (Fig. 35). It is found that the Ca^{2+} is still able to enter the cells and is expelled. So, it can be understood that Ca^{2+} loss is not dependent on Ca^{2+} pumps.
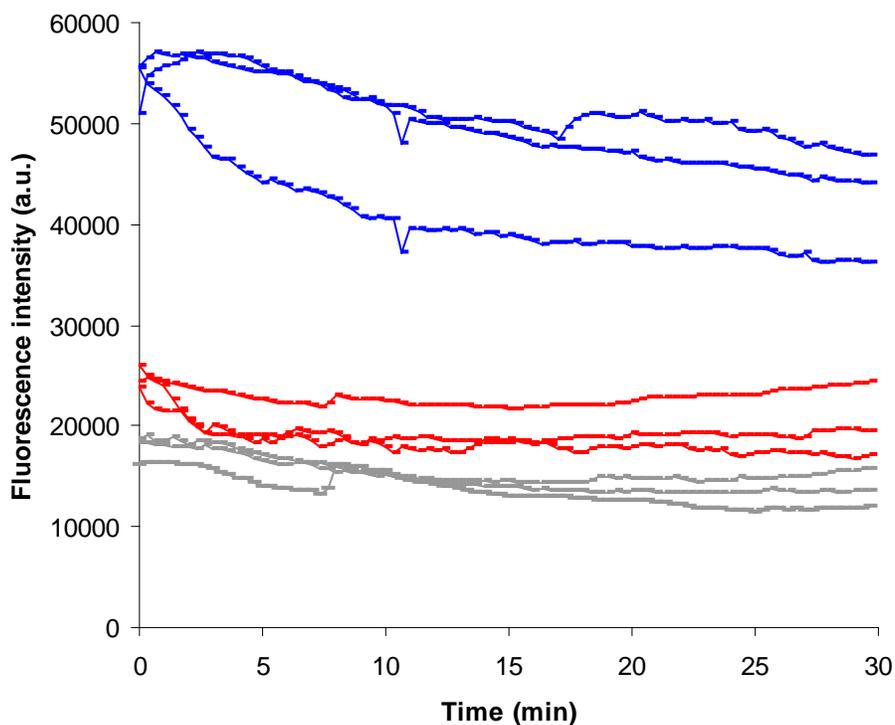
Fig. 35: Caco-2 cells in the presence of O-vanadate (80 µM) with different external Ca^{2+} concentrations. Three experiments are presented with different external Ca^{2+} concentrations for a time period of 30 min (▬ 10 mM Ca^{2+}, ▬ 2 mM Ca^{2+} and ▬ 0 mM Ca^{2+}). Each curve represents a single cell.

The role of ABC transporters cannot be neglected in this mechanism and suitable inhibitors like Cys A (10 µM) has been used. ABC transporters are involved in the expulsion of a wide variety of substances from the cell interior to extracellular space (Gatmaitan and Arias, 1993; Schinkel, 1997). The outcome of the experiment is not different even after the addition of Cys A as the Ca^{2+} loss was not inhibited in the presence of the inhibitor (Fig. 37).

It was necessary to estimate the Ca^{2+} content of a single Caco-2 cell to understand whether the mechanism was mediated simply by diffusion via Ca^{2+} channels or pumped out against concentration gradient in carcinoma cell line. The Ca^{2+} content determined by using fluorescent Fura-2 AM which is a ratiometric dye and excited in UV range. To chelate the external Ca^{2+}, EGTA (30 mM) has been added to the buffer. It was found that

the intracellular Ca^{2+} of single Caco-2 cells is in the micromolar range of 0.5-2.5 µM which is similar to the intestinal epithelium (Fig. 36).
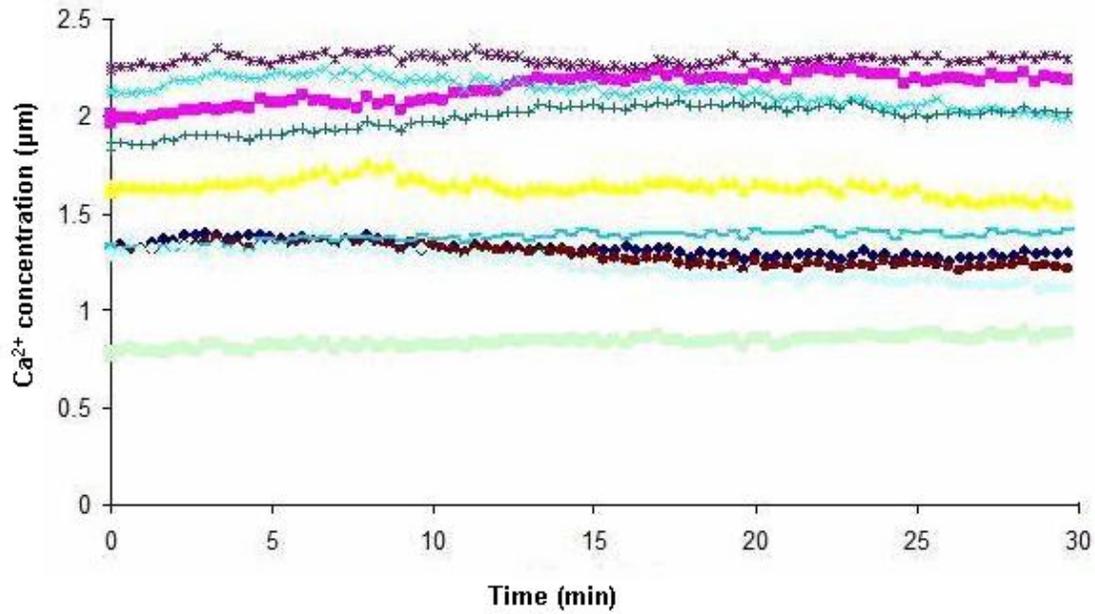
Fig. 36: Quantitative estimation of Ca^{2+} concentration inside the Caco-2 cells determined using the fluorescent dye Fura-2 AM. Each curve represents a single cell.
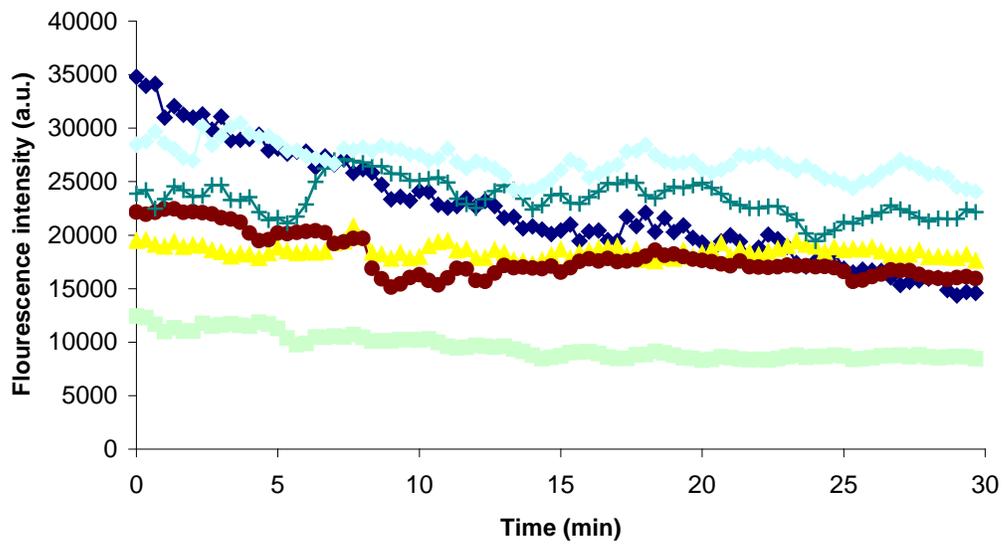
Fig. 37: Ca^{2+} transport of Caco-2 cells incubated with p-gp inhibitor Cyclosporin A (10 µM) and in the presence of 2 mM of external Ca^{2+} for time period of 30 min. Each curve represents a single cell.

Generally, for blocking the L-type Ca^{2+} channels there are three types of antagonists available. They include phenylalkylamines, benzodiazepines, and dihydropyridines. These antagonists interact at the specific binding site of the channel protein (Godfraind *et al*., 1986; Striessnig *et al*., 1987). Nifedipine (10 µM), a dihydropyridine, specifically blocks L-type Ca^{2+} channels is also applied for inhibiting the Ca^{2+} loss. Nifedipine is also used as an anti-anginal and anti-hypertensive agent. From the data, nifedipine action was insignificant to inhibit the Ca^{2+} loss (Fig. 38).
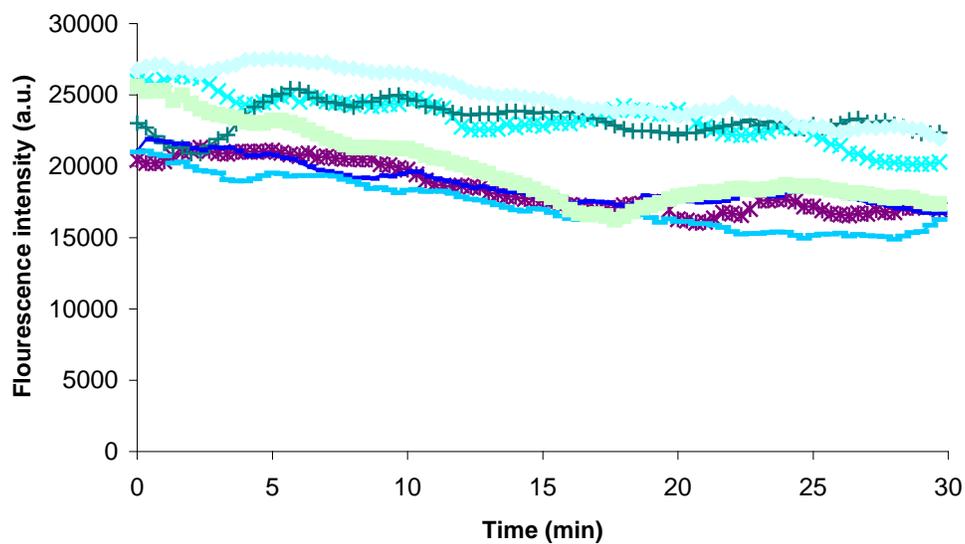
Fig. 38: Ca^{2+} transport of Caco-2 cells in the presence of L-type Ca^{2+} channel inhibitor nifedipine (10 µM) and with 2 mM of external Ca^{2+}. Each curve represents a single cell.

It has been assumed that along with p-gp, some other transporters are also involved in the Ca^{2+} loss of single Caco-2 cells. Experiments with cyclosporin A along with the other inhibitors of Ca^{2+} pump like O-vanadate and L-type channel Ca^{2+} inhibitor nifidipine have been used (Fig. 39 and 40). It has been observed that different combinations of inhibitors have no influence in inhibiting the Ca^{2+} loss of single Caco-2 cells. In all experiments the external Ca^{2+} concentration is maintained constant at 2 mM. Diltiazem-Cl which is also a specific inhibitor similar to nifedipine for L-type Ca^{2+} channels has been used, and the experiments are shown in Fig. 41 and Fig. 42. It is

found that the kinetics of fluorescence intensity of Caco-2 cells after the addition of Diltiazem-Cl appears to be stable for a time period of 30 min.
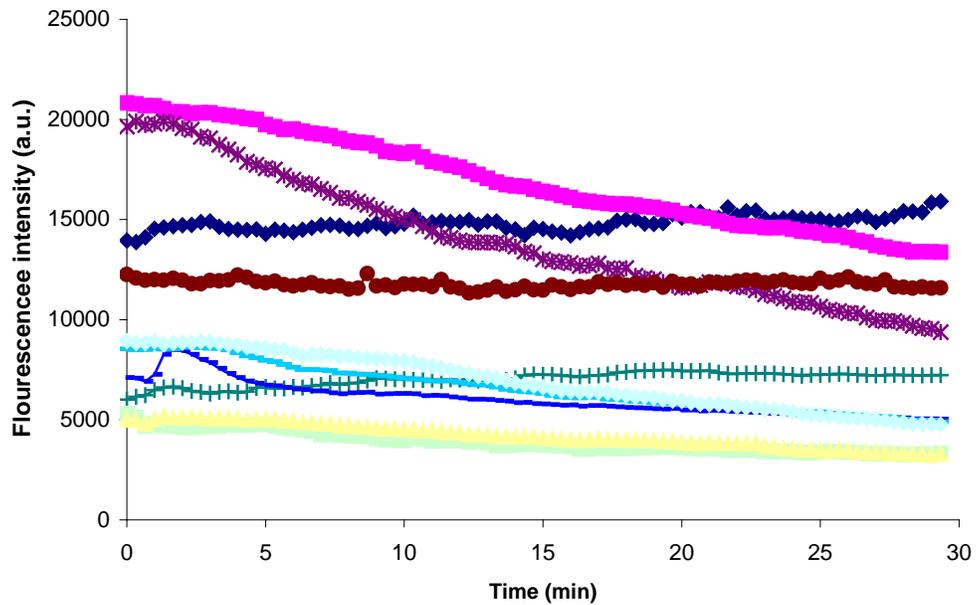
Fig. 39: Fluorescence kinetics of Ca^{2+} transport of Caco-2 cells in the presence of nifedipine (10 µM) and Cyclosporin A (10 µM) in the presence of 2 mM of external Ca^{2+} for a time period of 30 min. Each curve represents a single cell.
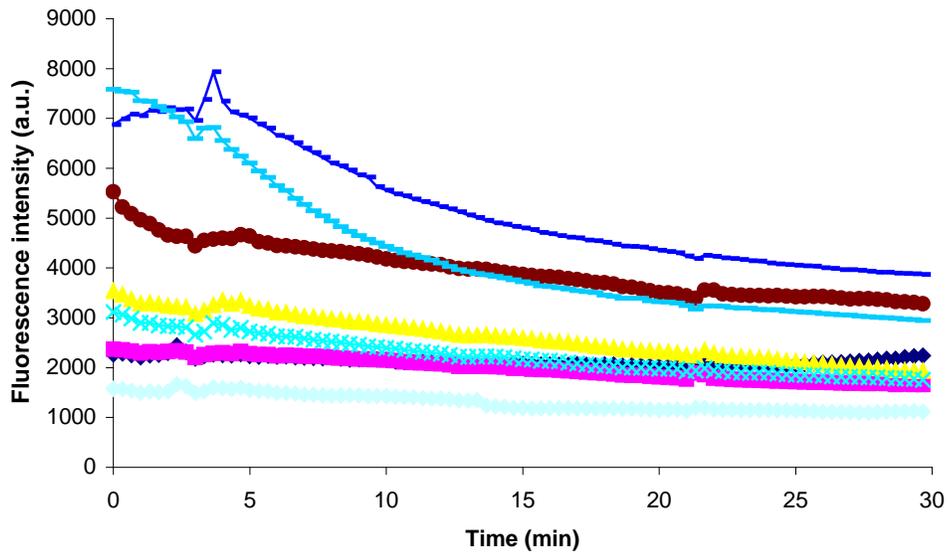
Fig. 40: Fluorescence kinetics of Ca^{2+} transport of Caco-2 cells in the presence of O-vanadate (80 µM), Cyclosporin A (10 µM) and with 2 mM of external Ca^{2+} for a time period of 30 min. Each curve represents a single cell.
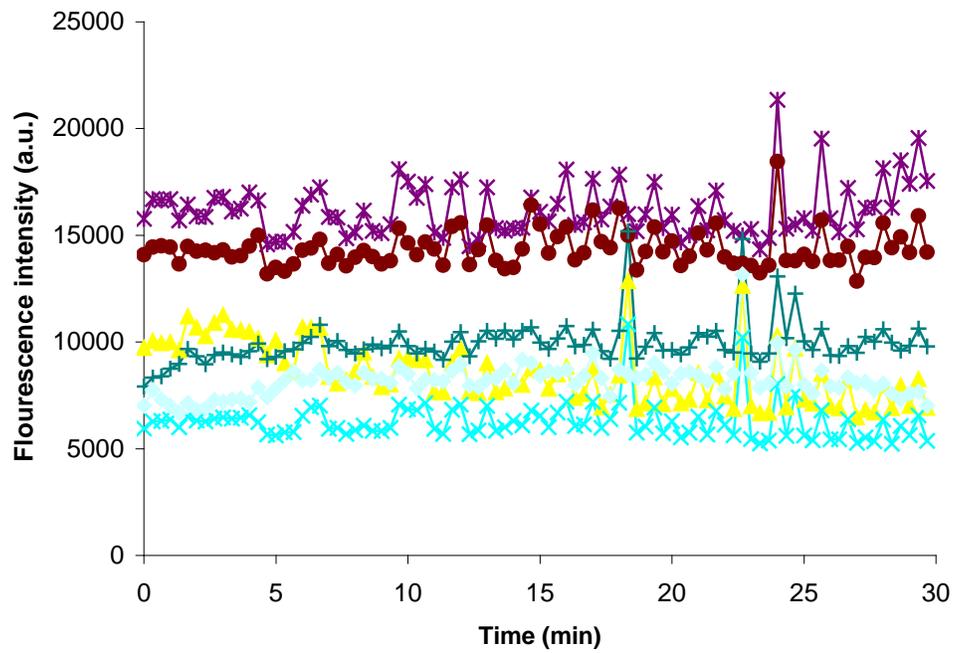
Fig. 41: Ca^{2+} transport of Caco-2 cells in the presence of Diltiazem-Cl (1 µM) in the presence of 2 mM of external Ca^{2+} for a time period of 30 min. Each curve represents a single cell.
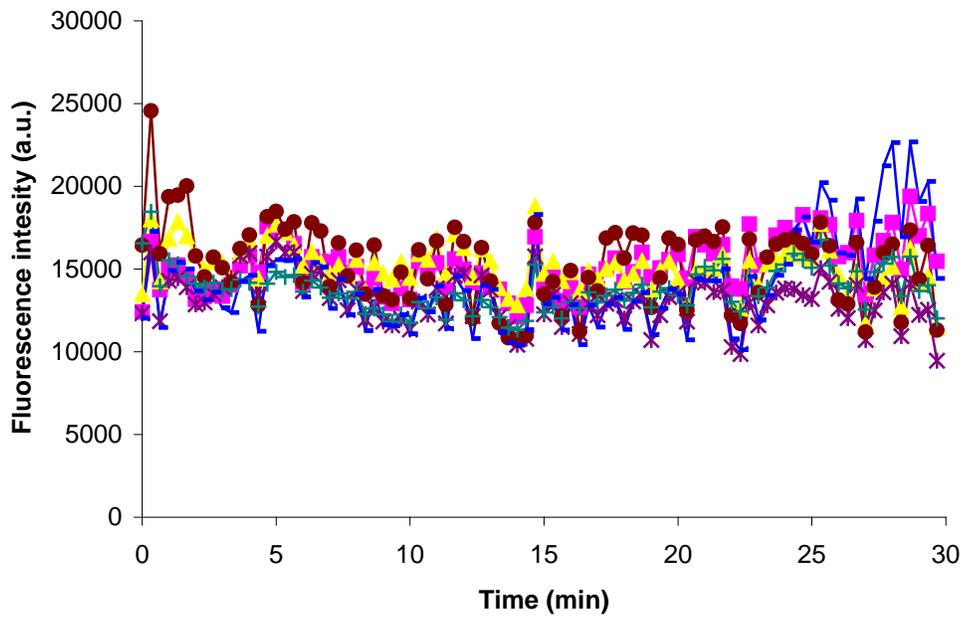
Fig. 42: Ca^{2+} transport of Caco-2 cells in the presence of Diltiazem-Cl (1 µM) and in the presence of 10 mM of external Ca^{2+} for a time period of 30 min. Each curve represents a single cell.

To our knowledge, it is the first report showing such behaviour of Ca^{2+} loss of a single Caco-2 cell and studied mechanism. We have observed that disruption of epithelium results in the Ca^{2+} release from a single Caco-2 cell. In a series of experiments with various inhibitors and drugs none of them could block the Ca^{2+} loss in physiological conditions except Diltiazem-Cl. Moreover, different combinations of inhibitors for pumps and L-type Ca^{2+} channels were also not able to inhibit the Ca^{2+} loss. Our data suggest that only Diltiazem-Cl is able to block slow or L-type Ca^{2+} channels effectively similar to previous findings (Kanaya *et al*., 1983; Lee and Tsien, 1983). Diltiazem-Cl is also responsible in the regulation of Ca^{2+} release from the intracellular stores of neutrophils (Rosales *et al*., 1992). Additionally, Diltiazem-Cl stimulates 1, 4-dihydropyridine binding to Ca^{2+} channels. It also acts as a coronary vasodilator and increases the coronary blood flow in humans (Vrolix *et al*., 1991).

In summary, our data suggest that L-type channels are involved the Ca^{2+} loss of single Caco-2 cells. Diltiazem-Cl effectively inhibits the Ca^{2+} loss of single Caco-2 cells, detached from the epithelium, in physiological conditions. Additionally, it also inhibits the Ca^{2+} loss of single Caco-2 cells at higher external Ca^{2+} concentrations (10 mM) also. It would be interesting to study such effect with other epithelial cell types or does this phenomenon is limited to Caco-2 cell line only.

Chapter 6: Effect of nano-structured surfaces and nano-particles on physiological processes of RBCs and Caco-2 cells

The experiments presented in this chapter were done together with Dr. Lyubomira Ivanova and Melanie Zimmer.

6.1 Influence of nano-structures on cellular processes

Cells respond significantly to the local nano-scale patterns of surface chemistry and topography (Stevens *et al.*, 2005). Several reports have shown that osteoblasts, fibroblasts, smooth muscle cells, chondrocytes and endothelial cells are sensitive towards the differences at nanometer scale compared with conventional surface roughness (Kay *et al.*, 2002; Webster *et al.*, 2001). Surface properties of materials as well as biophysical constraints at the biomaterial surface are of major importance since these features will direct the cell responses and cell behaviour (Meyer *et al.*, 2005). Nano-structured surfaces were utilised to study the actomyosin motility, osteoblasts functions improved on nano-structured surfaces of carbon and alumina on nano-structured surfaces (Price *et al.*, 2003). There are several reports regarding the influence of nano-structured surfaces on cell behaviour (Von Recum *et al.*, 1995 and Curtis *et al.*, 2001), cell migration, cell adhesion (Curtis *et al.*, 2001), and also gene expression (Dalby *et al.*, 2002). Endothelial cells cultured on the extracellular matrix textured surfaces spread faster and resemble to the cells in their native arteries than cells grown on normal surfaces (Goodman *et al.*, 1996).

Ca^{2+} is the most important ion in the human body which is responsible for many cellular processes. Ca^{2+} acts as a universal intracellular messenger which participates in neurotransmission and muscle contraction. Cells regulate the intracellular and extracellular Ca^{2+} levels very precisely. Such regulation is important for the cell growth differentiation and apoptosis (Santella *et al.*, 1998 and Nicotera *et al.*, 1998). An increase in intracellular pH was shown to be an essential prerequisite for many cellular processes like DNA synthesis, cell proliferation, and activation of glycolysis (Grinstein *et al.*, 1989). Rich and his co-workers have shown an increase of approximately 0.4 units of intracellular pH in various leukemia cell lines as compared to peripheral blood mononuclear cells from healthy donors (Rich *et al.*, 2000). Besides, cell growth and proliferation, a wide variety of cellular processes and properties such as metabolism, cell volume, and tubulin polymerization are affected by intracellular pH (Busa *et al.*, 1984; Lang *et al.*, 1998). Intracellular pH is an important parameter which influences cell physiology and metabolism of a cell. Thus, it would be of importance to study the

changes in the intracellular pH of RBCs and Caco-2 cells on different surfaces and materials. We have chosen RBCs and Caco-2 cells a model for our experiments.

6.2 Results

All the investigations have been carried out at single cellular level using fluorescence imaging. The kinetics of Ca^{2+} and H^+ transport of RBCs and Caco-2 cells has been studied on various nano- and chemically modified surfaces. The results obtained are compared with the corresponding kinetics on ordinary borosilicate glass surface over 30 min. The surfaces tested include:

- Borosilicate glass surface
- Micro/Nano-structured surfaces
- Nano-structured PMMA surfaces
- Chemically modified surfaces
- Glass surfaces coated with organic polymer

6.2.1 Kinetics of Ca^{2+} transport of RBCs

The RBCs are labeled with Fluo-4 marker which is suitable to study the kinetics of Ca^{2+} transport. The response of RBCs after incubation of the dye is studied on glass surface for a time period of 30 min are shown in Fig. 43.
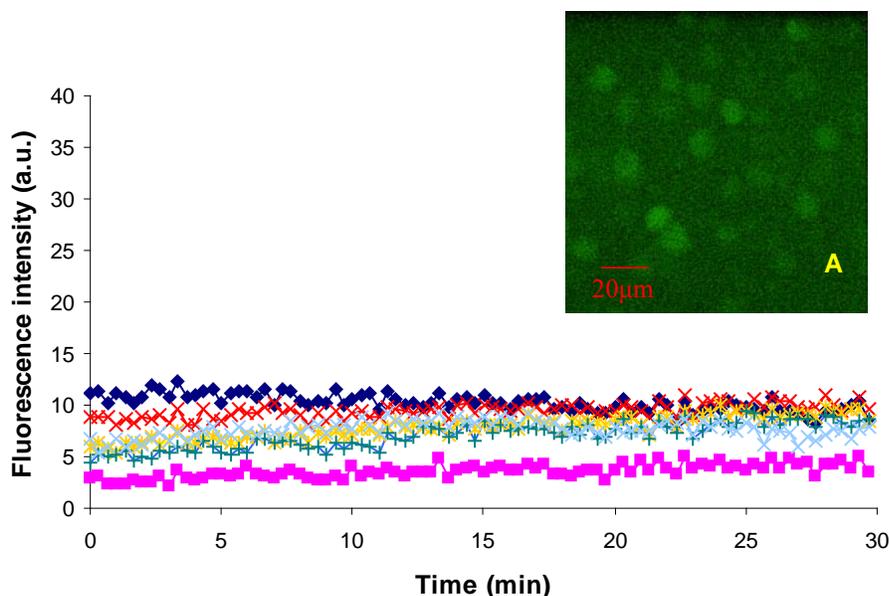
Fig. 43: Kinetics of Fluo-4 fluorescence intensity of RBCs in the presence of 2 mM external Ca^{2+} on normal glass surface over a time period of 30 min. A: Fluorescence image with RBCs. Each curve represents a single cell.

All the cells show a low and stable fluorescence kinetics which is characteristic of RBCs under such conditions. This experiment serves as a reference for following experiments with different nano-structured surfaces having different patterns and textures. Similar conditions like incubation time of the dye and 2 mM external Ca^{2+} are maintained for all the experiments.

Kinetics of Ca^{2+} transport of RBCs on Micro/Nano-structured surfaces

The micro- and nano-structured surfaces have been produced by modifying the glass surface using various methods (Chapter 3). The combined fluorescence and bright field images of surface texture of GPTS, ETC and nano-structured surfaces (KLN), and also the corresponding surfaces with RBCs respectively (Fig. 44). The artificial surfaces of GPTS and ETC have micro imprints on their surface and the KLN surface has nano patterns. A detailed description of the preparation and pattern of materials used here in this chapter are explained in the chapter Materials and methods. The Kinetics of Fluo-4 fluorescence intensity of RBCs in the presence of 2 mM external Ca^{2+} over different surfaces with respect to control (glass surface) for a time period of 30 min is shown in Fig. 45. The kinetics of Ca^{2+} transport of RBCs on PMMA surfaces is dealt separately as a different kinetics with respect to other surfaces has been observed.
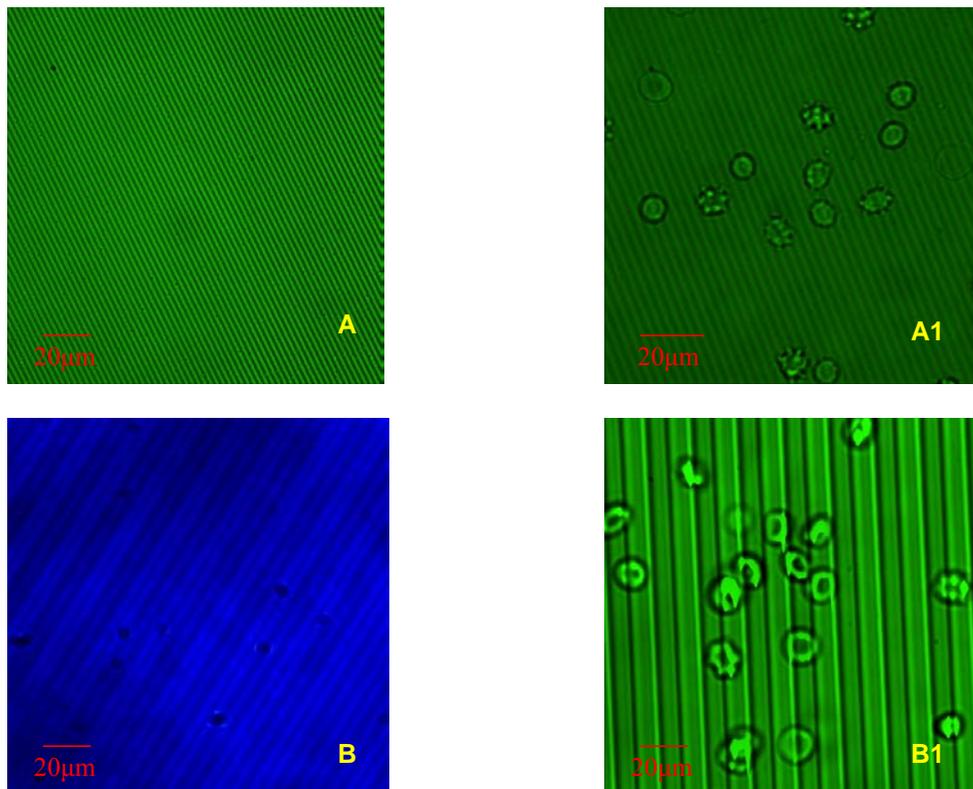
Fig. 44: Images A, B, C represent the combined fluorescence and bright field images of surface texture of GPTS, ETC and nano-structured surfaces (KLN), and A1, B1, C1 represent the corresponding surfaces with RBCs.
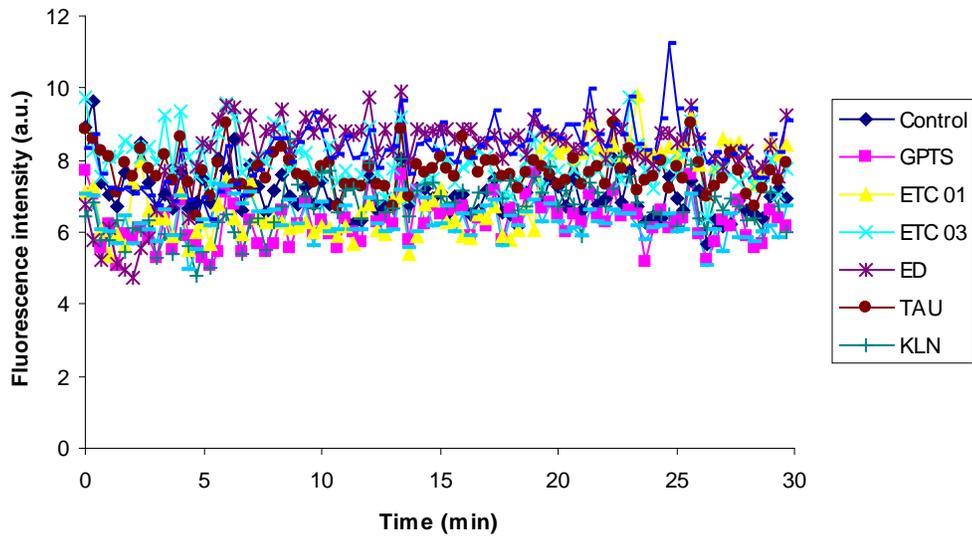
Fig. 45: Kinetics of Fluo-4 fluorescence intensity of RBCs in the presence of 2 mM external Ca^{2+} over different surfaces for a time period of 30 min. Each curve represents the average of 3-5 cells.

Kinetics of Ca^{2+} transport of RBCs on PMMA Surfaces

The surfaces obtained from Science park, Barcelona differ from the ordinary glass surface and other modified surfaces in the nature of material and thickness. A detailed description regarding the pattern of these structures is explained in Materials and methods (chapter 3). Combined bright field and fluorescence images of different PMMA structures are depicted in Fig. 46.
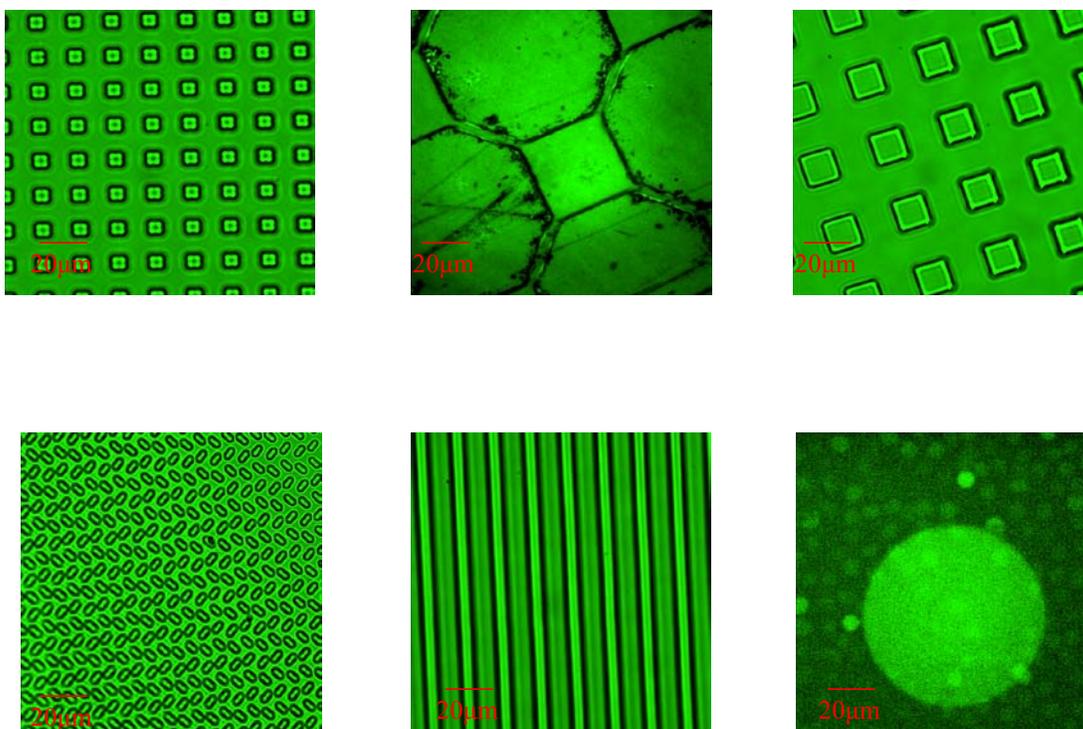
Fig. 46: Combined bright field and fluorescence images of various surface patterns of PMMA surfaces.

The kinetics of fluorescence intensity of Fluo-4 on the micro- and nano-structured surfaces has shown that the impact caused by these patterns is negligible. The fluorescence intensity of RBCs on PMMA surfaces (shown in Fig. 47) is unstable compared to glass or other modified surfaces. The results with PMMA surfaces show that it has some influence on Ca^{2+} transport of RBCs. Experiments have been done on every pattern of PMMA surfaces separately. It has been observed that the kinetics of fluorescence intensity of RBCs is unstable on every pattern. In some cases, an increase in the fluorescence intensity has been obsereved compared to other surfaces. The design or the precursor material of PMMA surfaces might have influenced the fluorescence kinetics of RBCs.
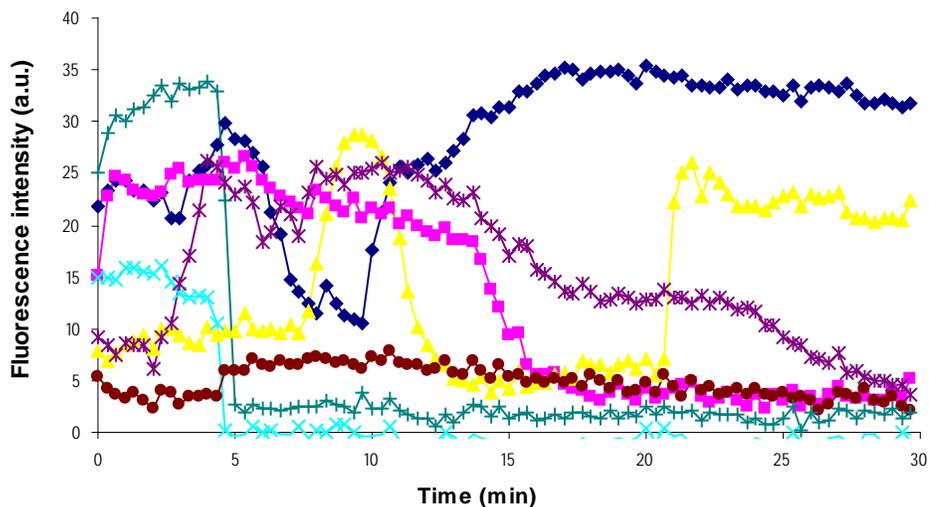
Fig. 47: Kinetics of Fluo-4 fluorescence intensity of RBCs in the presence of 2 mM external Ca^{2+} over PMMA surface for 30 min. Each curve represents a single cell.

6.2.2 Kinetics of Ca^{2+} transport of Caco-2 cells

Ca^{2+} transport of Caco-2 cells has been studied similar to RBCs. The cells are labeled with Fluo-4 which is a Ca^{2+} indicator suitable to study the kinetics of fluorescence intensity on glass and various artificial surfaces for a time period of 30 min. Caco-2 cells show a strong fluorescence signal compared to RBCs and lose Ca^{2+} in physiological conditions as explained before in the Chapter 5. Caco-2 cells on glass surface with Ca^{2+} loss can be seen in Fig. 48, and this experiment serves as a reference for following modified surfaces.
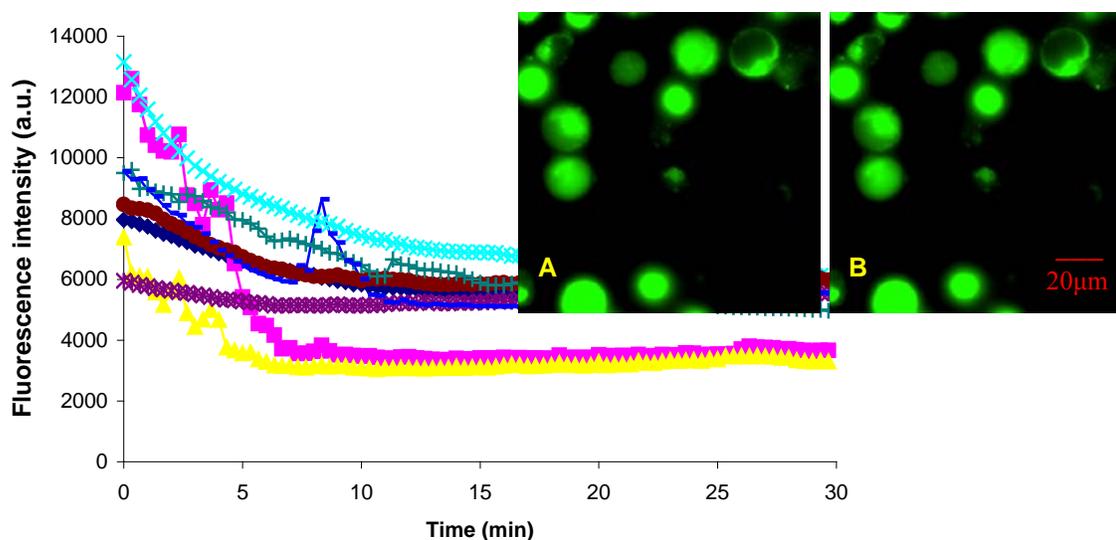
Fig. 48: Kinetics of Fluo-4 fluorescence intensity of Caco-2 cells with 2 mM external Ca^{2+} over glass surface for 30 min. Fig. A and B represent the fluorescence image of Caco-2 cells at 0 and 30 min of experiment, respectively. Each curve represents a single cell.

Kinetics of Ca^{2+} transport of Caco-2 cells on Micro/Nano-structured surfaces

The kinetics of fluorescence intensity of Caco-2 cells with different surfaces (shown in Fig. 49) follows a similar pattern with respect to glass surface. All the modified surfaces (GPTS, ETC and KLN) and the chemically modified surfaces (ED and TAU) do not differ from the control (glass surface) on the Ca^{2+} transport of Caco-2 cells. A similar pattern of fluorescence kinetics has been observed on every surface tested with respect to glass surface.
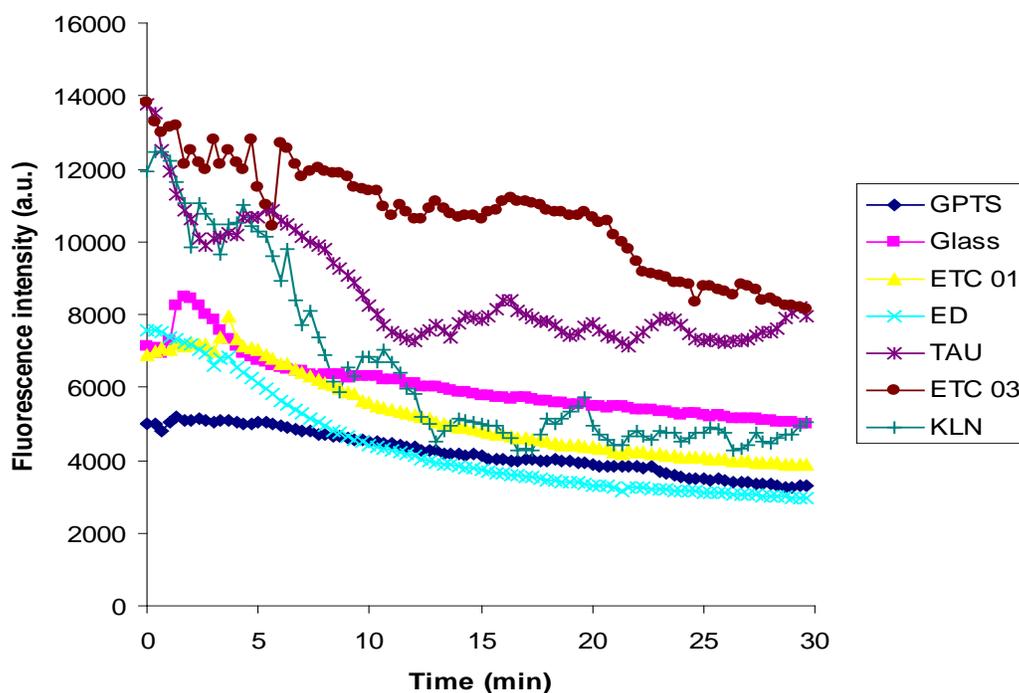
Fig. 49: Kinetics of Fluo-4 fluorescence intensity of Caco-2 cells in the presence of 2 mM external Ca^{2+} over different surfaces for 30 min. Each curve represents the average of 3-5 cells on different surfaces.

Kinetics of Ca^{2+} transport of Caco-2 cells on PMMA surfaces

Significant decrease in the fluorescence intensity compared to glass surfaces has been observed in the case of PMMA surfaces has been observed (Fig. 50). It is also seen that fluorescence intensity of Caco-2 cells on these surfaces is somewhat stable except for few cells compared to the kinetics Fluo-4 fluorescence intensity on glass surfaces over a time period of 30 min. From the data obtained, it is clearly evident that none of the

modified surfaces (GPTS, ETC 01 and 03, ED, TAU and KLN) except PMMA surfaces influence the Ca^{2+} transport of RBCs. The pattern or the precursor material might have some impact on the reduced fluorescence intensity.
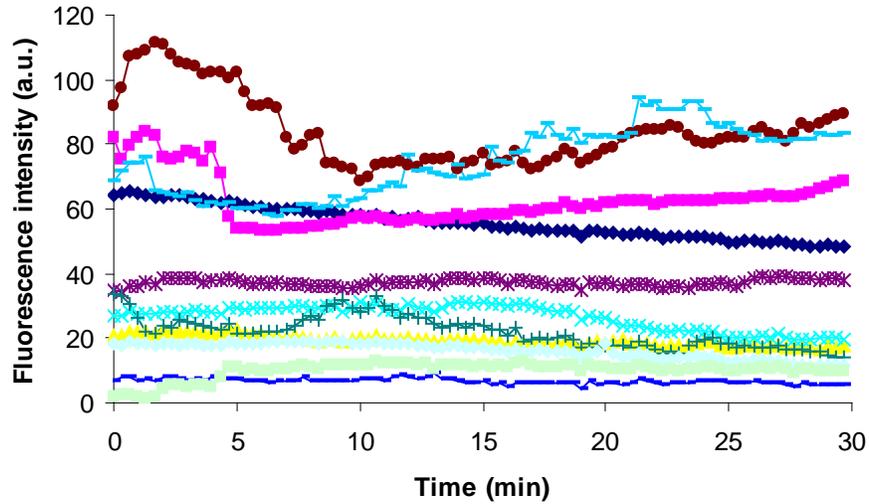
Fig. 50: Kinetics of Fluo-4 fluorescence intensity of Caco-2 cells in the presence of 2 mM external Ca^{2+} over PMMA surface for a time period of 30 min. Each curve represents a single cell.

6.2.3 Intracellular pH measurements of RBCs

We have investigated the influence of the surface constraints on the pH of RBCs in physiological conditions using BCECF dye and the ionophore nigericin. A calibration curve is plotted at a pH range of 7 to 8 exciting the dye at 450 and 490 nm shown in Fig. 51.
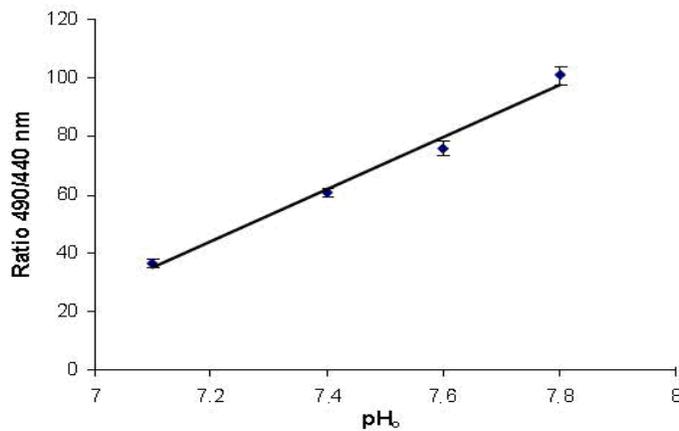
Fig. 51: Calibration curve plotted for intracellular pH of RBCs using BCECF dye and ionophore nigericin on glass surface.

In physiological conditions RBCs maintain a pH of 7.2-7.4 and it remains constant for a time period of 30 min (Fig. 52).
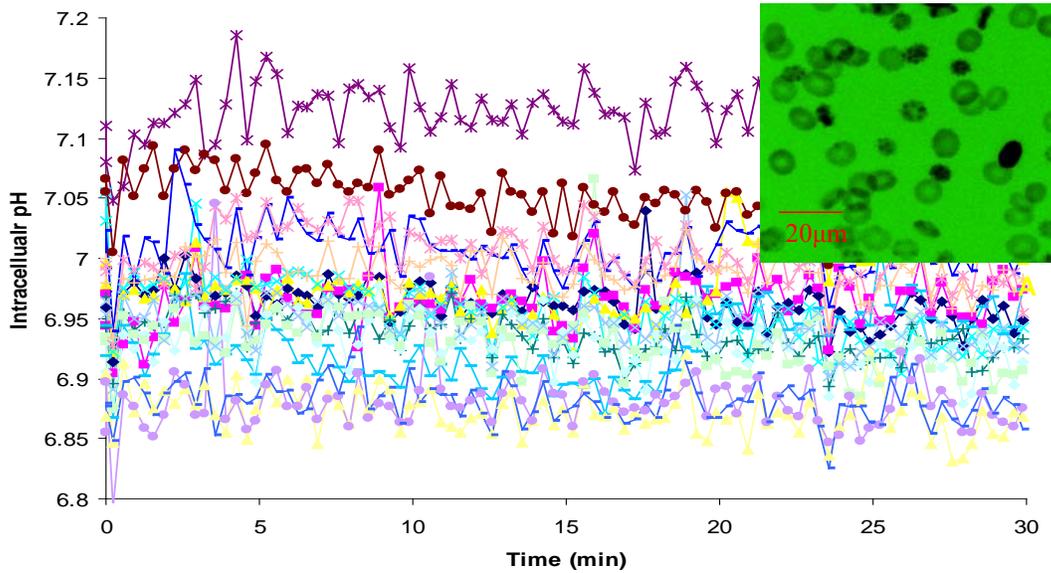
Fig. 52: Kinetics of pH change of RBCs incubated with pH indicator, BCECF-AM, on glass surface for a time period of 30 min. A. Ratio image of red blood cells of two fluorescence wavelengths at 450/490 nm on the glass surface. Each curve represents a single cell.

Intracellular pH measurements of RBCs on Micro-/ Nano-structured surfaces

The modified surfaces (GPTS, KLN and ETC) and the chemically modified surfaces (ED and TAU) did not influence the intracellular pH of RBCs (Fig. 53). The fluorescence intensity is stable and constant on these surfaces similar to the glass surface.
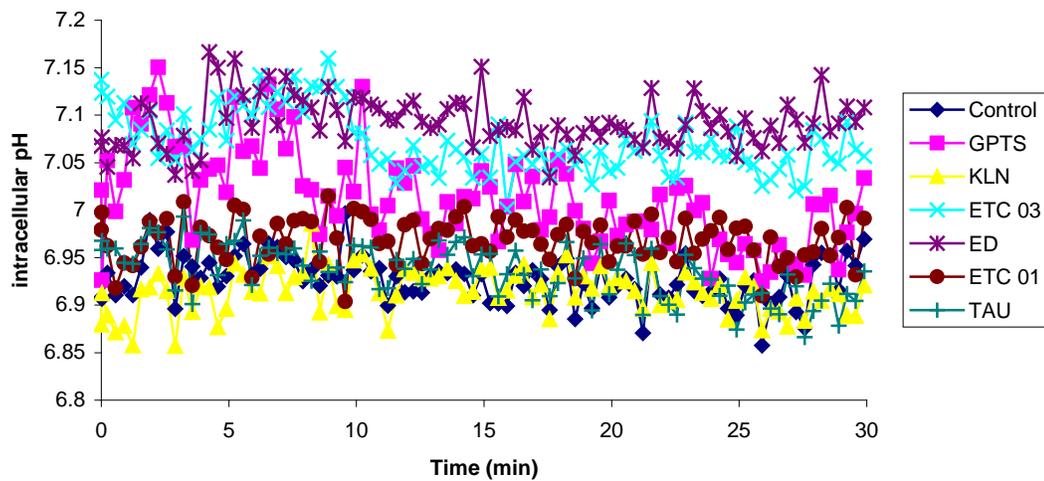
Fig. 53: Kinetics of pH changes of RBCs incubated with pH indicator, BCECF-AM, on different surfaces for a time period of 30 min. Each curve represents the average of 3-5 cells over different surfaces.

Intracellular pH measurements of RBCs on PMMA surfaces

The PMMA surfaces have different material and surface texture compared to the other tested and ordinary glass surface. The kinetics of pH change of RBCs over PMMA surfaces is shown below (Fig. 54). The PMMA surfaces have shown a different fluorescence kinetics compared to the above mentioned surfaces. Although, the intracellular pH lies within the range of physiological conditions, a slight decrease in the pH has been observed. It is difficult to correlate this behaviour with respect to the nature of material.
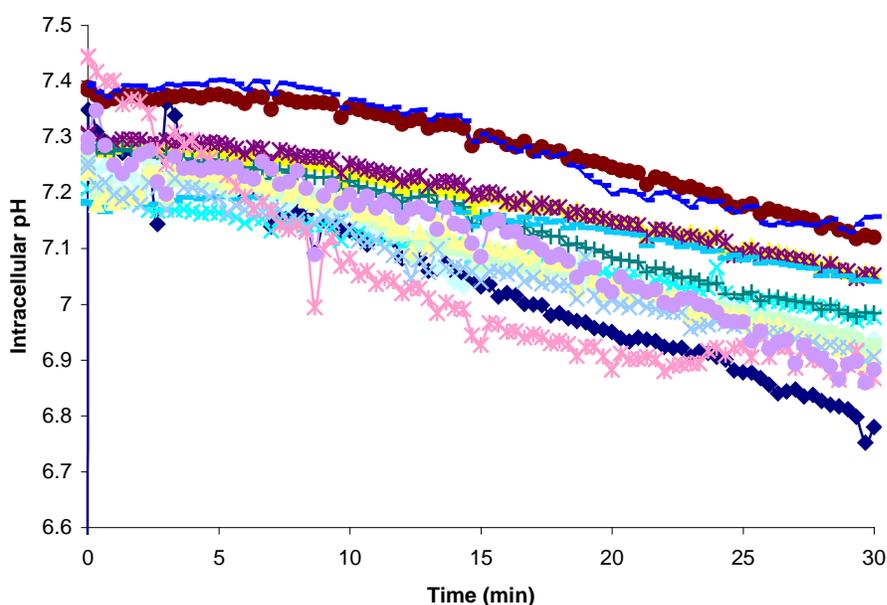
Fig. 54: Kinetics of pH change of RBCs incubated with pH indicator, BCECF-AM, on PMMA surface for a time period of 30 min. Each curve represents a single cell.

6.2.4 Intracellular pH measurements of Caco-2 cells

Changes in the intracellular pH of Caco-2 cells have been studied similar to RBCs using BCECF-AM dye and K^+/H^+ ionophore, nigericin. A calibration curve is plotted is shown in Fig. 55. Caco-2 cells after labeling with the dye have been studied on various nano- and micro- modified surfaces and chemically modified surfaces. The experiments on glass surface are used as a reference for the following experiments. In physiological conditions, Caco-2 cells maintain a constant pH of 6.8-7.2 for a time period of 30 min (Fig. 56). It is clearly evident from the kinetics of pH changes that single Caco-2 cells on

different surfaces have negligible effect (Fig. 57). In contrast, the experiments with PMMA surfaces, the kinetics of fluorescence intensity of Caco-2 cells is rather unstable with reference to glass surface. A decrease in the intracellular pH has been observed on PMMA surfaces over a time period of 30 min (Fig. 58).
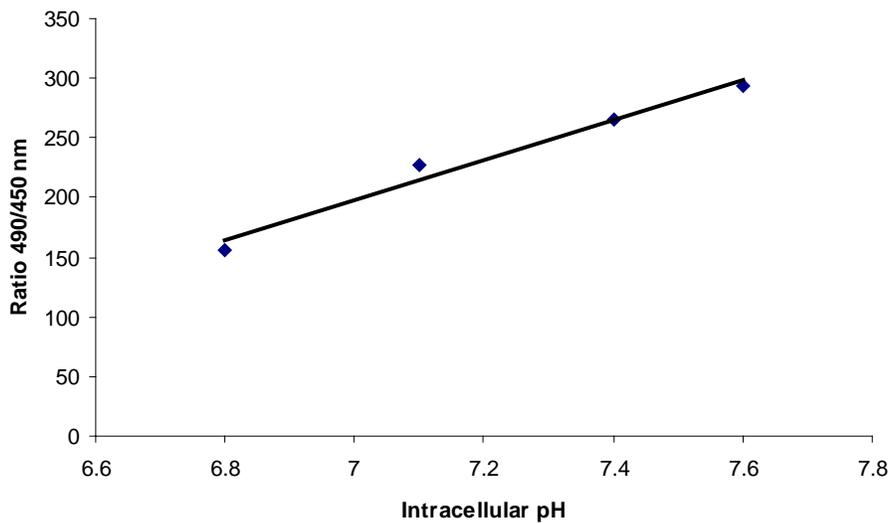
Fig. 55: Calibration curve plotted for intracellular pH of Caco-2 cells using BCECF dye and ionophore nigericin on glass surface.
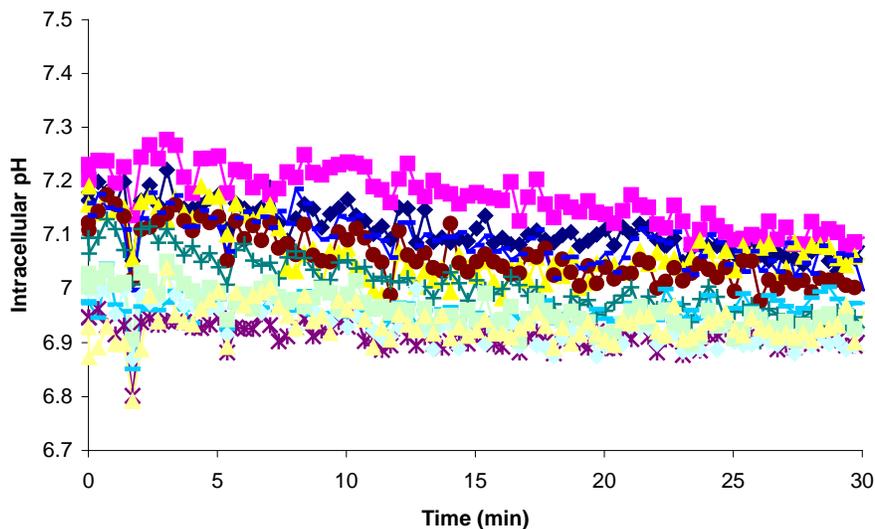
Fig. 56: Kinetics of pH changes of Caco-2 cells incubated with pH indicator, BCECF-AM, on glass surface for a time period of 30 min. Each curve represents a single cell.
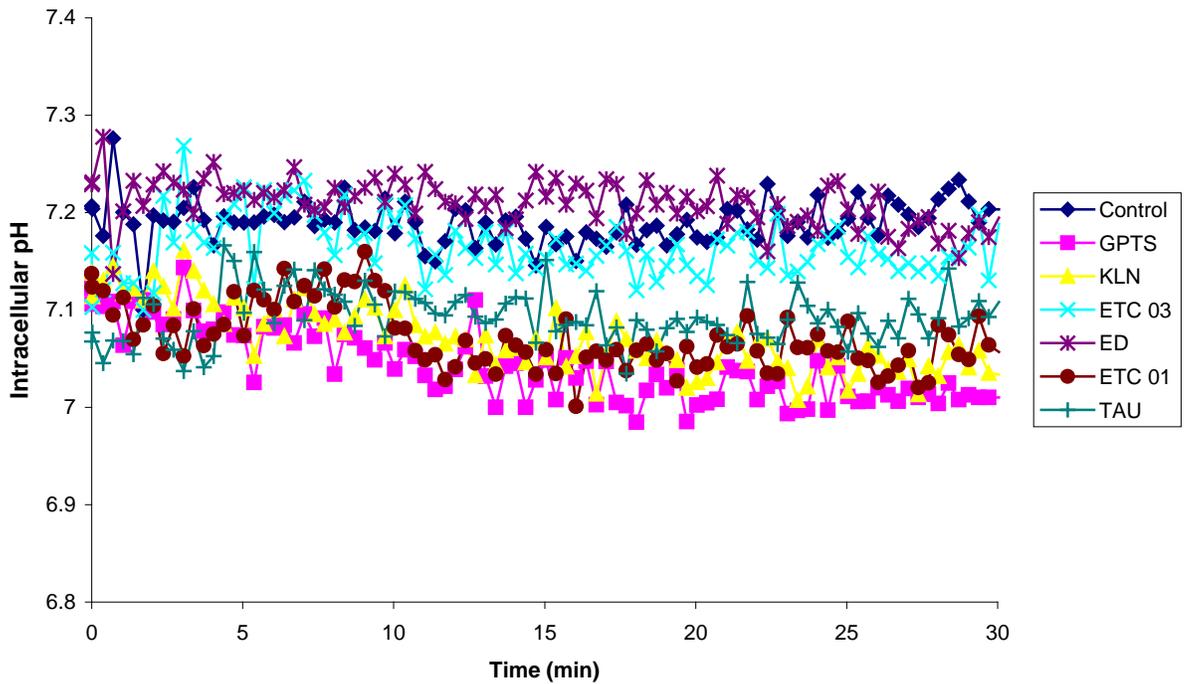
Fig. 57: Kinetics of pH changes of Caco-2 cells incubated with pH indicator, BCECF-AM, on different surfaces for a time period of 30 min. Each curve represents the average of 3-5 cells over different surfaces.
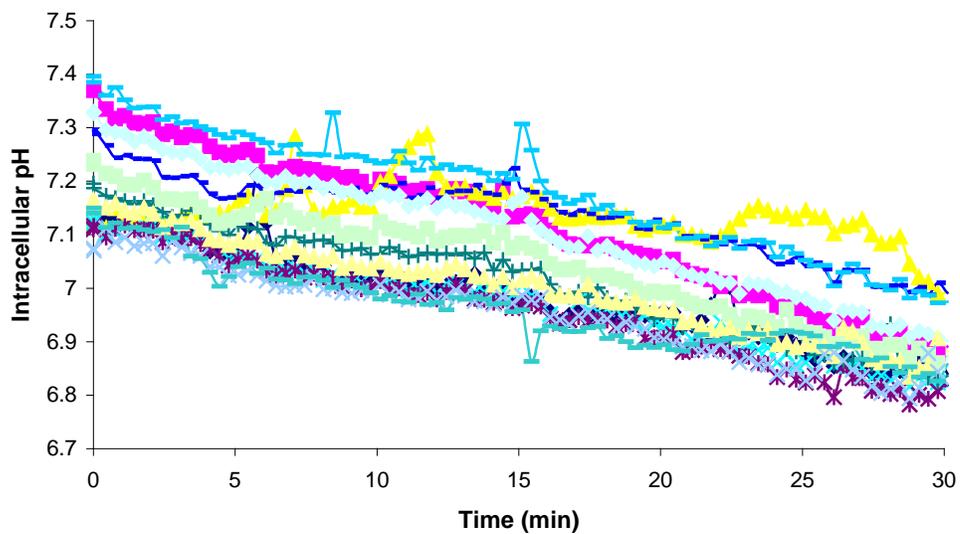
Fig. 58: Kinetics of pH changes of Caco-2 cells incubated with pH indicator, BCECF-AM on PMMA surface over a time period of 30min. Each curve represents a single Caco-2 cell.

From the data, the effect of PMMA surfaces on the kinetics of pH changes of single Caco-2 cells is significant compared to other modified surfaces and glass surface.

Intracellular pH measurements of RBCs on organic polymer surfaces

The organic polymer surfaces I and II obtained from the Department of Organic Chemistry, Sofia University, Bulgaria are bipolar in nature. The cells could not settle down on the surface even after a time period of 1 h, which makes it difficult to carry the Ca^{2+} and pH measurements (Fig. 59-61). Cells are transformed into echinocytes with these surfaces and clumping of cells has been observed. The other polymer surface III is negatively charged, and a transformation of RBCs to echinocyte shape has been observed after 30 min of the experiment. Experiments with Caco-2 cells were not possible as the surfaces are meant for single use.
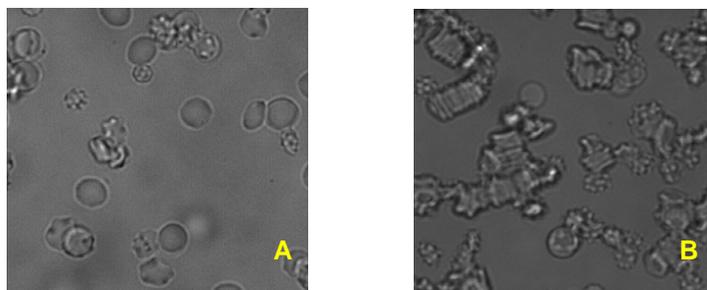
Fig. 59: Bright field image of RBCs over organic polymer surface I after 5 min (A) and 30 min (B) of the experiment.
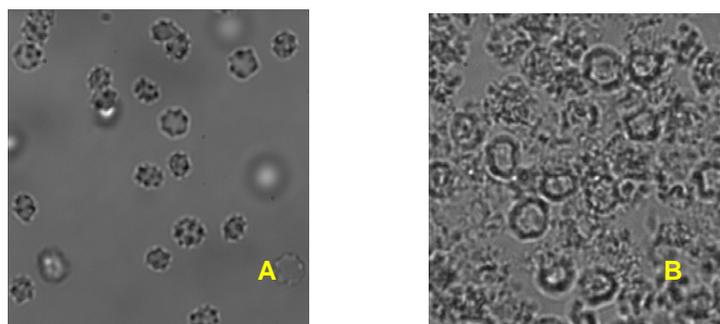
Fig. 60: Bright field image of RBCs over organic polymer surface II after 5 min (A) and 30 min (B) of the experiment.
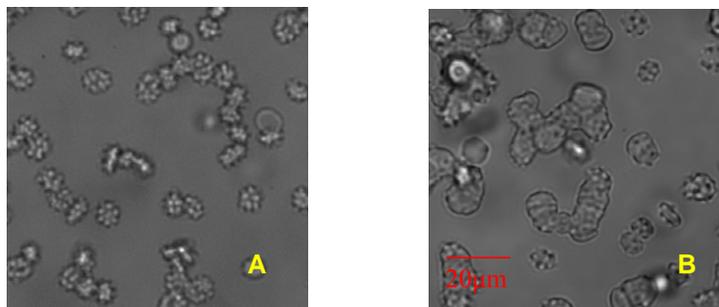
Fig. 61: Bright field image of RBCs over organic polymer surface III after 5 min (A) and 30 min (B) of the experiment.

6.2.5 Interaction of Nano-particles with RBCs and Caco-2 cells

Nano-particle based drug delivery systems are helpful for delivering the drug to specific locations in the human body. Nano-particles having few nanometers to few hundred nanometers emerged as potential applicants in the field of medicine and industry. Nano-particles are also used in neurosurgery. Generally, cellular uptake mechanisms include pinocytosis, endocytosis and receptor-mediated endocytosis. Encapsulation of macromolecules and DNA with nano-particles will help in avoiding the lysosomal degradation and specific delivery to the target. The membrane crossing ability of nano-particles with RBCs and Caco-2 cells and their possible physiological effects at single cellular level has been investigated. Nano-particles of different physical and chemical properties have been investigated with human RBCs and Caco-2 cells. The possible penetration of the particles into the cells and their distribution inside the cells has been investigated. A comparison of the effect on the 2 cell types is of importance since RBCs do not exhibit endocytosis.

The nano-particles investigated include f-PLGA, (poly lactic-co-glycolic acid) coupled with WGA (wheat germ agglutinin) are of 520 nm in diameter. The properties like biodegradability and biocompatibility make PLGA as a suitable choice for tissue engineering and drug delivery. The poor bio-adhesion of PLGA can be overcome by conjugating it with a suitable lectin like WGA. Both human RBCs and Caco-2 cells were studied after the incubation with the nano-particles for 30 min at 4°C. Washed human RBCs were incubated with nano-particles at a concentration of 2.5 mg/ml for a time period of 30 min. The fluorescence and bright field images of RBCs with nano-particles is shown in Fig. 62. It is found that the tested nano-paricles accumulated outside the cell

(Fig. 62B and C) and are unable to cross the membrane. The experiments with RBCs are done with Caco-2 cells also. Caco-2 cells are washed carefully to remove the RPMI medium and re-suspended in physiological solution. Caco-2 cells with nano-particles (f-PLGA+WGA) of 520 nm size at a concentration of 1 mg/ml are tested at 488 nm. Both bright field image and fluorescence images are shown in Fig. 63B and C. It has been observed that the nano-particles get accumulated at the cell membrane and are unable to cross the membrane barrier.
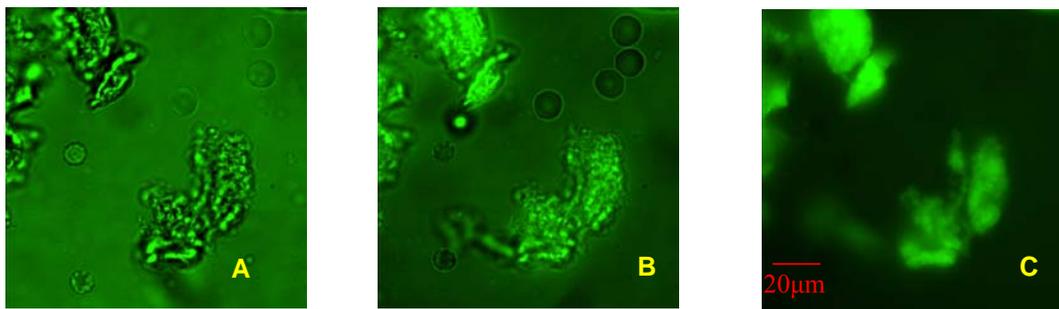
Fig. 62: RBCs with nanoparticles (f-PLGA+WGA) with a size of 520 nm at a concentration of 2.5 mg/ml (A: Bright field image, B: Bright field and fluorescence image, and C: Fluorescence image).
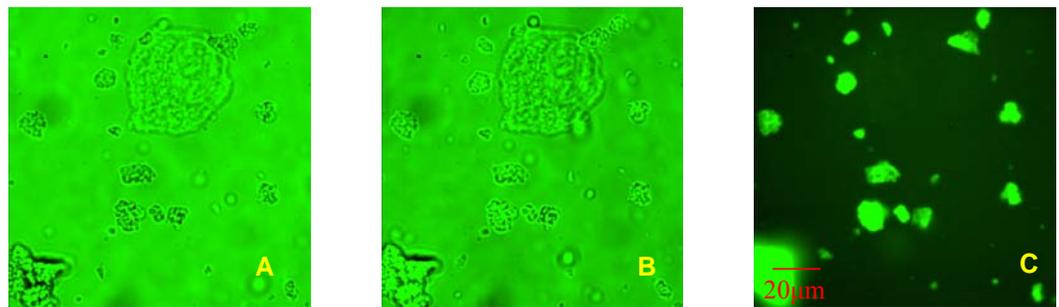
Fig. 63: Caco-2 cells with nano-particles (f-PLGA+WGA) of 520 nm size at a concentration of 1 mg/ml (A: Bright filed image, B: Bright field and fluorescence image, and C: Fluorescence image).

The nano-particles with magnetic iron oxide core on which an organic layer (dye) is grafted with a phosphate entity are of 10 nm in diameter. Particularly, iron oxide particles are helpful in diagnosis of brain tumors and lesions in the brain using MRI (Mendonca *et al.*, 1986). Precise conjugation of an antibody to a magnetic nano-particle

enables to label specific molecules, structures, viruses and microorganisms. For the uniform distribution of nano-particles, ultrasonic techniques have been used. All the experiments for the nano-particles with magnetic oxide core have been carried out at 340 nm. It has been observed from the fluorescence image that the nano-particles are attached to the cell membrane of Caco-2 cells (Fig. 64B).
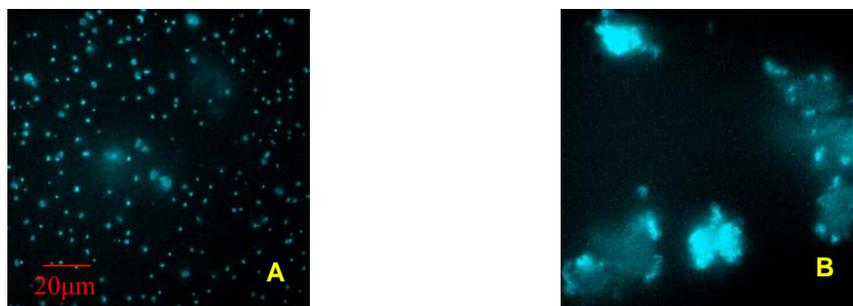
Fig. 64: Caco-2 cells with magnetic iron oxide particles of 12 nm sizes at 340 nm and at a concentration of 1 mg/ml. A: Fluorescence image of particles and B) Fluorescence image of Caco-2 cells with nano-particles.

6.3 Discussion

In this work, changes in the intracellular pH and Ca^{2+} transport of RBCs and single Caco-2 cells has been studied on various modified surfaces from various sources. The changes in these physiological processes imply valuable information about cell homeostasis and cell metabolism. Our results clearly indicate that the textures, patterns and modifications on the glass surface do not influence the Ca^{2+} transport and pH of RBCs and Caco-2 cells. In contrast, PMMA surfaces which are fabricated with different material other than borosilicate have significant influence on these physiological processes. In case of RBCs, PMMA surfaces influence the Ca^{2+} transport of RBCs by altering the band-3 protein conformation. As band-3 occupies most of the RBCs membrane structure, it would be appropriate to consider the role of band-3 protein. Changes in the pH of RBCs can be attributed to the effect of PMMA surface on Na^+/H^+ exchanger. The kinetics for Ca^{2+} transport of Caco-2 cell over PMMA surfaces is more or less similar (Ca^{2+} loss), but the fluorescence intensity decreases considerably. The alterations in the organisation of cytoskeletal matrix of Caco-2 cell on this surface might influence the Na^+/H^+ exchanger, thereby a decrease in the pH has been observed.

The nano-particles examined with different sizes and characteristics could not pass through the membranes of both RBCs and Caco-2 cells. Moreover, a conglomeration or accumulation of these nano-particles at the cell surface of both cell types has been observed. After conglomeration of the nano-particles it seems that they do not cross the membrane. In summary, nano-particles were unable to cross the membrane barrier because of their large size or chemical composition. From the cell morphology point of view, the nano-paricles could not induce any abnormal changes for both the cell types.

The investigations with the magnetic iron core nano-particles have been carried out in collaboration with Prof. Begin-Colin, Institute of Physics and Chemistry of Materials Strasbourg (IPCMS).

Summary

The RBC membrane differs from a simple bilayer membrane by its mechanical properties, shear viscoelasticity and by the long range mobility of integral membrane proteins. The influence of transmembrane potential of human RBCs on the lateral diffusion of Na^+/H^+ exchanger and membrane lipid analogue Bodipy-HPC has been studied using fluorescence correlation spectroscopy (FCS). Variable changes in the diffusion constants of Na^+/H^+ exchanger at different transmembrane potentials and corresponding cytoskeleton interactions have been explained. The role of volume changes of RBCs on the diffusion constant of Na^+/H^+ has been studied. The obtained data suggest that the transmembrane potential has no significant influence on the lateral diffusion of lipid analogue Bodipy-HPC.

Additionally, the mechanism behind the Ca^{2+} loss of a single Caco-2 cell in physiological conditions has been studied in detail. The mechanism behind such loss and the suitable inhibitor to block this loss has been studied. Different inhibitors for Ca^{2+} channels and pumps have been used to understand the responsible mechanism has been found out. It has been demonstrated, that the detached single Caco-2 cell, from the epithelium, loses Ca^{2+} through L-type channels.

Moreover, the influence of nano-structured surfaces and nano-particles on the physiological processes like Ca^{2+} transport and intracellular pH of RBCs and Caco-2 cells has been studied. Changes in the intracellular pH and Ca^{2+} transport on living cells have impact on the cell metabolism and physiology. It has been shown that most of the surfaces with various patterns and textures on the glass surface do not influence the Ca^{2+} transport and intracellular pH. Polymer surfaces with different precursor material other than glass (borosilicate) have shown to exert significant influence on both Ca^{2+} transport and pH of RBCs and Caco-2 cells.

Zusammenfassung

Die Membran der roten Blutzelle (RBC) unterscheidet sich von einer einfachen Bilayer-Membran durch ihre mechanischen Eigenschaften, viskoelastische Scherkräfte und durch die große Beweglichkeit von integralen Membranproteinen. Der Einfluss des Membranpotentials von menschlichen RBCs auf die laterale Diffusion des Na^+/H^+-Austauschers und des Membranlipid-Analogons bodipy-HPC wurde mittels Fluoreszenz-Korrelations-Spektroskopie (FCS) untersucht. Die Variation der Diffusionskonstante des Na^+/H^+ Austauschers bei verschiedenen Transmembranpotentialen und den korrespondierenden Cytoskelett-Interaktionen wurde erklärt. Die Rolle von Volumenänderungen bei RBCs auf die Diffusionskonstante von Na^+/H^+ wurde studiert. Die gewonnenen Daten deuten darauf hin, dass das Transmembranpotential keinen signifikanten Einfluss auf die laterale Diffusion des Lipid-Analogons bodipy-HPC hat.

Zusätzlich wurde im Detail der Mechanismus hinter dem Ca^{2+}-Verlust einer Caco-2-Zelle in physiologischen Bedingungen und einem geeigneten Inhibitor, um diesen Verlust zu blocken, untersucht. Verschiedene Inhibitoren für Ca^{2+}-Kanäle und Pumpen wurden benutzt, um den verantwortlichen Mechanismus zu verstehen. Es wurde gezeigt, dass eine einzelne, aus Epithel isolierte, Caco-2-Zelle durch L-Typ-Kanäle Ca^{2+} verliert.

Darüber hinaus wurde der Einfluss von nanostrukturierten Oberflächen und Nanopartikeln auf physiologische Prozesse wie den Ca^{2+}-Transport und den intrazellulären pH von RBCs und Caco-2-Zellen betrachtet. Veränderungen im intrazellulären pH und dem Ca^{2+}-Transport in lebenden Zellen haben einen Einfluss auf den Stoffwechsel und die Physiologie von Zellen. Es wurde gezeigt, dass die meisten nanostrukturierten Oberflächen mit verschiedenen Mustern und Texturen in der Glasoberflösche keinen Einfluss auf den Ca^{2+}-Transport und den intrazellulären pH haben. Polymeroberflächen mit verschiedenen Rohstoffen als Glas (Borosilikat) zeigen einen signifikanten Einfluss sowohl auf den Ca^{2+} -Transport als auch auf den pH von RBCs und Caco-2-Zellen.

References

Aickin CC and Thomas RC (1977). An investigation of the ionic mechanism of intracellular pH regulation in mouse soleus muscle fibres. J Physiol, 273: 295–316.

Alivisatos P (2004). The use of nano crystals in biological detection. Nature Biotechnol, 22: 47–52.

Alvarez J and Garcia-Sancho J (1989). An estimate of the number of Ca^{2+}-dependent K^+ channels in the human red cell. Biochim Biophys Acta, 903: 543–546.

Alvarez J, Montero M, Garcia-Sancho J (1992). High affinity inhibition of Ca^{2+}-dependent K^+ channels by cytochrome P-450 inhibitors. J Biol Chem, 267: 11789–11793.

Artursson P (1990). Epithelial transport of drugs in cell culture. I: A model for studying the passive diffusion of drugs over intestinal absorptive Caco-2 cells. J Pharm Sci, 79: 746–782.

Artursson P (1991). Cell culture as models for drug absorption across the intestinal mucosa. Crit Rev Ther Drug Carrier Syst, 8: 305–310.

Artursson P, Ungell AL and Lofroth JE (1993). Selective paracellular permeability in two models of intestinal absorption: cultured monolayers of human intestinal epithelial cells and rat intestinal segments. Pharm Res, 10: 1123–1129.

Axelrod D (1983). Lateral motion of membrane proteins and biological function. J Membr Biol, 75: 1–10.

Benga GH, Popescu O, Borza V, Pop VI, Muresan A, Mocsy I, Brain A and Wrigglesworth JM (1986). Water permeability of human erythrocytes. Identification of membrane proteins involved in water transport. Eur J Cell Biol, 41: 252–262.

Benga GH, Popescu O, Pop VI and Holmes RP (1986). Chloromercuribenzensulfonate binding by membranes proteins and the inhibition of water transport in human erythrocytes. Bioelectrochemistry, 25: 1535–1538.

Bennekou P, Barksmann TL, Kristensen BI, Jensen LR and Christophersen P (2004). Pharmacology of the human red cell voltage-dependent cation channel, Part II: Inactivation and blocking. Blood Cells Molecules and Diseases, 32: 356–361.

Bernhardt I (1994). Alteration of cellular features after exposure to low ionic strength medium. In: Cell Electrophoresis, Bauer J, (Ed.), CRC Press, Boca Raton, pp. 163–179.

Bernhardt I, Hall AC and Ellory JC (1991). Effects of low ionic strength media on passive human red cell monovalent cation transport. J Physiol, 434: 489–506.

Bernhardt I, Hall AC and Ellory JC (1988). Transport pathways for monovalent cations through erythrocyte membrane. Studia Biophys, 126: 5–21.

Bernhardt I, Kummerow D and Weiss E (2001). $K^+(Na^+)/H^+$ exchange in human erythrocytes activated under low ionic strength conditions. Blood Cells Molecules and Diseases, 27: 108–111.

Bernhardt I and Erwin W (2003). Passive membrane permeability for ions and the membrane potential. In: Bernhardt I and Ellory JC, (Eds.), Red cell membrane transport in health and disease, Springer Verlag, Berlin, pp. 83–109.

Blais A, Bissonette T and Berteloot A (1987). Common characteristics for Na^+-dependent sugar transport in Caco-2 and human fetal colon. J Membr Biol, 99: 113–125.

Bloom JA and Webb WW (1984). Photodamage to intact erythrocyte membranes at high laser intensities: methods of assay and suppression. J Histochem Cytochem, 32: 608–616.

Braun A, Hämmerle SP, Suda K, Rothen-Rutishauser B, Günthert M, Krämer SD and Wunderli-Allenspach H (2000). Cell cultures as tools in biopharmacy. Eur J Pharm Sci, 2: S51–S60.

Bronner F (1998). Calcium absorption– a paradigm for mineral absorption. J Nutr, 128: 917–920.

Bronner F and Spence K (1988). Non-saturable Ca^{2+} transport in the rat intestine is via the paracellular pathway. In: Bronner F and Peterlink M (Eds.), Cellular calcium and phosphate transport in Health and Disease. Progress in Clinical and Biological Research, New York, Liss, pp. 277–283.

Brown EM (1991). Extracellular Ca^{2+} sensing, regulation of parathyroid cell function, and role of Ca^{2+} and other ions as extracellular (first) messengers. Physiol Rev, 71: 371–411.

Brugnara C, Ha TV and Tosteson CC (1989). Role of chloride in potassium transport through a K-Cl cotransport system in human red blood cells. Am J Physiol, 256: C994–C1003.

Brugnara C, de Franceschi L and Alper SL (1993). Inhibition of Ca^{2+}-dependent K^+ transport and cell dehydration in sickle cell erythrocytes by clotrimazole and other imidazole derivatives. J Clin Invest, 92: 520–526.

Brungara C (1995). Erythrocyte dehydration in pathophysiology and treatment of sickle cell disease. Curr Opin Hematol, 12: 132–138.

Brungara C (1997). Erythrocyte membrane transport physiology. Curr Opin Hematol, 4: 122–127.

Busa WB and Nuccitelli R (1984). Metabolic regulation via intracellular pH. Am J Physiol, 246: R409–R438.

Cabantchik Z and I Rothstein A (1974). Membrane proteins related to anion permeability of human red blood cells. I. Localization of disulfonic stilbene bind binding sites in proteins involved in permeation. J Membr BioI, 15: 207–226.

Canessa M, Adragna W, Solomon HS, Connolly T and Tosteson DC (1980). Increased sodium-lithium countertransport in red cells of patients with essential hypertension. N Engl J Med, 302: 772–776.

Carafoli E (1992). The Ca^{2+} pump of the plasma membrane. J Biol Chem, 267: 2115–2118.

Carafoli E (1997). Plasma membrane calcium pump: structure, function and relationships. Basic Res Cardiol, 1: 59–61.

Christophersen P and Bennekou P (1991). Evidence for a voltage-gated, non-selective cation channel in the human red cell membrane. Biochim Biophys Acta, 1065: 103–106.

Chung Y, Song I, Erickson R, Sleisenger M and Kim Y (1985). Effect of growth and sodium butyrate on brush border membrane-associated hydrolases in human colorectal cancer cell lines. Cancer Res, 45: 2976–2982.

Curtis ASG, Casey B, Gallagher JO, Pasqui D, Wood MA and Wilkinson CDW (2001). Substratum nano-topography and the adhesion of biological cells. Are symmetry or regularity of nano-topography important?. Biophys Chem, 94: 275–283.

Cone CD Jr (1971). Control of somatic cell mitosis by simulated changes in the transmembrane potential level. Oncology, 25: 168–182.

Cone CD Jr (1970). Variation of the transmembrane potential level as a basic mechanism of mitosis control. Oncology, 24: 438–470.

Dalby MJ, Yarwood SJ, Johnstone HH, Affrossman S and Riehle MO (2002). Fibroblast signaling events in response to nanotopography: A gene array study, IEEE Trans Nanobiosc, 1: 12–17.

Danièle D, Carole M, Alain Z and Philippe Devaux F (1997). Aminophospholipid translocase and proteins involved in transmembrane phospholipid traffic. Biophys Chem, 68: 221–231.

De Franceschi L, Saadane N, Trudel M, Alper SL, Brugnara C and Beuzard Y (1994). Treatment with oral clotrimazole blocks Ca^{2+}-activated K^+ transport and reverses erythrocyte dehydration in transgenic SAD mice. A model for therapy of sickle cell disease. J Clin Invest, 93: 1670–1676.

Deitmer JW and Ellis D (1980). Interactions between the regulation of the intracellular pH and sodium activity of sheep cardiac Purkinje fibres. J Physiol, 304: 471–478.

Denker SP, Huang DC, Orlowski J, Furthmayr H and Barber DL (2000). Direct binding of the Na^+/H^+ exchanger NHE1 to ERM proteins regulates the cortical cytoskeleton and cell shape independently of H^+ translocation. Mol Cell, 6: 1425–1436.

Denner K, Heinrich R and Bernhardt I (1993). Carrier-mediated residual K^+ and Na^+ transport of human red blood cells. J Membr Biol, 132: 137–145.

Dennis EK, Sheetz MP and Schindler M (1981). Matrix control of protein diffusion in biological membranes. Proc Nati Acad Sci USA, 78: 3576–3580.

Deuticke B (2003). Membrane lipids and proteins as a basis of red cell shape and its alterations. In: Bernhardt I and Ellory JC (Eds.), Red cell membrane transport in health and disease, Springer Verlag, Berlin, pp. 27–60.

Deutsch CJ, Holian A, Holian SK, Daniele RP and Wilson DF (1979). Transmembrane electrical and pH gradients across human erythrocytes and human peripheral lymphocytes. J Cell Physiol, 99: 79–93.

Devaux PF (1992). Protein involvement in transmembrane lipid asymmetry. Annu Rev Biophys Biomol Struct, 21: 417–439.

Dix CJ, Hassan H, Obray HY, Shah R and Wilson G (1990). The transport of vitamin B12 through polarized monolayers of Caco-2 cells. Gastroenterology, 98: 1272–1279.

Duhm J and Becker BF (1977). Studies on the lithium transport across the red cell membrane. Interindividual variations in the Na^+-dependent Li^+ countertransport system of human erythrocytes. Pflugers Arch, 370: 211–219.

Duhm J and Gobel BO (1984). Role of the furosemide-sensitive Na/K transport system in determining the steady-state Na and K content and volume of human erythrocytes in vitro and in vivo. J Membr Bioi, 77:243–54.

Dupont Y and Bennett N (1982). Vanadate inhibition of the Ca^{2+}-dependent conformational change of the sarcoplasmic reticulum Ca^{2+}-ATPase. FEBS Lett, 139: 237–240.

Elson El and Magde D (1974). Fluorescence correlation spectroscopy I. Conceptual basis and theory. Biopolymers, 13: 1–27.

Fairbanks G, Steck TL, and Wallach DF (1971). Electrophoretic analysis of the major polypeptides of the human erythrocyte membrane. Biochemistry, 10: 2606–2617.

Fleet JC and Wood RJ (1999). Specific 1,25(OH)$_2$D$_3$-mediated regulation of transcellular calcium transport in Caco-2 cells. Am J Physiol, 276: G958–G964.

Fleet JC, Eksir F, Hance KW and Wood RJ (2002). Vitamin D-inducible calcium transport and gene expression in three Caco-2 cell lines. Am J Physiol, 283: G618–G625.

Fogh J, Fogh JM and Orfeo T (1977). One hundred and twenty-seven cultured human tumor cell lines producing tumors in nude mice. J Natl Cancer Inst, 59: 221–225.

Forsyth PA, Marcelja S Jr, Mitchell DJ and Ninham BW (1977). Phase transition in charged lipid membranes. Biochim Biophys Acta, 469: 335–344.

Freedman JC and Hoffman JF (1979). The relation between dicarbocyanine dye fluorescence and the membrane potential of human red blood cells set at varying Donnan equilibria. J Gen Physiol, 74: 187–212.

Fromherz P (1988). Spatio-temporal patterns in the fluid-mosaic model of membranes. Biochim Biophys Acta, 944: 108–111.

Fujinag J, Tang XB and Casey JR (1999). Topology of the membrane domain of human erythrocyte anion exchange protein. J Biol Chem, 274: 6626–6633.

Funder J (1980). Alkali metal cation transport through the human erythrocyte membrane by the anion exchange mechanism. Acta Physiol Scand, 108: 31–37.

Funder J and Wieth JO (1966). Chloride and hydrogen distribution between human red cells and plasma. Acta Physiol Scand, 68: 234–245.

Gatmaitan Z and Arias I (1993). Structure and function of P-glycoprotein in normal liver and small intestine. Adv Pharmacol, 24:77–97.

Garcia MN, Flowers C and Cook JD (1996). The Caco-2 cell culture system can be used as a model to study food iron availability. J Nutr, 126: 251–258.

Gardoš G (1958). The function of calcium in the potassium permeability of human erythrocytes. Biochim Biophys Acta, 30: 653–654.

Giuliano AR and Wood RJ (1991). Vitamin D regulated calcium transport in Caco-2 cells; unique in vitro model. Am J Physiol, 260: G207–G212.

Glahn RP, Wien EM, Van Campen DR and Miller DD (1996). Caco-2 cell iron uptake from meat and casein digests parallels in vivo studies: use of a novel in vitro method for rapid estimation of iron bioavailability. J Nutr, 126: 332–339.

Godfraind I, Miller RC and Wibo M (1986). Calcium entry blockade and excitation-contraction coupling in the cardiovascular system. Pharmacol Rev, 38: 321–416.

Golan DE and Veatch W (1980). Lateral mobility of band 3 in the human erythrocyte membrane studies by fluorescence photobleaching recovery: Evidence for control by cytoskeletal interactions. Proc Natl Acad Sci USA, 77: 2537–2541.

Goodman SL, Sims PA and Albrecht RM (1996). Three-dimensional extracellular matrix textured biomaterials. Biomaterials, 17: 2087–2095.

Gopinath R M and Vincenzi FF (1977). Phosphodiesterase protein activator mimics red blood cell cytoplasmic activator of (Ca^{2+}-Mg^{2+}) ATPase. Biochem Biophys Res Commun, 77: 1203−1209.

Grinstein S, Cohen SS and Rothstein A (1984). Cytoplasmic pH regulation in thymic lymphocytes by an amiloride-sensitive Na^+/H^+ antiport. J Gen Physiol, 83: 341–369.

Grinstein S, Rotin D and Mason MJ (1989). Na^+/H^+ exchange and growth factor-induced cytosolic pH changes. Role in cellular proliferation. Biochim Biophys Acta, 988: 73–97.

Grygorczyk R and Schwarz W (1983). Properties of the Ca^{2+} activated K^+ conductance of human red cells as revealed by the patch-clamp technique. Cell Calcium, 4: 499–510.

Günther I and Vormann J (1985). Mg^{2+} efflux is accomplished by an amiloride sensitive Na^+/Mg^{2+} antiport. Biochem Biophys Res Commun, 130: 540–545.

Hall AC and Ellory JC (1986). Evidence for the presence of volume-sensitive KCl transport in 'young' human red cells. Biochim Biophys Acta, 85: 317–320.

Hauri HP, Sterchi EE, Bienz D, Fransen MA and Marxer A (1985). Expression of intracellular transport of microvillus membrane hydrolases in human intestinal epithelial cells. J Cell Biol, 101: 838–851.

Hidalgo I, Raub T and Borchardt R (1989). Characterization of the human colon carcinoma cell line (Caco-2) as a model system for intestinal epithelial permeability. Gastroenterology, 96: 736–749.

Hu HM and Borchardt RT (1990). Mechanism of L-α-methyldopa transport through a monolayer of polarized human intestinal epithelial cells Caco-2. Pharm Res, 7: 1313–1319.

Heinrich R, Brumen M, Jäger A, Müller P and Herrmann A (1997). Modelling of phospholipid translocation in the erythrocyte membrane. A combined kinetic and thermodynamic approach. J Theor Biol, 185: 295−312.

Jarrett HW and Penniston JT (1977). Partial purification of the Ca^{2+} –Mg^{2+}ATPase activator from human erythrocytes: its similarity to the activator of 3':5' - cyclic nucleotide phosphodiesterase. Biochem Biophys Res Commun, 77: 1210−1216.

Jay AW and Burton AC (1969). Direct measurement of potential difference across the human red blood cell membrane. Biophys J, 9: 115–121.

Jähnig F (1976). Electrostatic free energy and shift of the phase transition for charged lipid membranes. Biophys Chem, 4: 309–318.

Jorgensen PL (1982). Mechanism of the Na^+,K^+ pump: Protein structure and conformation of the pure (Na^+,K^+)-ATPase. Biochim Biophys Acta, 694: 27–68.

Kaestner L, Christophersen P, Bernhardt I and Bennekou P (2000). The non-selective voltage-activated cation channel in the human red blood cell membrane: Reconciliation between two conflicting reports and further characterisation. Bioelectrochem, 52: 117–125.

Kaestner L, Tabellion W, Weiss E, Bernhardt I and Lipp P (2006). Calcium imaging of individual erythrocytes: problems and approaches. Cell Calcium, 39: 13–19.

Kanaya S, Arlock P, Katzung BG and Hondeghem LM (1983). Diltiazem and verapamil preferentially block inactivated cardiac calcium channels. J Mol Cell Cardiol, 15: 145–148.

Kathleen ME (2007). The membrane and lipids as integral participants in signal transduction: lipid signal transduction for the non-lipid biochemist. Adv Physiol Educ, 31: 5–16.

Kay S, Thapa A, Haberstroh KM and Webster TJ (2002). Nanostructured polymer/nanophase ceramic composites enhance osteoblast and chondrocyte adhesion. Tissue Eng, 8: 753–761.

Keller RCA, Silvius JR and De Kruijff B (1995). Characterization of the resonance energy transfer couple coumarin-BODIPY and its possible applications in protein-lipid research. Biochem Biophys Res Comm, 207: 508–514.

Kummerow D, Hamann J, Browning JA, Wilkins R, Ellory JC and Bernhardt I (2000). Variations of intracellular pH in human erythrocytes via $K^+(Na^+)/H^+$ exchange under low ionic strength conditions. J Membr Biol, 176: 207–216.

Koppel DE, Sheetz MP and Schindler M (1981). Matrix control of protein diffusion in biological membranes. Proc Natl Acad Sci USA, 78: 3576–3580.

Korlach J, Schwille P, WebbWW and Feigenson GW (1999). Characterization of lipid bilayer phases by confocal microscopy and fluorescence correlation spectroscopy. Proc Natl Acad Sci USA, 96: 8461–8466.

Koynova R, Tarahovsky YS, Wang L, and MacDonald RC (2007). Lipoplex formulation of superior efficacy exhibits high surface activity and fusogenicity, and readily releases DNA. Biochim Biophys Acta, 1768: 375–386.

Lang F, Busch GL, Ritter M, Volkl H, Waldegger S, Gulbins E and Haussinger D (1998). Functional significance of cell volume regulatory mechanisms. Physiol Rev, 78: 247–306.

Lee KS and Tsien RW (1983). Mechanism of calcium channel blockade by verapamil, D600, diltiazem and nitrendipine in single dialysed heart cells. Nature, 302: 790–794.

Lew VL and Bookchin RM (1986). Volume, pH, and ion-content regulation in human red cells: analysis of transient behaviour with an integrated model. J Membr Biol, 92: 57–74.

Lew VL and Simonsen LO (1980). Ionophore A23187-induced calcium permeability of intact human red blood cells. J Physiol, 308: 60.

Loor F, Tiberghien F, Wenandy T, Didier A and Traber R (2002). Cyclosporins: structure-activity relationships for the inhibition of the human MDR1 P-glycoprotein ABC transporter. J Med Chem, 45: 4598–4612.

Lubman RL and Crandall ED (1994). Polarized distribution of Na^+/H^+ antiport activity in rat alveolar epithelial cells. Am J Physiol, 266: L138–L147.

Lux SE (1979). Spectrin-actin membrane skeleton of normal and abnormal red blood cells. Semin Hematol, 16: 21–51.

Magde D, Elson EL and Webb WW (1972). Thermodynamic fluctuations in a reacting system: measurement by fluorescence correlation spectroscopy. Phys Rev Lett, 29: 705–708.

Matsumoto H, Erickson R, Gum J, Yoshioka M, Gum E and Kim Y (1990). Biosynthesis of alkaline phosphatase during differentiation of the human colon cancer cell line Caco-2. Gastroenterology, 98: 1199–1207.

McCloskey M, Liu ZY and Poo MM (1984). Lateral electromigration and diffusion of IgE Fc receptors on rat basophilic leukemia cells: the effects of ligand binding. J Cell Biol, 99: 778–787.

McLaughlin S and Poo MM (1981). The role of electro-osmosis in the electric-field-induced movement of charged macromolecules on the surfaces of cells. Biophys J, 34: 85–93.

Mendonca DMH and lauterbur PC (1986). Ferromagnetic particles as contrast agents for magnetic resonance imaging of liver and spleen. Magn Reson Med, 3: 328–330.

Meunier V, Bourrié M, Berger Y and Fabre G (1995). The human intestinal epithelial cell line Caco-2; pharmacological and pharmacokinetic applications. Cell Biol Toxicol, 11: 187–194.

Murer H, Hopfer U and Kinne R (1976). Sodium, proton antiport in brush border membranes isolated from rat small intestine and kidney. Biochem J, 154: 597–602

Nicotera P and Orrenius S (1998). The role of calcium in apoptosis. Cell Calcium, 23: 173–180.

Numata M and Orlowski J (2001). Molecular cloning and characterization of a novel $(Na^+, K^+)/H^+$ exchanger localized to the trans-Golgi network. J Biol Chem, 276: 17387–17394.

Paradiso AM (1992). Identification of Na^+/H^+ exchange in human normal and cystic fibrosis ciliated airway epithelium. Am J Physiol, 262: L757–L764.

Preston GM and Agre P (1991). Isolation of the cDNA for erythrocyte integral membrane protein of 28 kilodaltons: Member of an ancient channel family. Proc Natl Acad Sci USA, 88: 11110–11114.

Pinto M, Robine LS and Appay MD (1983). Enterocyte-like differentiation and polarization of the human colon carcinoma cell line Caco-2 in culture. Biol Cell, 47: 323–330.

Pick U (1982). The interaction of vanadate ions with the Ca-ATPase from sarcoplasmic reticulum. J Biol Chem, 257: 6111–6119.

Politz JC, Browne ES, Wolf DE and Pederson T (1998). Intranuclear diffusion and hybridization state of oligonucleotides measured by fluorescence correlation spectroscopy in living cells. Proc Natl Acad Sci USA, 95: 6043–6048.

Price RL, Haberstroh KM and Webster T J (2003). Enhanced functions of osteoblasts on nanostructured surfaces of carbon and alumina. Med Biol Eng Comput, 41: 372–376.

Puskin JS, Gunter TE, Gunter KK and Russell PR (1976). Evidence for more than one Ca^{2+} transport mechanism in mitochondria. Biochemistry, 15: 3834–3842.

Rich IN, Worthington-White D, Garden OA and Musk P (2000). Apoptosis of leukemic cells accompanies reduction in intracellular pH after targeted inhibition of the Na^+/H^+ exchanger. Blood, 95: 1427–1434.

Richter S, Hamann J, Kummerow D and Bernhardt I (1997). The monovalent cation leak transport in human erythrocytes: An electro-neutral exchange process. Biophys J, 73: 733–745.

Rindler MJ and Saier MH Jr (1981). Evidence for Na^+/H^+ antiport in cultured Dog Kidney Cells (MDCK). J Biol Chem, 256: 10820–10825.

Rosales C and EJ Brown (1992). Calcium channel blockers nifedipine and diltiazem inhibit Ca^{2+} release from intracellular stores in neutrophils. J Biol Chem, 267: 1443–1448.

Santella L, Kyozuka K, De-Riso L and Carafoli E (1998). Calcium, protease action and the regulation of the cell cycle. Cell Calcium, 23: 123–130.

Sarkadi B and Tosteson DC (1979). Active cation transport in human red cells. In: Giebisch G, Tosteson DC and Ussing HH (Eds.), Membrane transport in biology, Springer, Berlin, 2: 117–160.

Schatzmann HJ (1975). Active calcium transport and calcium ion-activated ATPase in human red cells. Curr Topics Membranes Trans, 6: 125−168.

Schlessinger J, Koppel DE, Axelrod D, Jacobson K, Webb WW and Elson EL (1976). Lateral transport on cell membranes: mobility of concanavalin A receptors on myoblasts. Proc Natl Acad Sci USA, 73: 2409–2413.

Schlessinger J, Axelrod D, Koppel DE, Webb WW and Elson EL (1977). Lateral transport of a lipid probe and labeled proteins on a cell membrane. Science, 195: 307–309.

Schwille P, Haupts U, Maiti S and Webb WW (1999). Molecular dynamics in living cells observed by fluorescence correlation spectroscopy with one- and two-photon excitation. Biophys J, 77: 2251–2265.

Sheetz MP, Schindler M and Koppel DE (1980). Lateral mobility of integral membrane proteins is increased in spherocytic erythrocytes. Nature, 285: 510–512.

Schinkel AH (1997). The physiological function of drug-transporting P-glycoproteins. Semin Cancer Biol, 8:161–170.

Siebens AW and Kregenow FM (1985). Volume regulatory responses of amphiuma red cells incubated in an isotonic media: The effect of amiloride. J Gen Physiol, 86: 527–564.

Seigneuret M and Devaux PF (1984). ATP-dependent asymmetric distribution of spin-labeled phospholipids in the erythrocyte membrane: relation to shape changes. Proc Natl Acad Sci USA, 81: 3751–3755.

Singer SJ and Nicolson GL (1972). The fluid mosaic model of the structure of cell membranes. Science, 175: 720–731.

Steck TL (1972). Cross-linking the major proteins of the isolated erythrocyte membrane. J Mol Biol, 66: 295–305.

Steck TL (1974). The organisation of proteins in the human red blood cell membrane. J Cell Biol, 62: 1–19.

Steck TL (1978). The band 3 protein of the human red cell membrane: A review. J Supramolec Struct, 8: 311–324.

Stevens MM and George JH (2005). Interface exploring and engineering the cell surface. Science, 310: 1135–1138.

Streissnig J, Goll A, Moosberger K and Glossmann H (1986). Purified calcium channels have 3 allosterically coupled drug receptors. FEBS Lett, 197: 204–210.

Sundelacruz S, Levin M, and Kaplan DL (2008). Membrane potential controls adipogenic and osteogenic differentiation of mesenchymal stem cells. PLoS ONE, 3: 1–15.

Sundqvist KG and Ehrnst A (1976). Cytoskeletal control of surface membrane mobility. Nature, 264: 226–231.

Takahashi Y, Bark N, Kinjo M and Rigler R (2003). Fluorescence correlation spectroscopy (FCS) analysis of human red blood cell system. Optical Review, 10: 596–599.

Tilney LG and Detmers P (1972). Actin in erythrocyte ghosts and its association with spectrin. Evidence for nonfilamentous form of these two molecules in situ. J Cell Biol, 66: 508–520.

Träuble H and Eibl H (1974). Electrostatic effects on lipid phase transitions: membrane structure and ionic environment. Proc Natl Acad Sci USA, 71: 214–219.

Tse M, Levine S, Yun C, Brant S, Counillon L, Pouyssegur J and Donowitz M (1993). Structure/function studies of the epithelial isoforms of the mammalian Na^+/H^+ exchanger gene family. J Membr Biol, 135: 93–108.

Tsien RY (1989). Fluorescent indicators of ion concentration. Methods Cell Biol, 30: 127–156.

Von Recum AF and Van Kooten TG (1995). The infuence of micro-topography on cellular response and the implications for silicone implants. J Biomater Sci Polym, 7: 181–198.

Vrolix MC, Sionis D, Piessens JH, Van Lierde J, Willems JL and H De Geest (1991). Coronary hemodynamics and coronary flow reserve after intracoronary diltiazem in humans. Am J Cardiol, 68: 1633–1637.

Webster TJ, Ergun C, Doremus RH, Siegel RW and Bizios R (2000). Enhanced functions of osteoblasts on nanophase ceramics. Biomaterials, 21: 1803–1810.

West JL and Halas NJ (2000). Applications of nanotechnology to biotechnology. Curr Opin Biotechnol, 11: 215–217.

Wiley J S and Cooper RA (1974). A furosemide-sensitive cotransport of sodium plus potassium in the human red cell. J Clin Invest, 53: 745–755.

Wilson G, Hassan IF, Dix CJ, Williamson I, Shah R, Mackay M and Artursson P (1990). Transport and permeability properties of human Caco-2 cells: an in vitro model of the intestinal epithelial cell barrier. J Controlled Rel, 11: 25–40.

Wong FH, Kamstra JS, Chen NL and Fradin C (2007). Localized photodamage of the human erythrocyte membrane causes an invagination as a precursor of photohaemolysis. J Microsc, 226: 6–17.

Zachowski A (1993). Phospholipids in animal eukaryotic membranes transverse asymmetry and movement. Biochem J, 294: 1–14.

Zwaal RFA and Schroit AJ (1997). Pathophysiologic implications of membrane phospholipid asymmetry in blood cells. Blood, 89: 1121–1132.

Zweibaum A, Triadou N, Dedinger M, Augeron C, Robine-Leon S, Pinto M, Rousset M and Haffen K (1983). Sucrase-isomaltase: A marker of fetal and malignant epithelial cells of the human colon. Am J Cancer, 32: 407–412.

Statement/Erklärung

I hereby declare that I have independently done this dissertation. I did not use any unauthorized assistance and unmentioned materials.

Hiermit erkläre ich an Eides statt, die vorliegende Dissertation selbstständig angefertigt zu haben. Ich habe keine unerlaubten sowie unerwähnten Hilfen benutzt.

Saarbrücken,

13.10.2010

Acknowledgements

I would like to express my sincere gratitude to my doctor-father, Prof. Dr. Ingolf Bernhardt, for his invaluable support, patience and encouragement throughout my doctoral studies. Both his scientific insights and editorial skills helped me to complete the work for this dissertation.

I would like to acknowledge the collaborative work with Prof. Dr. Gregor Jung (Dept. of Biophysical Chemistry) and his valuable suggestions throughout my work.

I am highly grateful to Dr. Seena Veettil for analyzing the FCS curves and troubleshooting during the collaborative work.

My thanks go to all my coworkers Erwin Weiß, Dr. Lyubomira Ivanova, Dr. Nguyen Duc Bach, Daniel Mörsdorf, Melanie Zimmer, Lisa Wagner and Jörg Riedel for creating an enjoyable and stimulating atmosphere.

I express my thanks to Shiva Shankar, Harish Bokkasam and all other friends.

Finally, I am grateful to my parents Venkataiah and Vimala, my wife and daughter for their love, and support.

Appendices

CURRICULUM VITAE

ARAVIND PASULA

EDUCATION

2003-2008	**PhD in Biophysics**
	Universität des Saarlandes, Saarbrücken, Germany.
1998-2000	**Masters Degree in Biochemistry**
	Osmainia University, Hyderabad, India.
1995-1998	**Bachelor's Degree in Microbiology**
	Osmainia University, Hyderabad, India.
1991-1993	**Pre-degree in Science**
	Board of Intermediate, A.P., India.

EXPERIENCE

Jan 2003- Sept 2008	**PhD student**
	Central Isotope laboratory, Biophysics, Universität des Saarlandes, Saarbrücken, Germany.
Jan 2001- Dec 2002	**Junior research fellow**
	Department of Biochemistry, Osmainia University, Hyderabad, India.

TECHNICAL SKILLS

■ Laser Scanning Confocal Microscopy ■ Fluorescence Spectroscopy ■Fluorescence Microscopy ■ Cell culture ■ Electrophoresis techniques ■Chromatography techniques ■ DNA Isolation ■ RNA Isolation ■ Plasmid Isolation ■ Mini, Midi and Maxi Prep ■ PCR ■ Electrophoresis techniques ■ ELISA ■ Protein expression & Pull down assays ■ Enzyme assays

PERSONAL DETAILS

Date of Birth	18 April 1976
Place of Birth	Mahabubnagar, India
Sex	Male
Nationality	Indian
Languages known	English (good), German (basic), Hindi (good), Telugu (mother tongue)